



Tectonics

RESEARCH ARTICLE

10.1002/2016TC004293

This article is a companion to *Rutte et al.* [2017] doi:10.1002/2016TC004294.

Key Points:

- Thrust sheets and fold nappes record ~66% mid-upper crustal shortening in the Central Pamir
- Syn-convergent, ~N-S extension exhumed the Central Pamir gneiss-dome rocks from ~30 km
- Dextral wrenching and ~E-W extension record collapse of the Pamir-plateau crust into the Tajik depression

Supporting Information:

- Figure S1
- Figure S2
- Table S1

Correspondence to:

D. Rutte,
drutte@bgc.org

Citation:

Rutte, D., L. Ratschbacher, S. Schneider, K. Stübner, M. A. Stearns, M. A. Gulzar, and B. R. Hacker (2017), Building the Pamir-Tibetan Plateau—Crustal stacking, extensional collapse, and lateral extrusion in the Central Pamir: 1. Geometry and kinematics, *Tectonics*, 36, doi:10.1002/2016TC004293.

Received 29 JUN 2016

Accepted 10 NOV 2016

Accepted article online 11 JAN 2017

Building the Pamir-Tibetan Plateau—Crustal stacking, extensional collapse, and lateral extrusion in the Central Pamir: 1. Geometry and kinematics

Daniel Rutte^{1,2} , Lothar Ratschbacher¹, Susanne Schneider¹, Konstanze Stübner^{1,3} , Michael A. Stearns^{4,5}, Muhammad A. Gulzar¹, and Bradley R. Hacker⁴ 

¹Geologie, TU Bergakademie Freiberg, Freiberg, Germany, ²Now at Berkeley Geochronology Center and Earth and Planetary Sciences, University of California, Berkeley, California, USA, ³Now at Geowissenschaften, Universität Tübingen, Tübingen, Germany, ⁴Earth Sciences, University of California, Santa Barbara, California, USA, ⁵Now at Geology and Geophysics, University of Utah, Salt Lake City, Utah, USA

Abstract Asian deep crust exposed in the Pamir permits determination of the amount, sequence, and interaction of shortening, extension, and lateral extrusion over ~30 km of crustal section during the India-Asia collision. In the Central Pamir, gneiss domes and their hanging walls record Paleogene tripling of the 7–10 km thick Phanerozoic upper crustal strata; total crustal thickness may have amounted to 90 km. Two thrust sheets, comprising Cambro-Ordovician, respectively, Carboniferous to Paleogene strata, straddle the domes. Amphibolite-facies metamorphic rocks within the domes—equivalent to lower grade rocks outside the domes—form fold nappes with dome-scale wavelengths. E-W stretching occurred contemporaneously with top-to-~N imbrication and folding. At ~22–12 Ma, bivergent (top-to-N and top-to-S), normal-sense shear zones exhumed the crystalline rocks; most of the extension occurred along the northern dome margins. Shortening resumed at ~12 Ma with opposite-sense thrusting and folding focused along the dome margins. Throughout the building of the Central and South Pamir, dominant ~N-S shortening interacted with ~E-W extension along mostly dextral shear/fault zones. In the Neogene, shear is concentrated along a dextral wrench corridor south of the domes. We interpret the Paleogene shortening to record thickening and northward growth of the Pamir-Tibetan Plateau and short-lived Miocene crustal extension as gravitational adjustment, i.e., collapse, of the thickened Asian crust to Indian slab breakoff. Synconvergent Paleogene lateral extrusion thickened the Afghan Hindu Kush crust west of the India-Asia collision, and the Miocene-Recent dextral shear and ~E-W extension have accommodated collapse of the Pamir Plateau into the Tajik depression.

1. Introduction

The Pamir—together with the western Tian Shan—forms the northwestern tip of the India-Asia collision zone. Following *Ruzhentsev and Shvolman* [1981], *Burtman and Molnar* [1993] estimated “more than 300 km” N-S shortening across the Pamir interior (Central and South Pamir; Figure 1) and assigned dome-shaped exposures of crystalline rocks—the Pamir gneiss domes—to Precambrian microcontinents, interspersed with Paleozoic-Mesozoic magmatic arc and subduction-accretion systems [*Schwab et al.*, 2004]. *Robinson et al.* [2004], *Schwab et al.* [2004], *Schmidt et al.* [2011], *Stübner et al.* [2013a, 2013b], *Stearns et al.* [2013, 2015], and *Smit et al.* [2014] showed that these domes contain amphibolite-facies sedimentary and igneous rocks, buried, metamorphosed, and exhumed in the Cenozoic. Here we analyze the Muskol and Shatput domes, two ~150 × 20 km sized, east trending antiforms that continue into the Muztaghata dome of the Chinese Pamir (Figures 1 and 2a) [*Robinson et al.*, 2007]. Together with the Sarez and Yazgulem domes farther west, they expose the structurally deepest units of the Central Pamir (Figure 1b) and allow studying processes in the Asian part of the India-Asia collision zone to depths of ~30 km [*Schmidt et al.*, 2011; *Stearns et al.*, 2015].

In part 1 of this paper series, we explore the geometry, kinematics, and amount of deformation in the eastern Central Pamir; part 2 [*Rutte et al.*, 2017] reports the timing. We show that Paleogene ~N-S shortening by imbrication and folding led to middle-upper crustal thickening and coeval orogen-parallel lateral (~ESE-WNW) extrusion of the buried ductile crust. Two Miocene normal-sense shear zones—the North and South Muskol shear zones (NMSZ and SMSZ)—exhumed the deep crust. Miocene to Recent deformation

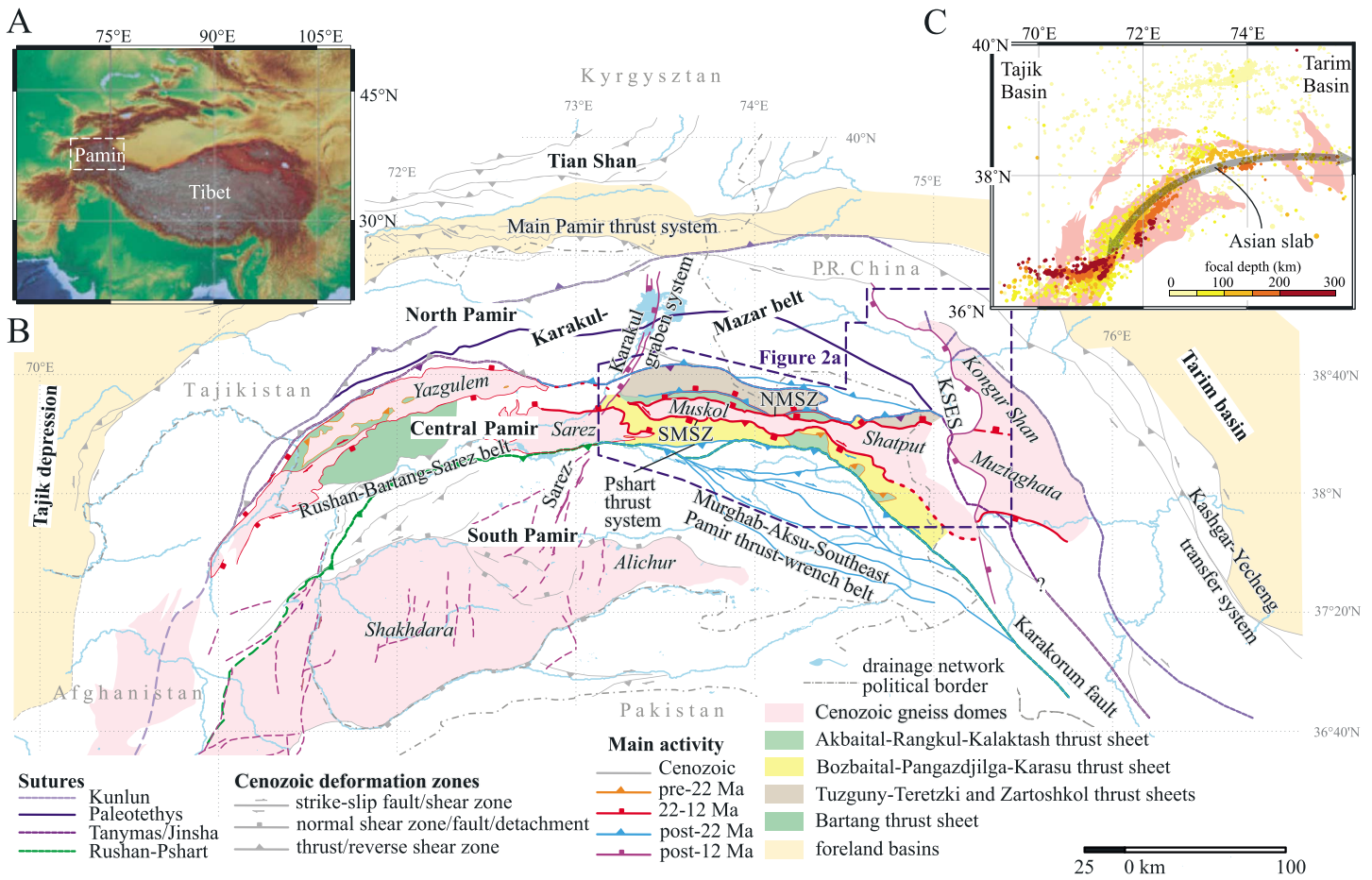


Figure 1. (a) The Pamir orocline at the northwestern margin of the Tibetan Plateau. (b) Simplified geologic-structural map of the Pamir orocline showing the Paleozoic-Mesozoic sutures, Cenozoic gneiss domes, major faults, and thrust sheets. Structures and sutures are from this study and modified from Vlasov *et al.* [1991], Leven [1995], and Schwab *et al.* [2004]. NMSZ, North Muskol shear zone; SMSZ, South Muskol shear zone; KSES, Kongur Shan extensional system. (c) Location of intermediate-depth seismicity plotted in relation to the location of the South and Central Pamir domes; modified from Sippl *et al.* [2013b].

reactivated the domes with bivergent, ~N-S thrusting-folding, dextral wrenching, and ~E-W extension, establishing a corridor along which the Central and South Pamir rocks were extruded approximately westward during prevailing ~N-S convergence.

Gneiss domes bounded by normal-sense shear zones are common in extensional settings. More rarely, they occur in collisional orogens, either with extension parallel to orogenic convergence, as in the North Himalayan gneiss domes [e.g., Lee *et al.*, 2000] and the South Pamir Shakh dara dome [Stübner *et al.*, 2013a], or with extension normal to orogenic convergence, as in the Muztaghata-Kongur Shan domes of the Chinese Pamir [e.g., Brunel *et al.*, 1994] or the Tauern Window of the Eastern Alps [e.g., Ratschbacher *et al.*, 1989]. Gravitational orogenic collapse [e.g., Dewey, 1988], blind thrusts beneath the domes [e.g., Lee *et al.*, 2000], vertical extrusion [e.g., Vannay *et al.*, 2004], diapirism [e.g., Rey *et al.*, 2011], and crustal buckling [e.g., Burg and Podladchikov, 1999] may explain the formation of orogen-parallel extensional domes. Here we describe the Central Pamir domes as composite features formed by gravitational collapse initiated by Indian slab breakoff [Stearns *et al.*, 2015], followed by buckling due to ongoing convergence. In this, the domes are time markers, tracing disequilibria between compressive boundary forces and gravitational potential energy in the orogenic system over time. Rey *et al.*'s [2010] generic thermomechanical numerical models suggest that gravitational plateau collapse is realized by the competing and coupled mechanisms of gravitational sliding of plateau margins toward the foreland, lower crustal channel flow, upward mass transfer in metamorphic core complexes, and foreland deformation; significant melt fractions, high lower crustal buoyancy, and weak foreland upper crust favor the development of hinterland core complexes. With our study, we contribute to the understanding of the role these processes play in gneiss-dome formation.

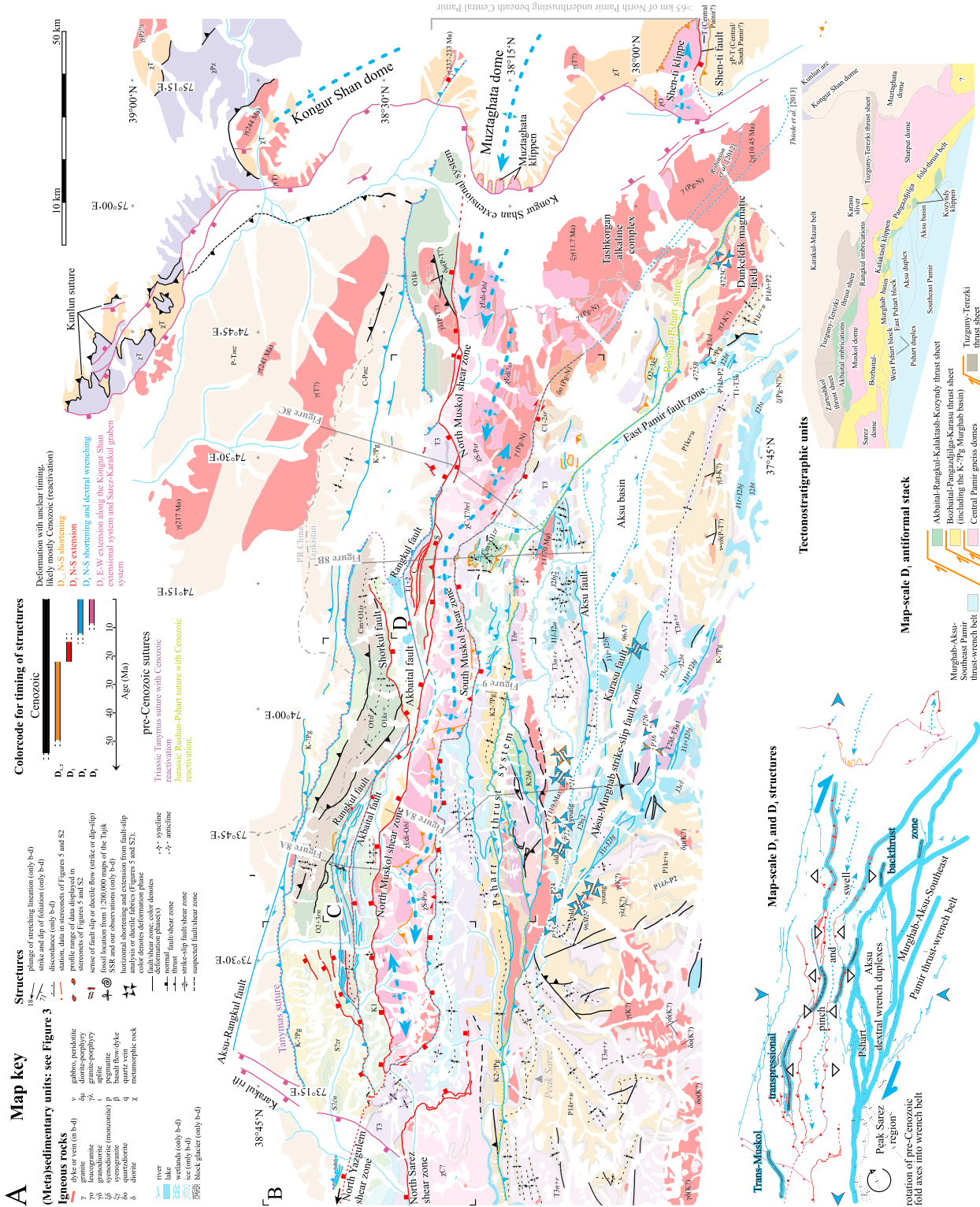


Figure 2. (a-d) Geologic-structural maps of the eastern Pamir. Frames in Figure 2a show locations of detailed maps in Figures 2b to 2d. The Tajik part is based on Yushin et al. [1964], the stratigraphic revisions of Vlasov et al. [1991] and Dronov et al. [2006], and our mapping from five expeditions (1993 to 2013); period, epoch, and lithologic "suite" abbreviations (Cm, Cambrian to N2, Pliocene; e.g., Cm+O1is, Isiiskaja suite) follow these authors and are detailed in Figure 3. The Chinese part is redrawn from Robinson et al. [2007, 2012] and Thiede et al. [2013], and modified based on our correlations with the Tajik Central Pamir [Rutte et al., 2017]. The lines mark cross-section traces (Figures 8 and 9). Ages (U-Pb) of magmatic rocks from Robinson et al. [2004], Schwab et al. [2004], Bershaw et al. [2012], Jiang et al. [2012], and Malz et al. [2013]. Insets at bottom in Figure 2a outline the map-scale structures, locate the tectonostratigraphic units discussed in the text, and depict the stacking geometry of the major thrust sheets and fold nappes.

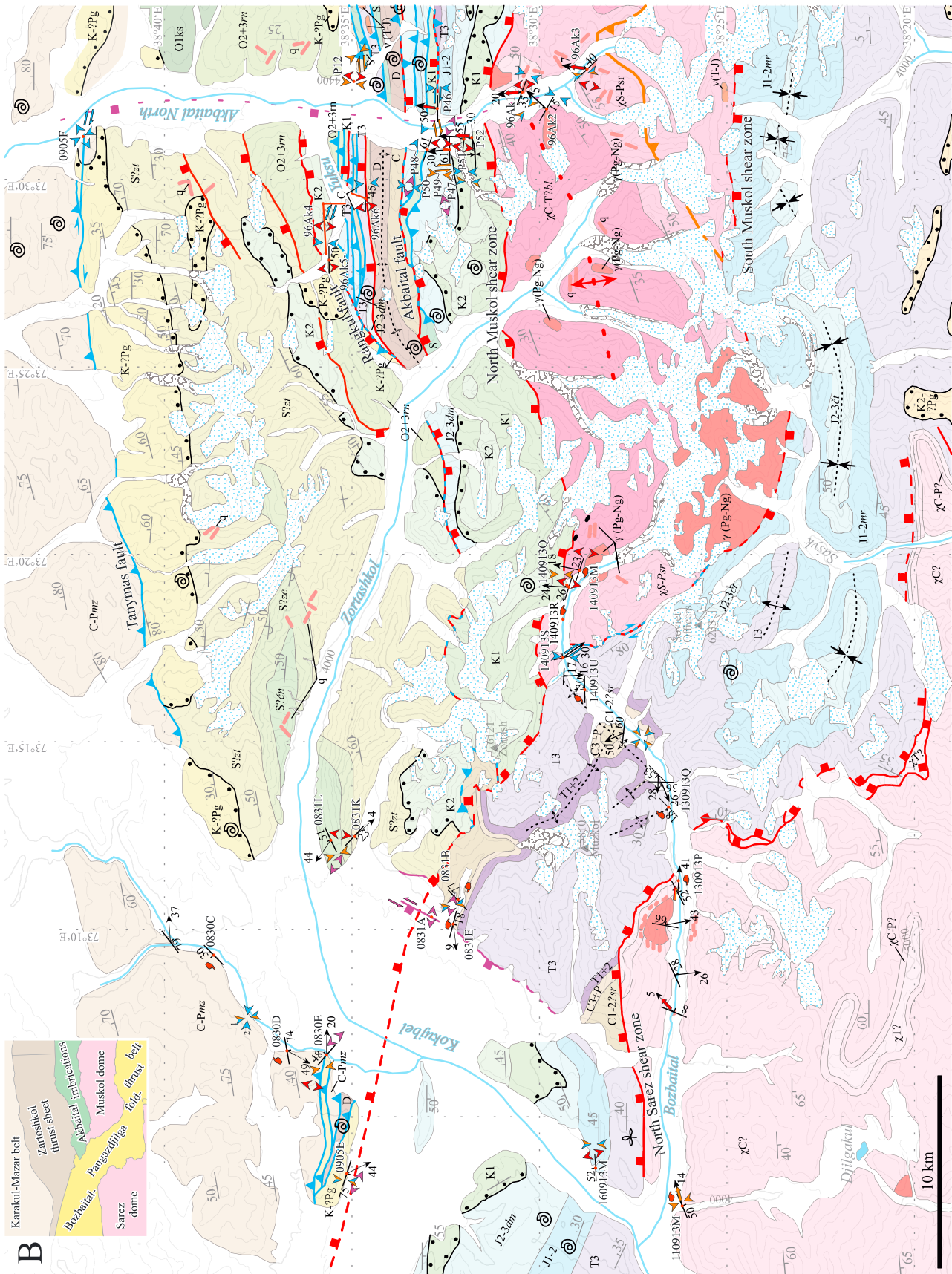


Figure 2. (continued)

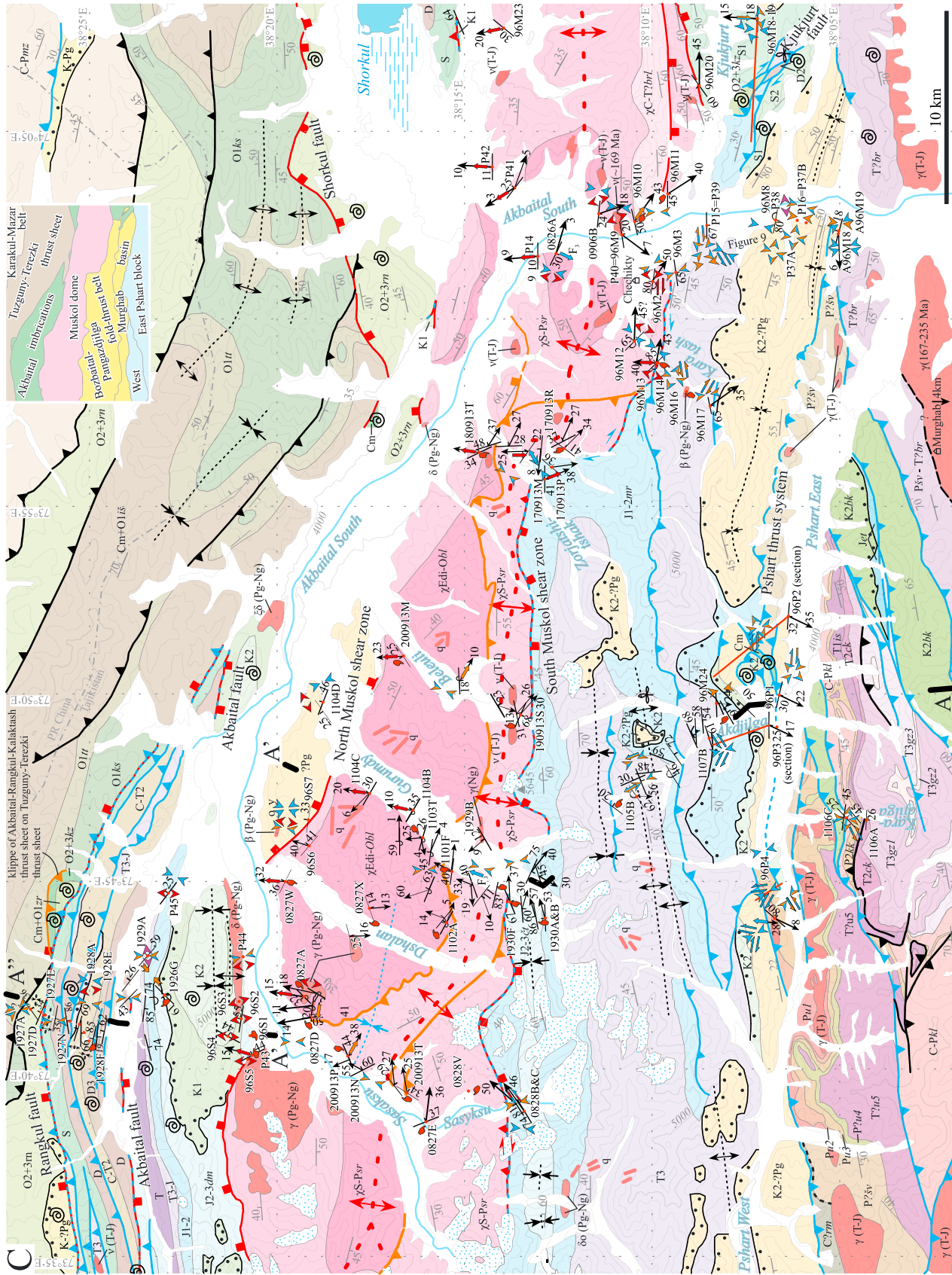


Figure 2. (continued)

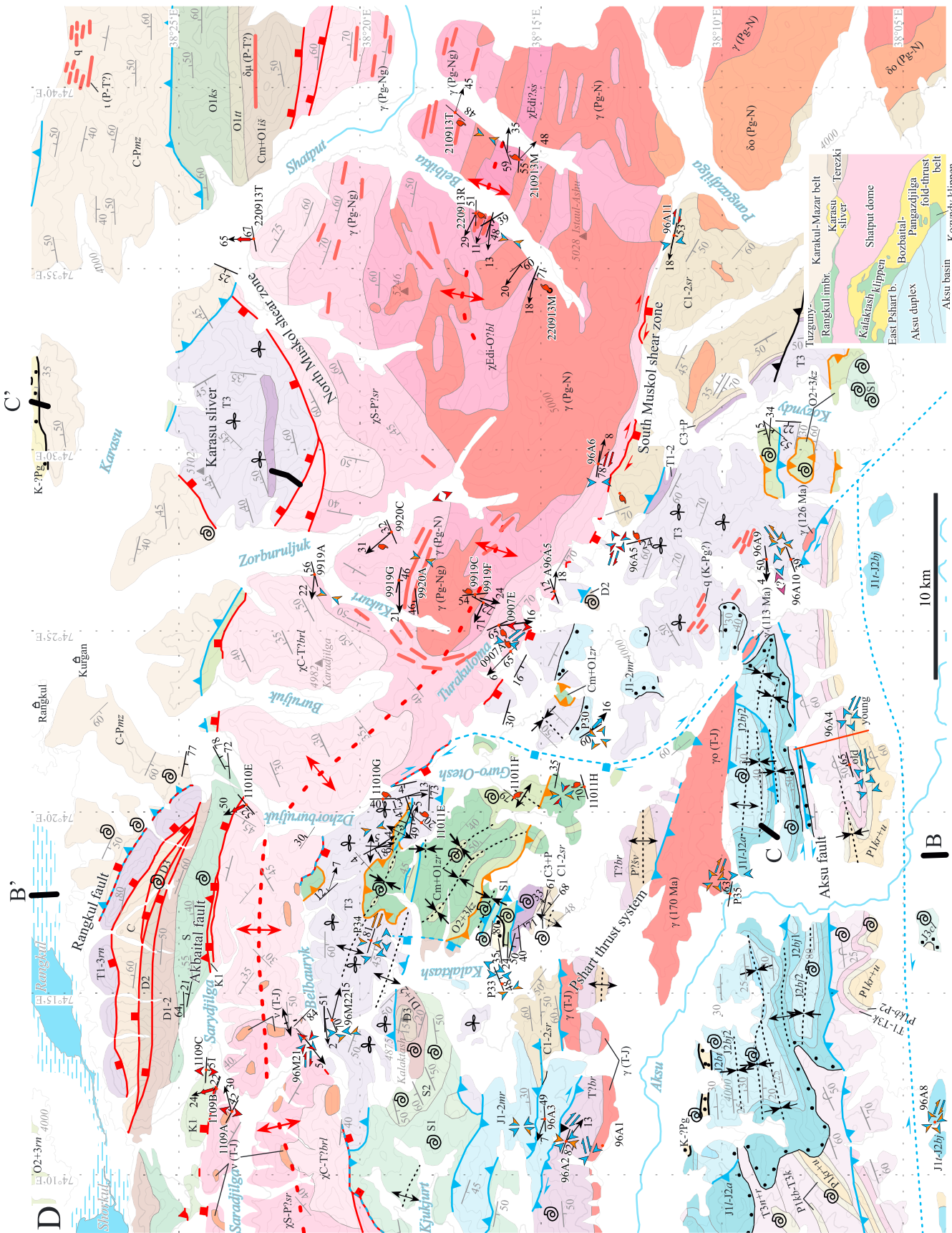


Figure 2. (continued)

The Pamir-Hindu Kush features intense intermediate-depth (~90–250 km) seismicity in an intracontinental setting [e.g., Pegler and Das, 1998; Sippl et al., 2013a], demonstrating vigorous geodynamic processes in the mantle beneath thickened (60–70 km) Asian crust [Mechie et al., 2012]. The seismicity beneath the Pamir [Schneider et al., 2013; Sippl et al., 2013b] outlines an arcuate, S to E dipping slab (Asian slab; Figure 1c). Kufner et al. [2016] inferred that northward advancing cratonic Indian lithosphere (“Cratonic India,” i.e., India excluding the extended northern parts of Greater India) is currently forcing delamination and roll back of cratonic Asian lithosphere (“Cratonic Asia,” i.e., North Pamir, Tarim, basement of Tajik basin, not including Cimmerian fragments without lithospheric keel [cf. Kufner et al., 2016]). They derived that delamination of ~380 km of Asian lithosphere at ~34 mm/yr—the India-Asia convergence rate in the western part of the collision zone [Molnar and Stock, 2009]—has taken ~11 Myr. The ability of India to underthrust was likely established when Cratonic India with its buoyant and thick Proterozoic crust and depleted mantle lid [Kumar et al., 2001] arrived at the Himalayan subduction zone and the Greater Indian slab—the extended passive margin of India—broke off 25–20 Myr ago [e.g., DeCelles et al., 2002; Negrodo et al., 2007; Stearns et al., 2013, 2015]. Here we argue that the onset of exhumation of the Central Pamir gneiss domes coincided with the breakoff of the Indian slab, and the termination of exhumation and resumption of shortening corresponded to the onset of delamination and retreat of the Asian slab when deep Cratonic India met deep Cratonic Asia [Kufner et al., 2016]. Thus, the domes are key features, linking processes at mantle depth, i.e., Indian slab breakoff and Asian slab retreat, to processes operating in the crust.

Currently, the Pamir east of the Sarez-Karakul graben system moves north with little internal seismic deformation; at its northern boundary, the Pamir is overthrusting the Tajik basin with strong seismicity along the Main Pamir thrust system, reflecting focused shortening (Figures 1b and 1c) [Schurr et al., 2014; Sippl et al., 2014]. The western Pamir shows higher seismic deformation rates, expressed by strike slip and normal faulting, indicating ~E-W extension together with ~N-S shortening. Schurr et al. [2014] explained the active deformation field as the result of ongoing collapse of the western margin of the Pamir Plateau and westward (i.e., lateral) extrusion of Pamir rocks into the Tajik depression, where this causes thin-skinned, ~E-W shortening of the Tajik-basin rocks above an evaporitic décollement. The combined bulk northward movement and westward extrusion of the Pamir likewise causes the progressive rotation of GPS-determined surface velocities from ~NNW to ~WNW from the eastern Pamir to the Tajik basin [Zubovich et al., 2010; Ischuk et al., 2013].

The collapse of the Pamir Plateau into the Tajik depression likely initiated via crustal extension in the Shakh-dara [Stübner et al., 2013a] and Muztaghata domes (Figure 1b) [Robinson et al., 2004, 2007]. Stübner et al. [2013a, 2013b] described the kinematic evolution of the largest of the Pamir domes—the giant Shakh-dara migmatitic gneiss dome of the southwest Pamir—by a model of metamorphic core-complex formation, involving ~90 km synconvergent crustal extension and ≥ 35 km rock exhumation, from ~16–2 Ma. Robinson et al. [2004, 2007] determined ~34 km ~E-W extension along the Kongur Shan extensional system starting at ~9–7 Ma. Here we show that upper crustal shortening and extension in the Central and South Pamir interacted with lateral stretching already in the Paleogene. This occurred by orogen-parallel, subhorizontal flow in the middle crust (preserved in the domes) and distributed dextral shear interacting with reverse and normal-sense shear across the entire Central Pamir. In the Neogene, dextral wrenching (sensu Wilcox et al. [1973]) is concentrated in the Murghab-Aksu-Southeast Pamir thrust-wrench belt south of the domes (Figure 1b).

2. Geologic Setting and Tectonostratigraphic Subdivision

Paleozoic-Mesozoic sutures subdivide the Pamir into the North, Central, and South Pamir (Figure 1b) [e.g., Burtman and Molnar, 1993]. The Central and South Pamir were part of Gondwana until the Permian [Leven, 1993]. Rifting along the Rushan-Pshart zone then separated the Central and South Pamir, and the opening of the Neotethys south of the South Pamir-Hindu Kush-Karakorum rifted them from Gondwana in the Permian-Triassic [e.g., Gaetani, 1997]. In the Triassic, the Central Pamir collided with the Kunlun arc and the intervening Karakul-Mazar accretionary wedge—both accounted to the North Pamir—closing the Paleotethys (Figure 1b); its southward subducting branch closed along the Tanymas suture [Schwab et al., 2004]. The closure of the Rushan-Pshart ocean and the collision of the Central and South Pamir occurred in the Late Triassic to Early Jurassic [Leven, 1995; Angiolini et al., 2015].

In the Russian literature, “suites” and “formations” subdivide the (litho)stratigraphy of the Pamir [Yushin et al., 1964; Vlasov et al., 1991; Leven, 1995; Dronov et al., 2006]. We adopted this subdivision, combined our field

observations and Zrn (zircon) U-Pb geochronology (Figure S1 in the supporting information) with the published data, and interpreted the stratigraphy in terms of the regional plate-tectonic evolution (e.g., rifting, passive margin formation, and subduction-accretion; Figure 3). The tectonostratigraphic units of the Central Pamir are (insert bottom right in Figures 2a and 3) (i) the gneiss domes; (ii) the Akbaital-Rangkul imbrications, the Karasu sliver, and the Tuzguny-Terezki and Zortashkol thrust sheets north of the gneiss domes (in the hanging wall of the NMSZ); (iii) the Bozbaital-Pangazdjilga fold-thrust belt, including the Murghab basin, and the Kalaktash-Kozyndy klippen south of the domes (in the hanging wall of the SMSZ); and (iv) the Murghab-Aksu-Southeast Pamir thrust-wrench belt of the southernmost Central and southeast Pamir. We show that the Akbaital-Rangkul imbrications and the Kalaktash-Kozyndy klippen form one thrust sheet—the Akbaital-Rangkul-Kalaktash thrust sheet—that straddles the domes and constitutes the structurally highest tectonic unit of the Central Pamir. The Bozbaital-Pangazdjilga fold-thrust belt connects with the Karasu sliver (see below and section 3.8), constituting the Bozbaital-Pangazdjilga-Karasu thrust sheet, which also straddles the domes. The dome rocks include Ediacaran to Triassic strata and resemble the lower Paleozoic strata of the Tuzguny-Terezki and Zortashkol thrust sheets and the upper Paleozoic strata of the structurally overlying thrust sheets; they form fold nappes and represent—together with the overlying thrust sheets—an antiformal stack (section 4).

The Central Pamir gneiss domes are asymmetric, partly overlapping antiforms with approximately east trending axes; they extend 10–40 km N-S and extend >400 km from the Afghan to the Chinese Pamir (Figure 1b). Four rock suites—in total >4.5 km thick—define the crystalline rocks of the Muskol and Shatput domes (Figure 3). The Sassyk suite comprises banded, locally migmatitic gneisses cut by granitic dykes that make up 10–40% of the rock volume. In the Muskol dome, we included the Sassyk suite into the Sarylshilin suite (see below), as it is lithologically and structurally identical with the latter. The Beleutin suite contains gneisses, quartzite, and micaschist increasing in abundance upsection. Local metatuff Zrn U-Pb ages (~540, ~533, and ~502 Ma) and the youngest detrital Zrn U-Pb age clusters (~590–580 Ma) in paragneiss and schist suggest an Ediacaran to Cambrian protolith (Figures 3 and S1). The Sarylshilin suite—about 1.1 km thick in the central Muskol dome, thinner in the eastern Muskol dome, and thicker again in the Shatput dome—comprises coarse white marble, grey to black, locally Ms (muscovite) bearing Bt (biotite) schist, and rare calcsilicate; some layers contain garnet (Grt) ± staurolite (St) ± aluminosilicates. The marble and metapelite-dominated members alternate in packages of 40 to 100 m. The youngest detrital Zrn U-Pb age cluster (~295 Ma, Figure S1) in quartzite at the top of the Sarylshilin suite suggests a Permian protolith. The structurally higher Buruliuk suite comprises Bt ± Grt ± Ms paragneiss, quartzite, Bt schist, rare marble, and conglomerate; the latter contains ≤15 cm pebbles in the upper third of the suite. The lithologies of the Buruliuk suite resemble the clastic Triassic units of the Bozbaital-Pangazdjilga fold-thrust belt (Figure 3). The Zrn U-Pb ages demonstrate imbrication/recumbent folds (section 4), and the presence of Paleozoic and possibly Triassic strata within the domes.

Lu-Hf garnet (35–26 Ma) [Smit *et al.*, 2014], U-Th-Pb monazite (28–14 Ma) [Robinson *et al.*, 2007; Stearns *et al.*, 2013], and U-Pb titanite (36–19 Ma) [Stearns *et al.*, 2015] ages date the high-grade prograde and retrograde metamorphism in the crystalline rocks of the domes. Peak conditions were 0.7–1.1 GPa and 500–775°C [Schmidt *et al.*, 2011; Stearns *et al.*, 2015]. Prograde, crustal-thickening metamorphism was replaced by retrograde metamorphism due to crustal extension (see section 3) at ~22 Ma; the retrograde metamorphism is dated by U-Th-Pb in monazite reflecting garnet breakdown, and U-Pb in titanite formed or recrystallized during retrograde mineral reactions [Stearns *et al.*, 2013, 2015]. Top-to-~N and top-to-~S normal-sense shear zones bound the domes in the north (NMSZ) and south (SMSZ), respectively (Figure 2a) [this study; Schmidt *et al.*, 2011; Stearns *et al.*, 2013].

The Akbaital-Rangkul imbrications north of the domes contain >7 km of Cambro-Ordovician to Cretaceous strata (Figures 2b to 2d and 3). The Paleozoic strata—rich in mollusks, brachiopods, and crinoids [Dronov *et al.*, 2006]—are a repetitive sequence of marine limestone, shale, and marl. Pebbly sandstone red beds above the Paleozoic strata—previously ascribed to the Permian—contain detrital Zrn as young as Early Triassic (youngest group is ~250 Ma; Figures 3 and S1). Triassic marine, often reworked carbonates, contains gastropods and mollusks. The Jurassic strata are massive to bedded limestones with layers rich in detrital sponge spicules, corals, and shells. Vlasov *et al.* [1991] and Dronov *et al.* [2006] ascribed disconformably overlying red silt/sandstones with conglomerate layers to the Paleogene, but later revised this to the Lower Cretaceous. The Upper Cretaceous contains basal conglomerates and thick-bedded carbonate. The youngest Zrn U-Pb

age group (~75 Ma) in structurally higher conglomerate and sandstone implies the presence of uppermost Cretaceous to possibly Paleogene strata (Figures 3 and S1). The Kalaktash-Kozyndy klippen south of the Muskol and Shatput domes (Figure 2a) resemble the Cambrian to Devonian pelite-limestone succession of the Akbaital-Rangkul imbrications [Dronov *et al.*, 2006]; together they constitute the Akbaital-Rangkul-Kalaktash thrust sheet (section 3.9).

The stratigraphic age of the ~2.5 km thick strata of the Tuzguny-Terezki and Zortashkol thrust sheets (Figure 2a)—based on fossil algae—is debated; Dronov *et al.* [2006] suggested a Meso-Neoproterozoic (Riphean) age; Vlasov *et al.* [1991] posited a Cambrian-Silurian age. The youngest detrital Zrn U-Pb age group of ~605 Ma in one sample supports the presence of Ediacaran strata. The Zortashkol thrust sheet contains >3 km of Silurian to Cretaceous strata. Strata that unconformably cover the Tuzguny-Terezki and Zortashkol thrust sheets were originally classified as Cretaceous and Paleogene [Yushin *et al.*, 1964] but revised to Cretaceous by Vlasov *et al.* [1991]. Dronov *et al.* [2006] questioned all evidence for Paleogene deposits.

The Bozbaital-Pangazdjilga fold-thrust belt south of the domes (Figure 2a) comprises >5 km of Carboniferous to Upper Cretaceous, possibly Paleogene (Murghab basin) strata [this study; Yushin *et al.*, 1964]. The Carboniferous strata are mostly silt/sandstones interlayered with shales and volcanic rocks. The Triassic is dominated by shales with detrital plant fossils; the Jurassic also comprises limestone. The Murghab-basin rocks (Figures 2a and 3) unconformably overlie the Triassic-Jurassic strata. In the first mapping effort [Yushin *et al.*, 1964], they were ascribed to the Cretaceous and Paleogene; Vlasov *et al.* [1991] assigned them to the Paleogene and Neogene. Dronov *et al.* [2006] reported >500 m of nonfossiliferous clastic rocks that contain at least one discordant contact above the uppermost fossil-bearing Maastrichtian rocks. The youngest detrital Zrn U-Pb age groups (Figures 3 and S1) confirm the age of the Mississippian to Middle Jurassic strata below the Murghab-basin rocks but are inconclusive for the age of the latter (youngest age group ~230 Ma). The Karasu sliver north of the Shatput dome (Figure 2a) exhibits Triassic rocks resembling those of the Bozbaital-Pangazdjilga fold-thrust belt regarding lithologies and detrital plant fossils [Dronov *et al.*, 2006]; together they constitute the Bozbaital-Pangazdjilga-Karasu thrust sheet (section 3.8).

The Murghab-Aksu-Southeast Pamir thrust-wrench belt comprises the West and East Pshart blocks, the southeast Pamir, and the Quaternary, perhaps older Aksu basin (Figures 2a and 3). The Pshart blocks are Carboniferous-Jurassic volcano-sedimentary units that align with the Rushan block (western Central Pamir) along the Rushan-Pshart suture zone [Leven, 1995]; imbricated Cretaceous strata document post-Jurassic deformation. Leven [1995] discriminated between a West Pshart block with Central Pamir stratigraphic and faunal affinities, and an East Pshart block with southeast Pamir affinities; accordingly, we place the Rushan-Pshart suture between these blocks. The southeast Pamir Cimmerian angular unconformity at the base of the Jurassic suggests Triassic-Jurassic suturing of the South and Central Pamir (Figure 3) [Dronov *et al.*, 2006; Angiolini *et al.*, 2015].

The Karakul-Mazar accretionary-wedge belt of the North Pamir formed before the Triassic by subduction of the Paleotethys (see above; Figures 1b, 2a, and 3) [Schwab *et al.*, 2004]. Carboniferous to Permian [Vlasov *et al.*, 1991; Robinson *et al.*, 2012] schist, phyllite, and rare marble and quartzite are intercalated with greenschist. Dronov *et al.* [2006] interpreted Devonian fossils as redeposited. The youngest detrital Zrns in metasilstone are ~335 Ma to ~265 Ma, agreeing with data from the Karakul-Mazar belt of the Chinese Pamir [Robinson *et al.*, 2012]. Schwab *et al.* [2004] correlated the Karakul-Mazar belt with the Songpan-Garzê-Hoh Xil system of Tibet.

3. Structural Geology

3.1. Definitions and Methods

Except for active faults [Strecker *et al.*, 1995], none of the structures of the Tajik eastern Pamir have previously been detailed. In the following, we establish the location, geometry, and kinematics of the major deformation zones. We document the structures in outcrop (decameter) scale “stations”—defined as single or closely spaced outcrops providing a consistent set of structural data—and link them by mapping along valleys (see valley names in Figures 2b to 2d) and ridges. Figures 4–6 present panoramic views of the dome structures, stereonet plots of structural orientations, sketches of field relations, deformation-time relationships, and field and thin section photos. Figure S2 completes the structural data set. Figures 2a–2d locate each



Figure 4. (a–d) Panoramic views of the Muskol dome. Distortion increases toward the image edges. Figures 4a and 4b are along section A in Figure 8. Thrusts and north vergent, recumbent, isoclinal folds in Figure 4d are in left part of Figure 4c. (e–h) Fault scarps in colluvial and alluvial deposits and range front normal faults along the active Sarez-Karakul graben system.

station (roman or *italic* lettering for Figures 5 and S2, respectively). Figures 7–9 provide cross sections and strain data.

We use the terms “brittle” and “ductile” in a scale-dependent fashion: brittle relates to macroscopic rock failure, whereas ductile denotes structures in which crystal plastic deformation of minerals—e.g., Qtz (quartz)—controlled the deformation, although other minerals—e.g., Fsp (feldspar)—may deform brittle. “Brittle–ductile” structures contain both deformation styles at macroscopic scale—e.g., faults associated with localized low-temperature (low- T) flow of Qtz or Cal (calcite). We estimated deformation intensity from the shape of deformed objects such as pebbles, the thickness and spacing of deformed zones, and the degree of grain-size reduction in comparison to the protoliths; locally, we quantified strain by using pebbles with the R_p/ϕ technique [e.g., Ramsay and Huber, 1983] and cross-section restoration. To establish the kinematics of deformation zones, we analyzed the sense of displacement in the field and thin sections, using offset markers, σ and δ

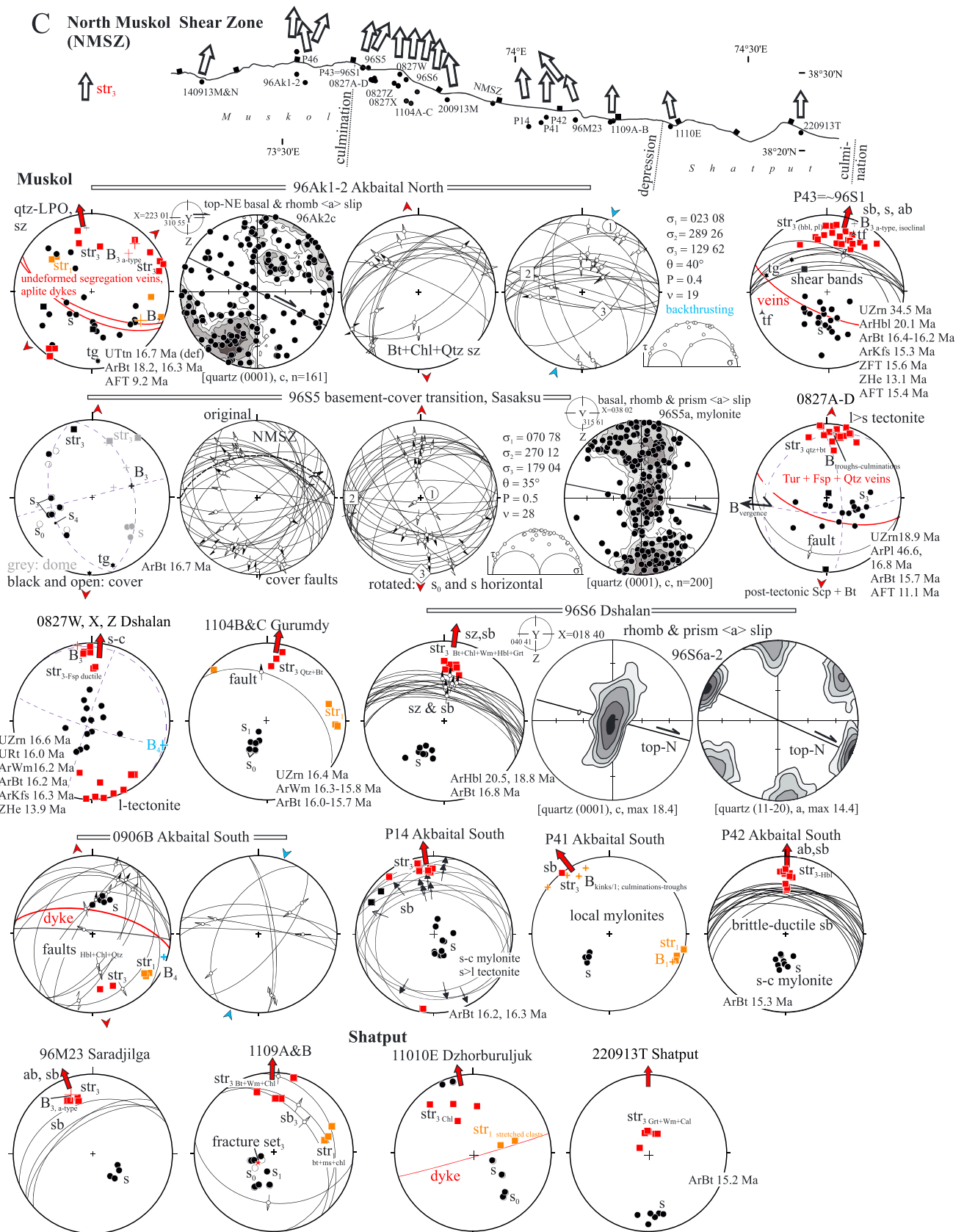


Figure 5. (continued)

D Hanging wall of the North Muskol shear zone

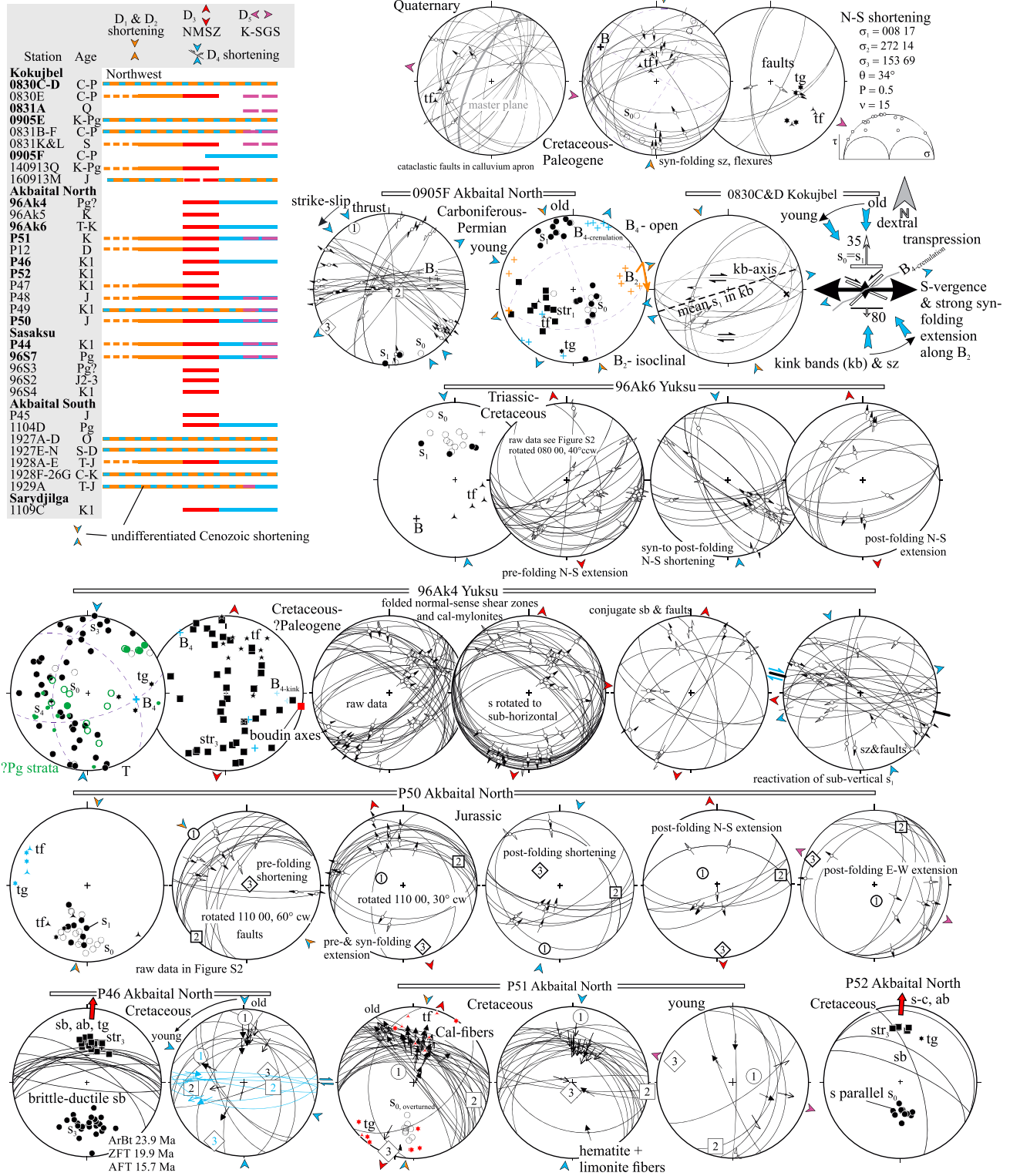
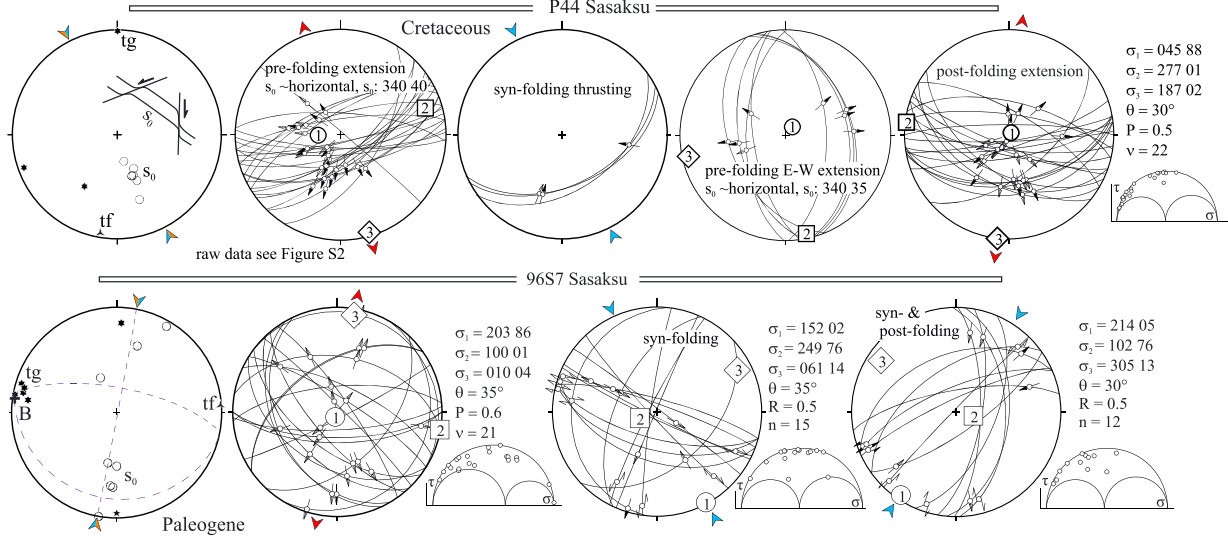


Figure 5. (continued)

Hanging wall of the North Muskol shear zone, continuation



E South Muskol shear zone (SMSZ)

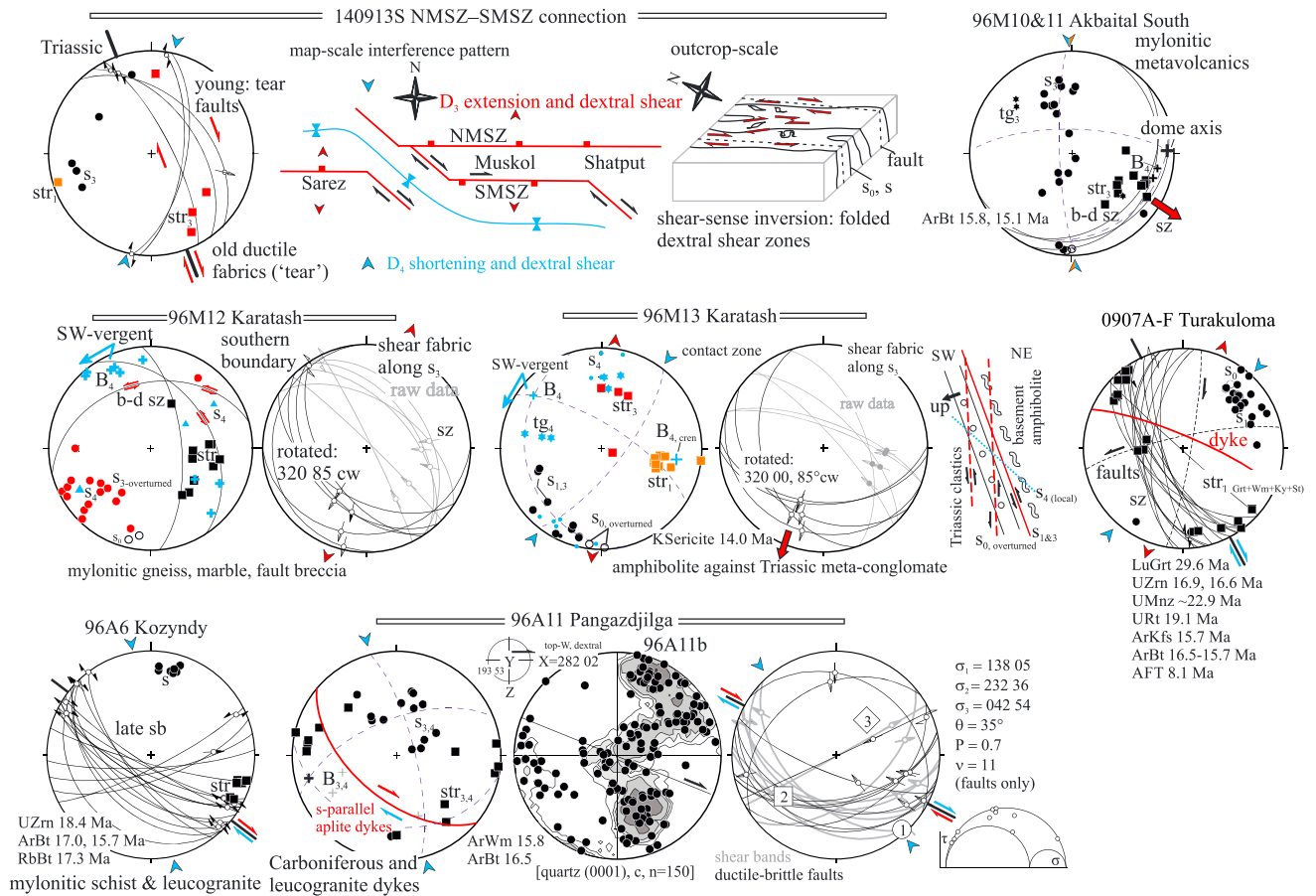


Figure 5. (continued)

F Hanging wall of the South Muskol shear zone

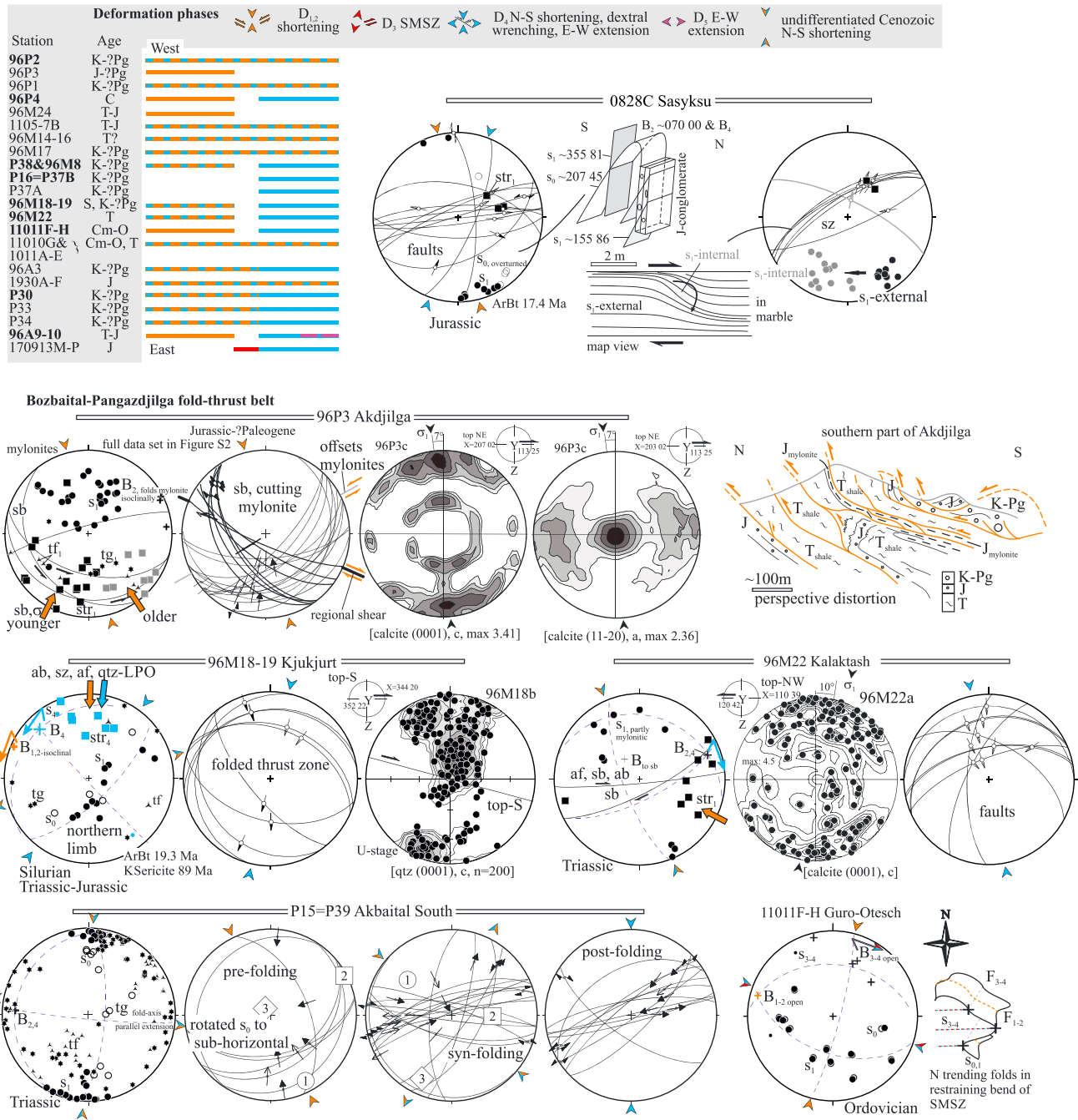
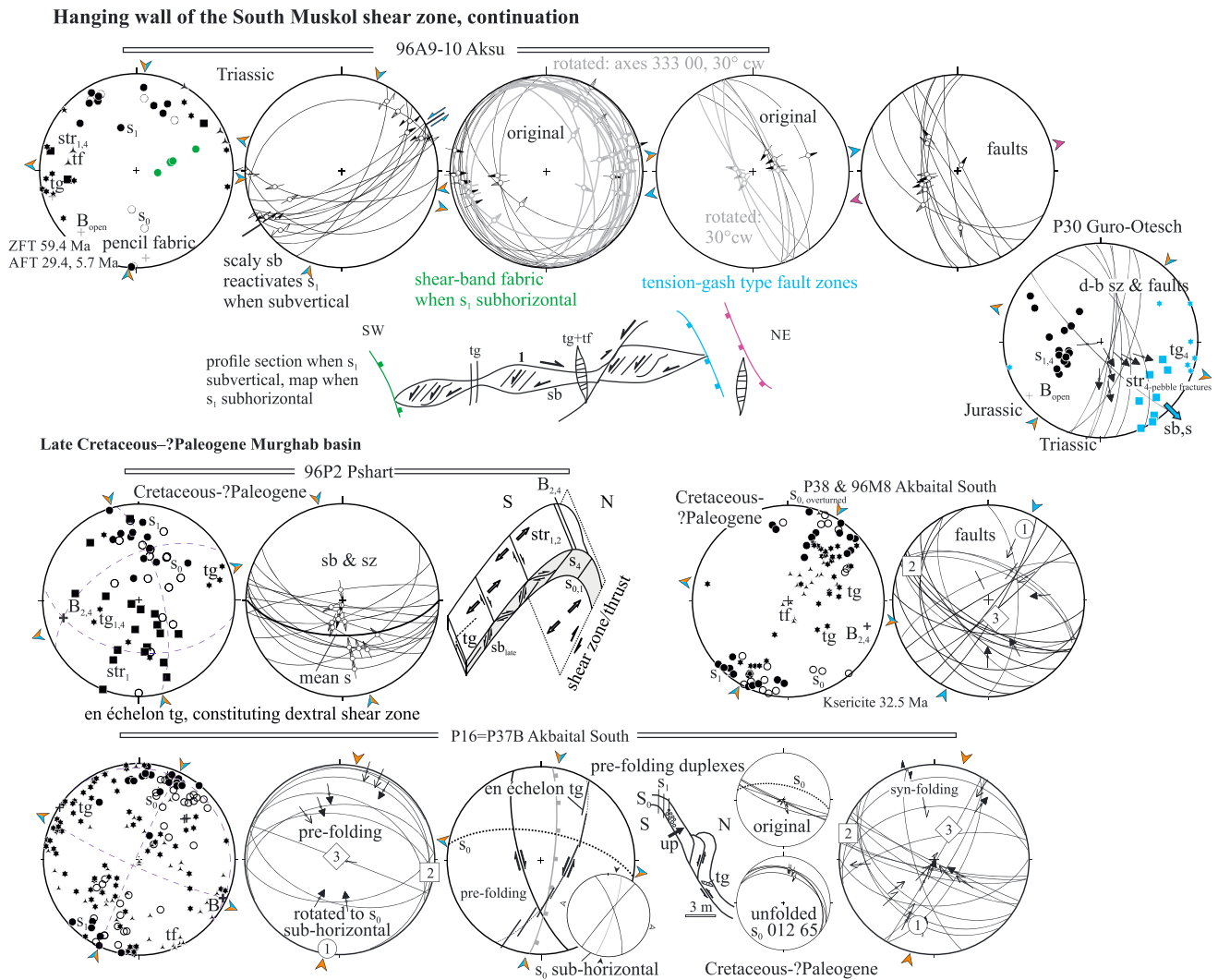


Figure 5. (continued)

porphyroclasts, shear zones (sz), shear bands (sb), asymmetric boudins (ab), asymmetric folds (af), schistosité-cisaillement (s-c) fabrics, and interpretations of U-stage and X-ray goniometer lattice-preferred orientation (LPO) measurements of Qtz and Cal. X-ray LPO analysis at Graz, Austria, employed the measurement and data-reduction procedures detailed in Kurz *et al.* [2002]. We based the LPO interpretations on comparisons to data from deformation zones where independent criteria, polycrystal-plasticity models, and experimental data constrain the path and temperature [e.g., Law, 1990]. To understand the kinematics of fault arrays, we applied “stress”-inversion techniques to fault slip data, employing the “numeric dynamic analysis”



implemented by *Sperner et al.* [1993] and *Sperner and Ratschbacher* [1994]. *Angelier* [1984], *Passchier and Trouw* [2005], and *Sperner and Zweigel* [2010] provided summaries and assessments of these methods.

Establishing the location, geometry, and kinematics of deformation in the Central Pamir for the first time requires the presentation and discussion of many observations. Each of the following sections starts with an overview about the observations (“Overview”), followed by descriptions of key stations (“Observations”). Given the interpretative nature of structural observations and the large number of stations necessary to characterize deformation over the eastern Central Pamir, the results are followed by their interpretations (“Interpretation”); a rigorous separation of observation and interpretation in separate results and discussion chapters would require massive repetition, which we try to avoid.

3.2. Structural Overview

A regional unconformity between Triassic and Jurassic strata, and Cretaceous strata unconformably covering the Tuzguny-Terezki and Zortashkol thrust sheets prove pre-Cenozoic deformation. Associated structures are (ENE trending folds in the Murghab-Aksu-Southeast Pamir thrust-wrench belt [e.g., *Vlasov et al.*, 1991], thrusts, and up to tight folds in the Bozbaital-Pangazdjilga fold-thrust belt and the Tuzguny-Terezki thrust sheet (Figure 2a). To assess Cenozoic deformation, we focused on profiles involving Jurassic and younger rocks and radiometric dating of deformation zones; Figures 5 and S2 report radiometric ages attached to

G Murghab-Aksu-Southeast Pamir thrust-wrench belt

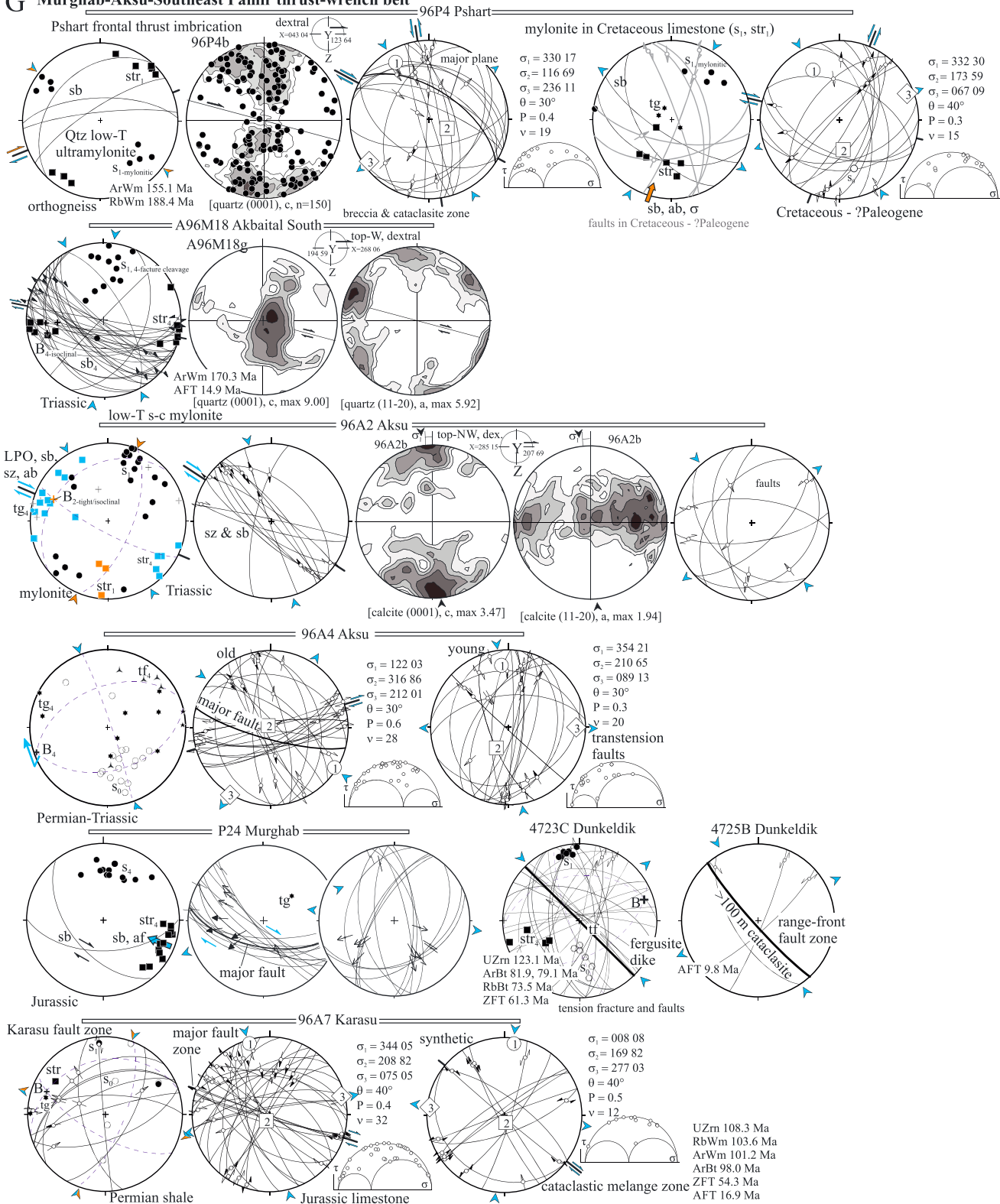


Figure 5. (continued)

the stereonet plots that are detailed in part 2 [Rutte *et al.*, 2017]. We identified five, partly temporally overlapping Cenozoic deformation phases (D_{1-5}). Where allocation to a phase is constrained by radiometric ages or overprinting relationships, we assign a subscript to the structural measurements (Figures 5 and S2); where no data exist or phases cannot be assigned with confidence, we do not apply a subscript designation.

D_1 involved ~N-S shortening, crustal thickening, and ~E-W stretching. The largest thrust sheets of the eastern Central Pamir—the Akbaital-Rangkul-Kalaktash and the Bozbaital-Pangazdjilga-Karasu thrust sheets—were emplaced during D_1 . In the dome interiors, subhorizontal flow zones show along-strike (~ESE-WNW) stretching with a penetrative D_1 fabric (first foliation, s_1 ; first stretching lineation, str_1). D_2 folded the D_1 fabric tightly to isoclinally during progressive deformation; structures include refolded D_1 mylonites in the Bozbaital-Pangazdjilga fold-thrust belt, and folds of bedding (s_0) and s_1 within the domes. D_1 – D_2 buried the rock sequence to peak pressure-temperature (P - T) conditions. Outside the domes, D_1 – D_2 can rarely be discriminated and are mostly summarized as D_1 . D_3 involved ~N-S extension by flow/slip along normal-sense shear/fault zones, mainly the NMSZ and SMSZ; normal-shear fabrics extend to the far north of the Muskol dome. D_4 , ~N-S shortening by folding and reverse faulting, overlapped but mostly outlasted D_3 . D_4 formed the main fabric of the top-to-~S Akbaital-Rangkul imbrications north of the domes, the thrusting of the Karakul-Mazar belt onto the Central Pamir, and the imbrication of the Tuzguny-Terezki and Zortashkol thrust sheets; it tightened the top-to-~N Bozbaital-Pangazdjilga fold-thrust belt and is the dominant phase in the formation of the Murghab-Aksu-Southeast Pamir thrust-wrench belt. This zone connects westward with the Rushan-Bartang-Sarez belt (Figure 1b). D_3 exhumed the crystalline rocks of the domes; together with D_4 , it shaped their geometry. D_5 encompasses the active ~E-W extension along the Kongur Shan and the Sarez-Karakul graben systems [Robinson *et al.*, 2004; Schurr *et al.*, 2014].

3.3. Internal Structure of the Eastern Sarez, Muskol, and Shatput Domes

3.3.1. Overview

The Muskol and Shatput domes constitute an asymmetric antiform [Pashkov and Dmitriyev, 1982] with the crest line along the southern part of the domes (Figures 2a and 4). The southern limb dips more steeply or similarly compared to the northern limb (Figures 2c and 2d, 4, and 5a). Tight to isoclinal, first- and second-generation folds (F_1 and F_2) fold s_0 , s_1 , and str_1 at the dome scale. In contrast to the map (kilometer) scale folds (forming fold nappes; section 4), which indicate ~N-S shortening and vertical thickening, the subhorizontal and mostly symmetric D_1 fabrics at the decameter scale imply along strike stretching (~ENE trending str_1). $D_{1,2}$ fabrics formed under prograde to peak P - T conditions. D_3 structures reflect distributed, ~N-S extension during retrograde metamorphism. D_4 —rare in the dome interiors—reflects resumed ~N-S shortening, with local open to tight F_4 . Figure 5a summarizes the observed structures.

3.3.2. Observations

S_0 comprises compositional layering; s_1 , in general, parallels s_0 but cuts it in local F_1 hinges (e.g., 0828X, Figure 6a). In the dome cores, str_1 on s_1 plunge and dip approximately east and approximately west

Figure 5. Structural data from selected outcrops (stations) plotted in lower hemisphere, equal area stereograms (see Figure S2 for the complete data set). Arrows around the stereograms indicate shortening and stretching directions (double arrows) or flow direction (single arrow) of brittle-ductile and ductile structures or subhorizontal maximum and minimum stress orientations determined from fault-slip analysis. Skewed arrows mark fold vergence. Some plots have explanatory sketches in map, cross section, or block-diagram view. Shear zones, shear bands, and faults are drawn as great circles and shear directions and striae (slickenlines) as arrows pointing in the direction of the displacement of the hanging wall. Confidence levels of slip-sense determination are expressed in the arrowhead style: solid, certain; open, reliable; half, unreliable; without head, poor. Reduced stress-tensor calculations: principal stress orientations (σ_{1-3}); θ , fracture angle used for calculation; R, shape factor of stress-ellipsoid = $(\sigma_2 - \sigma_3) / (\sigma_1 - \sigma_3)$; n , number of data used for calculation; dimensionless Mohr diagram visualizes normal versus shear stress relations for each fault (circles). X-ray goniometer and U-stage lattice preferred orientation measurements are contoured in multiples of random distribution. X, Y, and Z (principal strain axes) indicate orientations of the diagrams (normal to foliation and parallel to stretching lineation). Abbreviations: s_0 , bedding; s , foliation; s_{1-x} , foliation related to D_{1-x} ; str_{1-x} , stretching lineation related to D_{1-x} ; sz, shear zone; sb, shear band; B_{1-x} , fold axes of F_{1-x} folds related to D_{1-x} ; σ , sigma porphyroclast; δ , delta porphyroclast; tg, tension gash; tf, tension fracture; af, asymmetric fold; ab, asymmetric boudinage. Several plots provide the radiometric data obtained at these stations, which are reported in part 2 [Rutte *et al.*, 2017]. Abbreviations: Lu, Lu-Hf; U, U-Pb; Rb, Rb-Sr; Ar, ^{40}Ar - ^{39}Ar ; K, K-Ar; ZHe, zircon (U-Th)/He; ZFT, zircon fission track; AFT, apatite fission track; Grt, garnet; Zrn, zircon, Ttn, titanite; Rt, rutile; Hbl, hornblende; Amp, amphibole; Wm, white mica; Bt, biotite; Kfs, K-feldspar; Pl, plagioclase. (a) Summary of data from the Muskol and Shatput domes with schematic block diagram of the gneiss-dome structure, and color-coded time-deformation-metamorphism relations, applying to Figures 5a–5c. (b–g) Data from the structural units are discussed in the text. Map at top depicts along-strike orientation variation of str_3 along the North Muskol Shear Zone (Figure 5c). Table at top left provides color-coded deformation-time relationships and deformation phases observed in specific outcrops (Figure 5d). Same as Figure 5d but applying to Figures 5f and 5g. In these tables, bold stations mark stereograms shown in this figure, normal ones those shown in Figure S2. See text for interpretation.

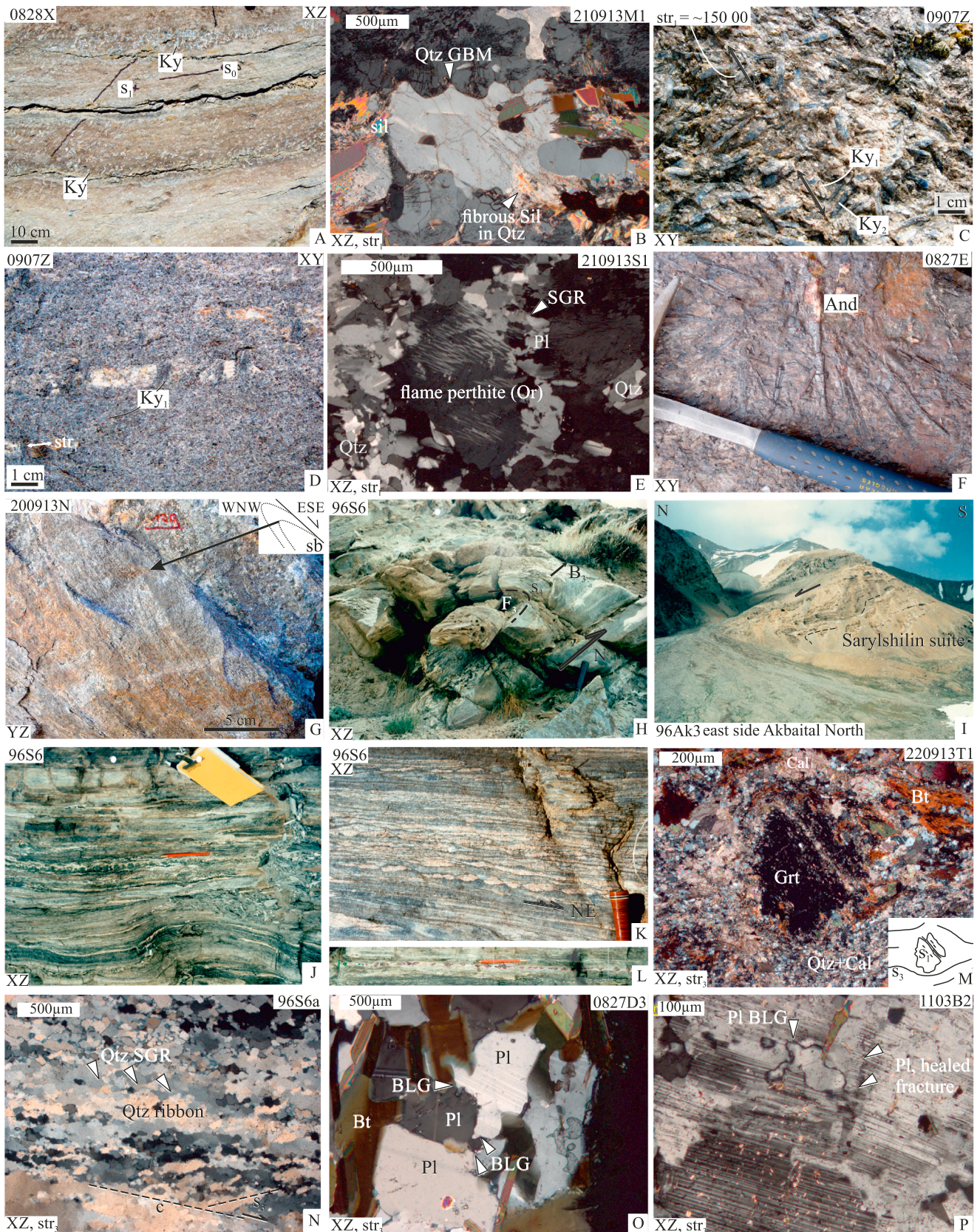


Figure 6

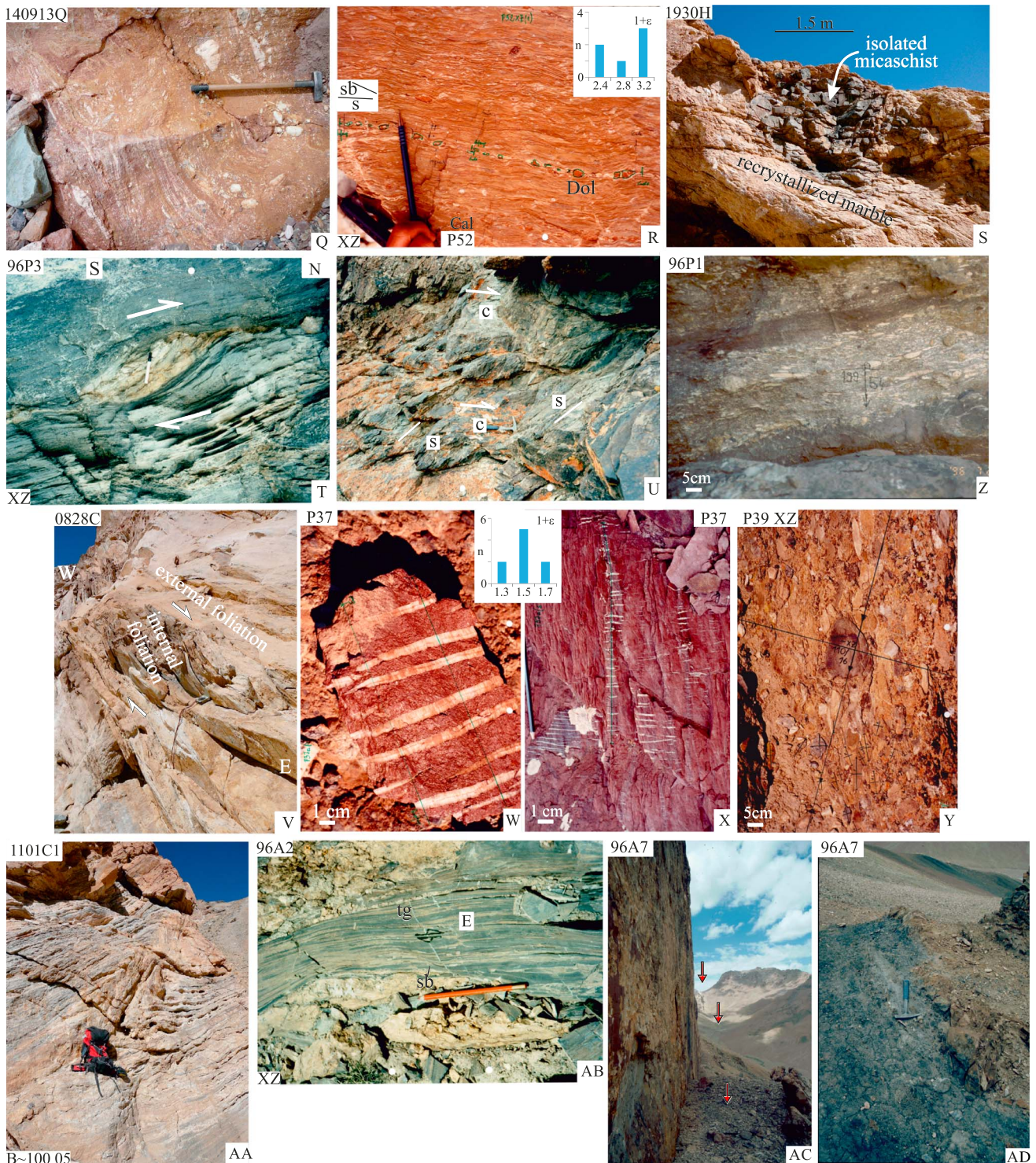


Figure 6. (continued)

(Figures 2b–2d and 5a and 5b). Both s_0 and s_1 follow great circle distributions, tracing F_2 to F_4 . Decameter-scale “a”-type [e.g., Malavieille, 1987] F_1 —with axes (B_1) parallel to str_1 —occur in high-strain zones (e.g., 9919A, Figure 5b). Str_1 is defined by Bt, Qtz, Ms, Fsp, Sil (sillimanite, e.g., 210913 M1, Figure 6b), St, Ky (kyanite, e.g., 0828X and 0907Z, Figures 6a, 6c, and 6d), Cpx (clinopyroxene), and Grt (e.g., 0907Z, Figure 6d). Microfabrics indicate that Qtz and Pl (plagioclase) deformed by grain-boundary migration (GBM; e.g., 210913 M1, Figure 6b) and

subgrain-rotation recrystallization (SGR; e.g., 210913S1, Figure 6e), respectively, or (orthoclase) shows flame perthite (e.g., 210913S1, Figure 6e). Locally, str_1 , e.g., defined by Ky_1 , is overgrown by randomly oriented Ky_2 (e.g., 0907Z, Figures 6c and 6d), and (andalusite, e.g., 0827E, Figure 6f), Scp (scapolite), and Bt. Sb (e.g., 200913N, Figure 6g) and af suggest a noncoaxial flow component; however, shear senses are inconsistent (110913M-130913P, 191913M-201913M, 200913N-T, 0828V-Y, 9919A, and 9919C-G, Figure 5b). F_2 occur on meter to kilometer scale, are recumbent, tight to isoclinal, and locally bounded by thrusts (Figures 4a and 4d and 6aa). They fold the D_1 fabrics, including s_1 parallel segregation veins that form rootless folds, and are mostly north vergent, except in overturned F_1 limbs (Figure 5a). The maximum $F_{1,2}$ wavelengths exceed the scale of the domes (section 4). B_2 are variable but mostly ~ESE trending. S_2 developed in hinges and as crenulations. The variable plunges of $B_{1,2}$ and B_4 (see below) outline culminations and depressions along the crest line of the dome antiforms and are reflected in the variable strike-normal width of the domes (“pinch and swell” geometry; Figure 2a).

Along the northern dome margins, str_3 on s_3 plunge and dip north or—rarely—shallowly south (Figures 2c and 2d). S_3 and str_3 contain a retrograde mineral assemblage (section 3.4). Locally, (e.g., 96Ak3, Figure 5b), two types of F_3 occur: a-type F_3 characterize high-strain zones and north vergent, open to tight F_3 fold s_3 and str_3 and are restricted to well-foliated or layered rocks (e.g., Figures 6h and 6i) along the NMSZ (section 3.4). Symmetric paragneiss and dolomite boudins in marble and Amp (amphibole) rich boudins in metatuff (e.g., Figure 6j) occur in ~E-W (parallel to str_1) and ~N-S sections (parallel to str_3). Toward the northern dome margins, the boudins are distinctly asymmetric, indicating top-to-~N shear (Figures 6k and 6l). Along the southern dome margins, s_3 and str_3 dip and plunge south, parallel to s_0 . F_4 are rare; they are upright to inclined, open to tight, often kinks, and fold s_1 and s_0 without an axial-plane foliation. In the Sasaku and Dshalan valleys, plunging str_3 outline a F_4 syncline (Figure 4c). On the southern and northern limbs of the dome antiform, F_4 are north and south vergent, respectively (e.g., 1930F, 0826A, Figure 5b).

3.3.3. Interpretation

The Muskol and Shatput domes comprise antiforms with north dipping to subvertical axial surfaces (Figures 2c and 2d, 4, and 5a). D_1 structures comprise s_1 , str_1 , and F_1 and indicate crustal thickening and ~ENE-WSW—along strike—stretching. S_1 and str_1 host the mineral assemblage that formed under prograde and peak P - T conditions [Schmidt *et al.*, 2011; Smit *et al.*, 2014; Stearns *et al.*, 2015]. Microfabrics in Fsp and Qtz indicate deformation temperatures of 500–700°C [Pryer, 1993; Stipp *et al.*, 2002], close to the peak metamorphic conditions. $Ky \pm And \pm Sil \pm Scp \pm Bt$ overgrew this fabric, indicating termination of D_1 prior to or synchronously with peak metamorphism. F_1 and F_2 fold the rock-suite boundaries at dome scale (section 4). We interpret F_2 to have followed F_1 in a kinematic continuum, and thus to also indicate crustal thickening. D_3 structures reflect ~N-S extension during retrograde metamorphism. Although normal-sense shear zones along the dome margins accommodated most of the exhumation (sections 3.4 and 3.7), D_3 fabrics are also distributed within the domes. F_3 , folding s_3 and str_3 in anisotropic rocks, likely constitute collapse folds [e.g., Faure *et al.*, 2003], related to noncoaxial, progressive shear (section 3.4). D_4 reflects resumed ~N-S shortening after exhumation of the dome rocks to a shallow crustal level. The opposing vergence of F_4 on the north and south limbs of the domes suggests F_4 formation contemporaneous with or after creation of the dome antiform.

Figure 6. Selection of structures in the gneiss domes, their hanging walls, and the Murghab-Aksu-Southeast Pamir thrust-wrench belt. Station numbers, orientation (X , Y , and Z ; principal strain axes), and some structural features are highlighted. (a) Compositional layering s_0 cut by s_1 hosting str_1 . Kyanite (Ky) defines s_1 . (b) Cross-polarized light micrograph of D_1 tectonite with lobate grain boundaries in quartz (Qtz) typical of grain-boundary migration recrystallization (GBM). Qtz includes fibrous sillimanite (Sil). (c) Ky_1 along str_1 is strongly overgrown by Ky_2 , indicating cessation of D_1 in the Ky stability field. (d) Ky_1 defines str_1 in paragneiss. (e) D_1 tectonite in cross-polarized light micrograph with undulose extinction and subgrains in plagioclase (Pl), characteristic of subgrain-rotation recrystallization (SGR), flame perthite in orthoclase (Or), and Qtz with lobate boundaries, characteristic of GBM. (f) Andalusite (And) overgrows s_1 . (g) WNW vergent, asymmetric fold in D_1 tectonite cut by shear band (sb) suggests a non-coaxial flow component. (h and i) F_3 “collapse folds” fold s_3 of the North Muskol shear zone (NMSZ) on different scales. (j) D_3 calcisilicate tectonite with symmetric boudins of amphibole-rich layers. (k and l) D_3 metatuff tectonite with asymmetric boudins, indicating top-to-~N flow. (m) Cross-polarized light micrograph of garnet (Grt) that includes rotated $s_{1,2}$ in s_3 tectonite of the North Muskol Shear Zone (NMSZ). (n) Cross-polarized light micrograph of Qtz-rich D_3 mylonite with ribbon grains and subgrains, characteristic of SGR; top-to-~N flow. (o) Cross-polarized light micrograph of D_3 tectonite with serrated grain boundaries in Pl, characteristic of bulging recrystallization (BLG). (p) Cross-polarized light micrograph of D_3 tectonite with deformation twins, healed fractures, and serrated grain boundaries (indicating BLG) in Pl. (q) Top of NMSZ: Brittle-ductile marble tectonite. (r) Dolomite (Dol) boudins in Cal s_3 -sb mylonite; inset shows stretch data (see text). (s) Top of South Muskol shear zone (SMSZ): Rootless micaschist boudin in ductile, posttectonically recrystallized Cal tectonite. (t) Mylonitic, low-grade Jurassic schist; top-to-~N shear from σ clast. (u) Scaly top-to-~N sb fabric in Triassic schist. (v) Rotated foliation in posttectonically recrystallized Cal tectonite along the SMSZ. (w and x) Gashes with tension fibers; inset shows extension data (see text). (y and z) Examples of joint faces in conglomerate with limestone pebbles used for R_f/ϕ strain analysis (Figure 9). (aa) F_2 in recrystallized marble tectonite (Gurumdy valley, Figure 4a). (ab) Low-temperature Cal mylonite with shear band (sb) and tension gash, indicating dextral strike-slip. (ac and ad) Karasu fault with cataclastic mélange of shale and limestone/dolomite.

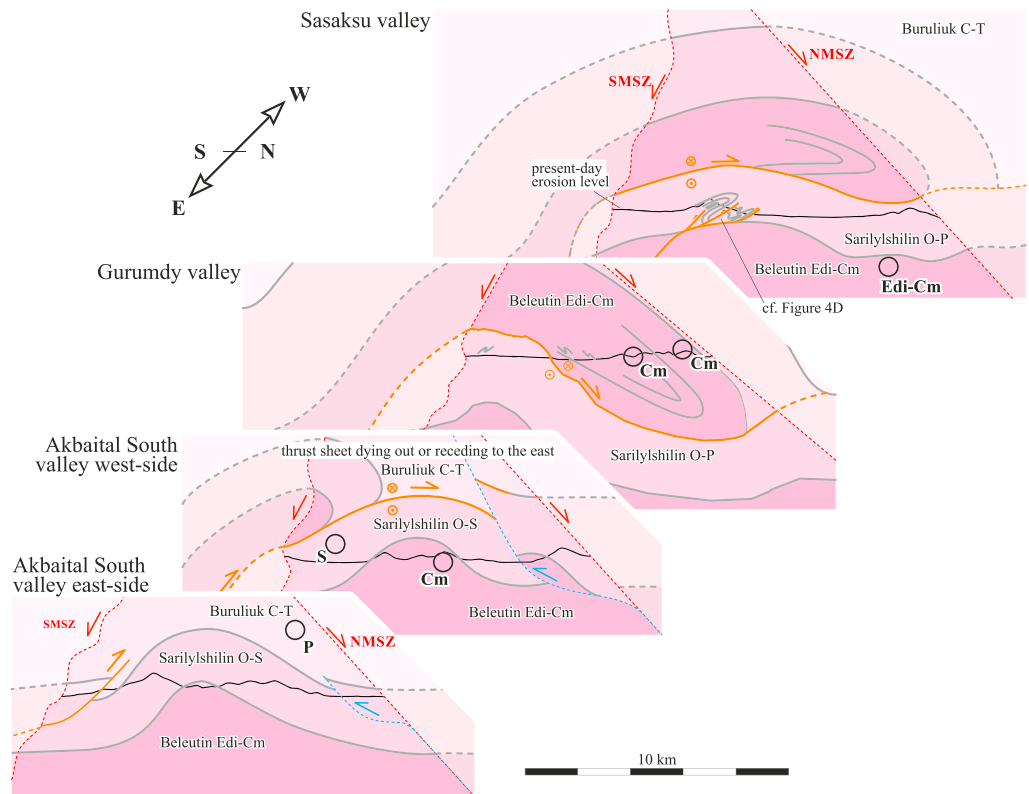


Figure 7. Schematic structural sections across the Muskol dome, visualizing the eastward, along-strike dying out or receding of a dome-spanning fold nappe. Black lines, topography; stippled red lines, North and South Muskol shear zones; orange and blue lines, predominant and postdominant thrusts, respectively. Map-view geometry (Figures 2b and 2c) and U-Pb zircon data demonstrate imbrication of the Beleutin suite. The sole thrust of the fold nappe crops out along the orographic left side of the Gurumdy valley (Figure 4a); the hinge of the fold nappe was not observed. Note the smaller fold nappe underlying the major fold nappe in the Sasaksu valley resembling its geometry (Figure 4d).

3.4. North Muskol Shear Zone

3.4.1. Overview

We mapped the 1.0–3.5 km thick, top-to-~N, normal-sense NMSZ for ~120 km from the Bozbaital valley (Sarez dome) in the west to the Shatput valley (Shatput dome) in the east (Figures 2b and 2d). It likely connects westward with the northern boundary of the Yazgulem dome; to the east, it is cut by the Kongur Shan extensional system and may continue north of the Muztaghata dome [Rutte *et al.*, 2017]; Robinson *et al.* [2007, 2012]). It has normal-shear fabrics that developed during exhumation of the NMSZ footwall from ductile to brittle conditions.

3.4.2. Observations

Metamorphic grade across the NMSZ changes from Ms + Bt + Grt ± Sil rocks in the footwall to low-grade and nonmetamorphosed rocks in the hanging wall; metamorphic grade rapidly decreases toward the top of the NMSZ, where shear zones transition into faults. The high-*T* deformation fabrics include syntectonic neocrystallization and/or recrystallization of Ms + Bt + Qtz + Fsp ± Hbl (hornblende) ± Grt along s_3 and str_3 (Figures 6m–6p), boudins of amphibolite in felsic layers where Pl and Qtz flow ductilely (Figures 6j and 6l), and fibrous Hbl in boudin necks and tension gashes. Qtz LPOs in mylonites record single or mixed basal, rhomb, and locally dominant prism <a> glide (96S6a-2 and 96Ak2 (Figure 5c) and 96S5 in Figure S2). Qtz was recrystallized by SGR (Figure 6n) and rarely by BLG. Pl was recrystallized by BLG and shows undulose extinction, deformation bands, tapered twins, and healed fractures (Figures 6o and 6p). Chl (chlorite) and Bt define str_3 in the low-grade transition zone between the Muskol and Shatput domes.

S_3 dips and str_3 plunges north; str_3 varies from 314° to 048° (Figure 5c, map at the top). Granitic pegmatite and aplite dykes and deformed and undeformed Qtz + Pl + Bt, Qtz + Hbl, Qtz + Chl, and Bt + Chl segregation

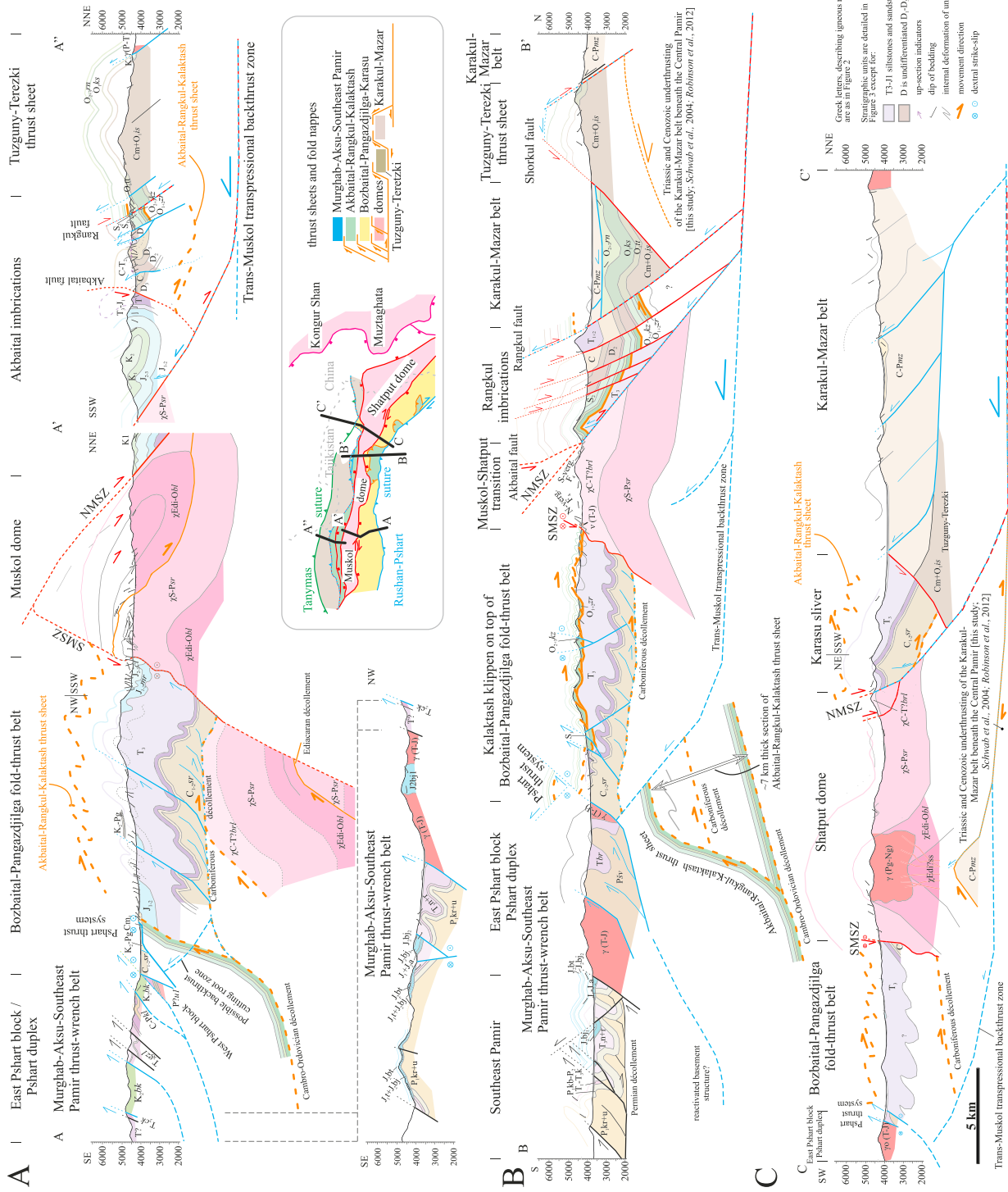


Figure 8. Structural sections across the Central Pamir (see Figures 2a to 2d for traces). Sections cross the northern southeastern Pamir and the Central Pamir, and end in the southern North Pamir. They parallel the flow direction during normal shear along the South and North Muskol shear zones (D₃) and the D_{1,2,4} shortening. Colors of thrusts and normal faults indicate their timing and correspond to Figures 2a to 2d. Tadpoles indicate dip of bedding or bedding-parallel penetrative foliation. The schematic ramp along the Cambro-Ordovician décollement below the Rushman-Pshart suture at the position of the Pshart thrust system (sections A and B) is the likely root zone of the Akbaital-Rangkul-Kalakatah thrust sheet. The dashed orange line in sections A and C trace the eroded base of the Akbaital-Rangkul-Kalakatah thrust sheet preserved in section B. The orange and blue lines below the sections outline the suspected deep structure, e.g., the underthrusting of North Pamir Karakul-Mazar rocks beneath the Central Pamir, as observed in the Chinese Pamir, and the reactivation of the Central Pamir by bivergent thrusting-folding and mostly after extensional dome formation. See text for details.

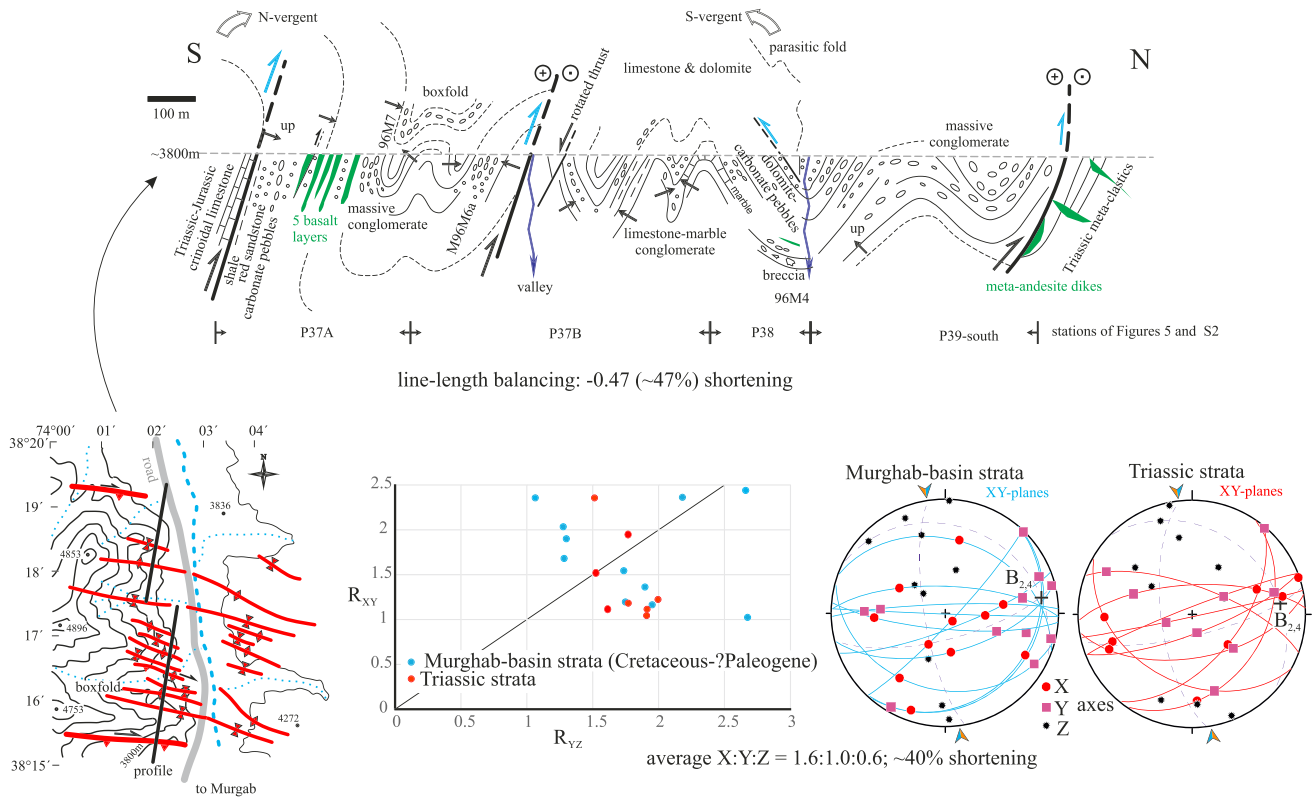


Figure 9. Map of and section across the Cretaceous-?Paleogene Murghab basin, part of the Bozbaital-Pangazdjilga fold-thrust belt, along the Akbaital South valley (Figure 2a). Strain, from deformed limestone pebbles of Murghab-basin conglomerates and underlying Triassic units (R/ϕ method), is at first order plane and invariant for the different units. Z (shortening) axes outline a great circle distribution and trace ~N-S shortening and tight folding; the Y and X axis distributions indicate both subvertical and subhorizontal ~E-W, along-strike extension. X-Y planes are, in general, vertical and trace the axial planes of upright folds.

veins strike normal to str_3 (e.g., 220913M-R and 0906B, Figure 5b). S_3 shows stronger along-strike variation than str_3 , outlining the culminations and depressions of the dome antiforms. Locally, open F_3 with B_3 parallel to str_3 or $L > S$ tectonites occur (e.g., 96Ak1-2, 0827A-D, and 0827W-Z, Figure 5c). Str_3 plunge increases eastward from 5–15° to 20–40° in the Muskol dome and up to 70° in the Shatput dome (e.g., 1104B and C, P14, P42, and 220913T, Figure 5c). S_b , s -c fabrics, σ and δ Fsp porphyroclasts, ab, af, and monoclinic Qtz LPOs consistently demonstrate top-to-~N flow (Figures 5c and 6h and 6i, 6k, and 6n). Str_3 (s_3 is difficult to discriminate from the sub-parallel s_1) occurs up to 3.5 km below the top of the NMSZ, defining its maximum thickness; the minimum thickness of the zone of penetrative deformation is given by the preservation of D_1 fabrics to within less than the top 1 km of the NMSZ. Roughly east trending, normal-sense, brittle-ductile sz , sb , fractures, and faults are common in the upper part of the NMSZ (e.g., 96S5, P43 = 96S1, 1104B, 1109A and B, and 96M23, Figure 5c). Their orientation spread is high, particular in outcrops with a-type open F_3 . The very top of the NMSZ shows locally cataclastic marble (Figure 6q) and fault gouge.

3.4.3. Interpretation

Exhumation of the NMSZ footwall occurred by top-to-~N normal-sense shear from amphibolite-facies to nonmetamorphic conditions. Ms + Bt + Grt + Hbl mylonites, with prekinematic to synkinematic Grt, likely formed at or above ~450°C. Qtz SGR recrystallization and crystal-plastic prism <a> glide indicate flow temperatures of 400–500°C, decreasing to 300–400°C during progressive deformation and varying due to position in the NMSZ (BLG; basal and rhomb <a> slip) [e.g., Stipp et al., 2002]. Fsp records flow at 400–500°C (undulose extinction, BLG, deformation twins, and bands) and <400°C (fracturing) [Ree et al., 2005; Ishii et al., 2007]. The development of brittle-ductile sb and faults within the NMSZ suggests that temperatures dropped below 250–300°C during continuous exhumation into the shallow crust. The NMSZ is up to 3.5 km thick, with penetrative deformation restricted to its upper part (<1 km). D_4 buckling may have tightened the domes and steepened the dip of the NMSZ; its steepest dip—north of Shatput dome—correlates with the area in which $^{40}Ar/^{39}Ar$ thermochronology suggests the strongest D_4 buckling [Rutte et al., 2017].

3.5. Akbaital-Rangkul Imbrications: The Hanging Wall of the North Muskol Shear Zone

3.5.1. Overview

We analyzed sections in the Akbaital North, Akbaital South, and Sarydjilga valleys (Figures 2b–2d and 5d). The Akbaital-Rangkul imbrications comprise tight (south) to open (north), symmetric to asymmetric, approximately south vergent folds and faults; they mostly formed during D_4 . The Akbaital fault is traceable for >100 km, separating Mesozoic strata in the south from mostly Paleozoic strata in the north (Figure 2a). It dips subvertical to the south in the Akbaital imbrications (Figures 2b and 2c); in the Rangkul imbrications, it dips to the north and the Mesozoic section is thinned to a slice of Cretaceous strata (Figure 2d). We interpret the Akbaital fault as a normal fault, antithetic to the NMSZ. D_4 shortening steepened it in the Akbaital imbrications and overturned it in the Rangkul imbrications. The Rangkul fault, one of several, mostly north dipping normal faults, synthetic to the NMSZ, bounds the Akbaital-Rangkul imbrications in the north.

3.5.2. Observations

D_1 and D_4 structures in the NMSZ hanging wall are difficult to distinguish; they are mostly reverse faults and folds recording ~N-S shortening. Several stations (e.g., P50, Figure 5d; 0830E, 0831K and L, P12, P48, 1928A-E, and 1919A, Figure S2) show reverse faults and ductile-brittle s_1 -c fabrics cut by normal faults; we classify these fabrics and s_1 and str_1 that carry the highest-grade metamorphic mineral assemblage (Bt, Chl) as D_1 fabrics. They include local open to tight F_1 with east trending B_1 . D_3 ~N-S extensional structures are prominent; they include Cal mylonites (e.g., 96Ak4, Figure 5d), locally with boudinaged dolomite layers and brittle-ductile s_3 -sb fabrics (e.g., P52, Figures 5d and 6r), Cal + Qtz + hematite \pm limonite mineralized normal faults (e.g., 96Ak4, P46, P51, P52, Figure 5d; P47, and 1928A-E, Figure S2), conjugate sets of strike-slip sb (e.g., P47, Figure S2), and ubiquitous gashes, commonly with fibers (e.g., 96Ak4, 96Ak6, Figure 5d; P47, and P48, Figure S2). The normal faults locally occur as conjugate sets (e.g., P50, Figure 5d) and contain cataclasite (e.g., P47 and 140913Q, Figure S2). The dolomite boudins in the Cal mylonite (e.g., P52, Figure 6r) yield an average subhorizontal stretch of 2.64 ($1 + e$; $e = (l-l_0)/l_0$; method of *Ferguson and Lloyd* [1984]); assuming plane strain, the foliation-normal shortening, compensating this stretch, amounted to $\leq 60\%$. F_4 fold D_3 structures. Consequently, the original normal-fault geometry is difficult to recognize, as the faults were rotated into apparent reverse-slip geometries or a consistent fault set (e.g., identical slickenside mineralization and consistent offset relationship to other structures) incorporates normal and reverse slip and associated oblique-slip sets (cf. raw data versus back-rotated plots in Figures 5d and S2). Reconstructing the original geometry illuminates extensional structures (e.g., horst-graben structures extending s_0 and faults cutting out layers) and maps these faults around decameter-scale folds. Some D_3 normal faults (and associated tensional structures) are tilted up to 40° (e.g., 96Ak6, 96Ak4, P50, and P44, Figure 5d); others cut across all preexisting structures (s_0 , s_1 , and s_3), often constituting conjugate sets. Other sb and normal fault sets formed close to the NMSZ, subparallel to and reactivating the north dipping s_0 and s_3 (e.g., P46, P52, Figure 5d; 96S2, and P45, Figure S2). At other stations, top-to-~S normal faults, antithetic to the NMSZ, prevail (e.g., P47, 96S3, and 96S4, Figure S2). Occasionally, we observed folded D_3 normal faults, overprinted by reverse slip, and in turn cut by normal faults (e.g., P50, P44, Figure 5d; P45, Figure S2).

D_4 structures comprise reverse faults, thrusts, and conjugate ~(N)E striking sinistral and ~NW striking dextral strike-slip faults (Figure 5d); top-to-~S reverse faults prevail (e.g., stations 0905E and F, P46, P51 (Figure 5d), P49, P45, and 1929A, Figure S2). In addition to the conjugate strike-slip faults, ~E-W extension is also manifested by stretch along B_4 , with gashes and tension fibers (e.g., 0830C and D, P50, and 96S7, Figure 5d). Most D_4 faults formed during folding (e.g., 96Ak6, P44, and 96S7, Figure 5d), and thus show considerable dip variation. Roughly east and west dipping normal faults (e.g., 0831A, P50, P51, Figure 5d; P48, P49, and 1929A, Figure S2) either relate to the stretch along B_4 or belong to D_5 . The D_5 normal faults are best developed along the Sarez-Karakul graben system (e.g., 0831A, Figure 5d; 0830E, 0831B-F, and 0831K and L, Figure S2); there, faults cut colluvium aprons (e.g., 0831A, Figure 5d) and form a cascade of at least three range-bounding normal faults (Figures 4e–4h; see also *Schurr et al.* [2014]).

3.5.3. Interpretation

We relate the D_1 structures to the emplacement of the Akbaital-Rangkul imbrications, as a part of the dome-straddling Akbaital-Rangkul-Kalaktash thrust sheet (section 3.9). Upper Cretaceous strata involved in D_1 indicate a Paleogene maximum emplacement age. The D_3 structures record ductile to brittle, ~N-S extension in the hanging wall of the NMSZ. Regionally distributed extension and local high-strain ductile ~N-S flow (e.g., the Cal mylonites) indicate stretching of the hanging wall of the NMSZ, i.e., a “stretching fault” geometry

[Means, 1989]; this increased the amount of displacement along the NMSZ (section 4). The folding of the D_3 structures and their local crosscutting relationships with D_4 structures, which record regional \sim N-S shortening, indicate that shortening locally interacted with but outlasted extension. D_5 \sim E-W extension traces the neotectonic deformation field [Strecker *et al.*, 1995; Schurr *et al.*, 2014]. The Akbaital fault is a D_3 normal fault antithetic to the NMSZ. D_4 steepened this fault in the Akbaital imbrications and overturned it in the Rangkul imbrications. The fault stack of the Akbaital imbrications comprises mostly D_4 , top-to- \sim S backthrusts associated with south vergent F_4 (Figures 2c and 5d). The folds and backthrusts imply refolding of the Akbaital fault, and reactivation of the NMSZ as a detachment for the hanging D_4 stack; either the NMSZ is the sole thrust of the Akbaital-Rangkul imbrications or a deeper blind thrust contributed to the dome architecture (Figures 8b and 8c and section 4). The Rangkul imbrications comprise top-to- \sim N normal faults, synthetic to the NMSZ (Figures 2d and 5d).

3.6. Tuzguny-Terezki and Zortashkol Thrust Sheets: The Hanging Wall of the North Muskol Shear Zone

3.6.1. Overview

The Tuzguny-Terezki and the Zortashkol thrust sheets expose the stratigraphically deepest units of the Central Pamir outside the domes; they form an east trending anticlinorium (Figure 2a). The youngest detrital Zrn U-Pb age cluster (1927B1: \sim 606 Ma, Figure S2) confirms the early Paleozoic to even Ediacaran age of the Tuzguny-Terezki rocks [Yushin *et al.*, 1964]. The northern margin of the thrust sheets and the Karakul-Mazar belt constitute a broad southvergent thrust-fold belt with Cretaceous and/or Paleogene strata in the footwalls. The southern boundary of the Tuzguny-Terezki and the Zortashkol thrust sheets—the Rangkul fault—is the roof thrust of the Akbaital-Rangkul imbrications (Figures 2a–2c). Normal faults, partially folded and mostly reactivated as reverse faults, extend \sim N-S extension far into the hanging wall of the NMSZ, emphasizing its role as the dominant dome-forming structure. A klippe of the Akbaital-Rangkul-Kalaktash thrust sheet on the Tuzguny-Terezki thrust sheet ($73^{\circ}45'E$, $38^{\circ}26'N$; Figure 2c) testifies to large-scale nappe tectonics prior to dome formation.

3.6.2. Observations

In the Kokujbel and Akbaital North valleys, north of the Sarez and Muskol domes (Figure 2b), three of four stations show that dextral strike slip accompanied top-to- \sim S thrusting (0830C and D, 0905E and F, Figure 5d; and 0830E, Figure S2) along the reactivated Tanymas suture. In the Zortashkol thrust sheet and the Akbaital imbrications west of Akbaital North (Figure 2b), stations 96Ak4–6 (Yuksu; Figures 5d and S2) document D_3 \sim N-S extensional structures that overprint an older fabric and are folded by F_4 ; several fault contacts place Cretaceous strata down onto Paleozoic strata. The top-to- \sim S Rangkul fault bounds the Zortashkol thrust sheet in the south (Figures 2a and 2b). Close to cross section A (Figures 2c and 8), Yushin *et al.* [1964] placed fossil-bearing Cambro-Ordovician strata as a klippe on the Tuzguny-Terezki thrust sheet. The nonmetamorphic limestone, shale, and sandstone of this klippe (classified as part of the Akbaital-Rangkul imbrications in Figure 3) differ distinctly in lithology and fossil content from the greenschist-facies mafic to felsic volcanic rocks, phyllite, quartzite, and limestone of the Ediacaran and Cambro-Ordovician strata of the Tuzguny-Terezki thrust sheet [Dronov *et al.*, 2006]. North of Lake Shorkul (eastern Muskol dome; Figure 2a), the Shorkul fault dips shallowly \sim SSE, tracing topography. It offsets the structurally highest units of the Tuzguny-Terezki thrust sheet against its antiformal core in the footwall (Figures 2a and 2c). The dextral Aksu-Rangkul fault (Figure 2a) interacts with the active Sarez-Karakul graben system in the west [Strecker *et al.*, 1995] and may extend eastward into the Chinese Pamir.

3.6.3. Interpretation

The unconformably overlying Cretaceous strata and the metamorphic hiatus between the rocks above and below this unconformity indicate that parts of the metamorphism, deformation, and exhumation of the Tuzguny-Terezki thrust sheet occurred pre-Cenozoic. We interpret the distinct (“exotic”) Cambro-Ordovician strata on the Tuzguny-Terezki thrust sheet as a klippe and as the northernmost remnant of the Akbaital-Rangkul-Kalaktash thrust sheet (emplaced during D_1 , see section 3.9), implying top-to- \sim N emplacement. The metamorphic hiatus between the rocks of the klippe and those of the Tuzguny-Terezki sheet further indicates pre-Cenozoic exhumation of the Tuzguny-Terezki rocks. The Zortashkol thrust sheet west of the Akbaital North valley—insufficiently studied so far—likely hosts refolded horst-graben structures and domes. We interpret the D_3 extensional structures, folded by F_4 , and the faults having Cretaceous strata in the hanging walls and older strata in their footwalls, as normal faults (Figures 2b and 2c). We speculate that the north dipping Rangkul fault in the Yuksu valley was a normal fault, reactivated as a D_4 top-to- \sim S thrust. The reactivated normal fault may be traced to the east of the Akbaital North valley, delimiting the Akbaital imbrications from the Tuzguny-Terezki thrust sheet with the exotic klippe in the hanging wall; it also joins the Akbaital (normal) fault in the Akbaital South valley, isolating the northern portion

of the Akbaital imbrications as a horst. We interpret the Shorkul fault as a normal fault that is antithetic to the NMSZ. The thrusts and folds that compose the top-to- \sim S back thrust belt along the northern and southern margins of the Tuzguny-Terezki and the Zortashkol thrust sheets—including the Akbaital-Rangkul imbrications—are dominantly D_4 structures; characteristically, dextral strike-slip shear accompanied and postdated thrusting-folding. The deepest exposure level in the Tuzguny-Terezki and Zortashkol thrust sheets is Cambrian, likely Ediacaran; we interpret the mafic to felsic metavolcanic rocks as stratigraphic equivalents to the Sassyk and Beleutin suite crystalline rocks within the Muskol and Shatput domes (Figures 2a and 3).

3.7. South Muskol Shear Zone

3.7.1. Overview

The SMSZ forms the southern boundary of the Muskol and Shatput domes; it separates amphibolite-facies crystalline rocks within the domes from greenschist-facies rocks south of them. This ductile to brittle-ductile normal-sense shear zone formed during D_3 , prior to and synchronous with D_4 dextral strike-slip shear. At the western tip of the Muskol dome, the SMSZ merges with the NMSZ. In the east, it may connect with the southern Shen-Ti fault in the Chinese Pamir (Figure 2a) [Robinson *et al.*, 2007, 2012].

3.7.2. Observations

At the western tip of the Muskol dome (Figure 2b), the SMSZ changes from its regional east strike to \sim NW and merges with the NMSZ as a dextral shear zone. The synclorium separating the Sarez and Muskol domes trends in an unusual NW direction and has tight \sim NW trending and open \sim NE trending folds. At 140913S (Figure 5e), sheared and isoclinally folded marble with δ and σ porphyroclasts indicate sinistral and dextral shear within different layers; there, kilometer-scale F_4 fold the dextral shear fabric (sketch next to station 140913S, Figure 5e). In the western central Muskol dome, Bt + Grt \pm St \pm Ky \pm Ms schist and marble are juxtaposed against Bt + Ab (albite) schists south of the SMSZ. The marble-metapelite Sarylshilin suite of the dome shows meter to decameter-scale tight to isoclinal, partly rootless folds, and meter-sized, isolated metapelite blocks surrounded by coarsely recrystallized marble (Figure 6s); similar mélangé fabrics occur along the SMSZ of the Shatput dome (96A5, Figure 2d). In the Jurassic strata of the SMSZ hanging wall, Ab (in metaclastic rocks) and Scp (in marble and calcisilicate) overgrew the subparallel s_0 and s_1 for at least 1.5 km south of the SMSZ (e.g., 1930B1 in Gurumdy and 0828B in Sasyksu); farther south, Chl schists locally contain <1 mm Bt porphyroblasts. In the Muskol-Shatput transition zone, Bt + Chl schists within the domes abut Triassic phyllite and metaconglomerate containing porphyroblasts of Bt + Chl south of the SMSZ. In the western Shatput dome (Turakuloma; Figure 2d), Ms + Grt \pm Sil \pm Bt schists border Bt bearing Triassic schists and metasandstone.

At the southern Gurumdy and Beleuli valleys (central Muskol dome), the SMSZ dips moderately to steeply south (Figures 2c and 4b). Axial trends of F_2 deviate by $\sim 30^\circ$ between the SMSZ footwall (1930F–J, 1101A–F, and 1929B–E, Figure 5b) and its hanging wall (1930A–F, Figure S2). Farther east (Zorjatshitshak; Figure 2c), ab and σ porphyroclasts indicate top-to- \sim SE shear in the SMSZ footwall (170913R–180913T, Figure 5b) and hanging wall (170913M–P, Figure S2). A major bend in the SMSZ occurs between the Zorjatshitshak and Karatash valleys (Figure 2c). In the latter, the ~ 5 m wide SMSZ is a \sim NE dipping mylonite zone. S_3 and str_3 developed in the rocks of the Muskol dome and overprint s_1 in its hanging wall; s_0 in the Triassic hanging wall conglomerate is overturned. Unfolding s_0 and $s_{1,3}$ (96M12–13, Figure 5e) yield a top-to- \sim S shear fabric; there, F_4 have a subvertical axial s_4 .

Still farther east (west side of the Akbaital South valley (Figure 2c) and 96M2, Figure S1), s_1 dips steeply \sim SE, whereas s_3 dips moderately to steeply south; s_0 is overturned to the south. There, the SMSZ dips south, with a late, dextral-oblique, brittle-ductile shear fabric. East of the Akbaital South valley (96M10–11, Figure 5e), s_3 in amphibolite and gneiss of the dome is folded by F_4 ; locally, the SMSZ is overturned toward approximately south. Brittle-ductile shear zones in mylonite show top-to- \sim SE flow. Along the transition between the Muskol and Shatput domes and in the Shatput dome, the SMSZ is, in general, subvertical to \sim SW dipping (Figures 2d, 5e, and S2); leucogranite dykes and Fsp + Qtz, Qtz + Bt + Chl \pm Tur (tourmaline) and pure Qtz segregation veins—deformed and undeformed—parallel its \sim NW strike. In the crystalline rocks of the domes (e.g., 0907A–F, 96A6, Figure 5e; and 96M21, Figure S2) and in the SMSZ hanging wall strata (e.g., 96A11, Figure 5e; and 96A5, Figure S2), the main fabric shows dextral shear along mylonitic sz and brittle-ductile faults. Dominant basal $<a>$ slip in Qtz (e.g., 96A11, Figure 5e) supports the regional observation of general low-T ductility along the SMSZ.

3.7.3. Interpretation

Regional mapping of the SMSZ is challenging, as it is often poorly defined by lithologic contrasts, separating marble and Bt-schist of the Sarylshilin suite in its footwall and Jurassic marble and Bt-schist in the hanging wall. Posttectonic annealing with static Cal recrystallization veils earlier high strain fabrics, e.g., rootless Bt-schist boudins in annealed marble. The increase in metamorphic grade from south to north, toward the SMSZ, documented by re/neo-crystallization of $\text{Cal} + \text{Ab} \pm \text{Bt} \pm \text{Scp}$, indicates metamorphic overprint of the SMSZ hanging wall through heat conduction from the rising dome. The posttectonic annealing in the hanging wall and the scarcity of brittle structures in the crystalline rocks of the domes indicate that deformation ceased at least locally under greenschist-facies conditions. The subvertical sections of the SMSZ characteristically have a dextral strike-slip shear component. In particular, the ~NW striking southern boundary of the Shatput dome is a late-stage, dextral strike-slip shear zone. Dykes and veins, subparallel to the boundary, record an earlier extensional component. Along the southern boundary of the Muskol dome, we documented transtensive SMSZ segments; F_4 caused subvertical to overturned $s_{1,3}$ and s_0 . We interpret the SMSZ as a D_3 normal-sense shear zone, interacting with and overprinted by D_4 dextral slip.

3.8. Bozbaital-Pangazdjilga Fold-Thrust Belt: The Hanging Wall of the South Muskol Shear Zone

3.8.1. Overview

The Bozbaital-Pangazdjilga fold-thrust belt stretches ~180 km along strike between the SMSZ in the north and the Murghab-Aksu-Southeast Pamir thrust-wrench belt in the south (Figure 1b). Its equivalent north of the Shatput dome is the Triassic Karasu sliver (Figures 2a, 2d, and 3 and section 2). Shortening occurred during D_1 overprinted by D_4 . Folds dominate over thrusts. The folds and fold nappes show along-strike segmentation: dextral-reverse shear zones connect sinistral oblique thrusts, accommodating ~N-S shortening with subvertical but also significant ~ESE-WNW stretching.

3.8.2. Observations

The hanging wall of the SMSZ comprises Carboniferous to Jurassic strata, unconformably overlain by Cretaceous and likely younger Murghab-basin rocks (section 2 and Figure 2c). South of the central Muskol dome (Akdjilga valley; Figure 2c), an erosional remnant of Murghab-basin rocks forms a cliff; here, the basin strata dip shallowly south on top of folded and steeply dipping Jurassic rocks. The Murgab-basin conglomerate and breccia contain ≤ 50 cm clasts of limestone/marble (some monomict layers), dolomite, basalt, chert, quartzite, foliated Chl phyllite schist, Cal mylonite, and undeformed two-mica granite; the rocks are mostly Cal cemented. Basalt-andesite dykes and at least one lava flow horizon occur in the basin strata as well as in the underlying Triassic-Jurassic strata. Metamorphic minerals are epidote (Ep) + Chl + Cal in the basalts and Cal + Chl + Ser (sericite) in the clastic rocks. The metabasalts yielded ~20 Ma K-Ar and $^{40}\text{Ar}/^{39}\text{Ar}$ whole-rock ages, within uncertainty equal to Ser K-Ar and Zrn fission track ages from the clastic rocks; they are equal to metamorphic formation or cooling ages in the adjacent Triassic-Jurassic rocks [Rutte *et al.*, 2017].

Metamorphism in the Bozbaital-Pangazdjilga fold-thrust belt increases northward, reaching the Bt isograd south of the SMSZ. There, Bt and Scp, locally Ab, and Amp postdate D_1 . Rare D_3 structures strongly hinder the discrimination of D_1 and D_4 , but the D_1 - D_4 structural evolution is characteristically from ductile (e.g., 0828C, Figures 5f and 6v) to brittle. S_0 - s_1 relationships indicate tight to isoclinal, ~N(NW) verging F_1 in the entire sequence; wavelengths reach at least 1 km. Axial planes dip variably but mostly vertically to moderately south with overturned limbs. Layer-parallel shortening structures with conjugate faults and decameter-scale duplexes (e.g., P16 = P37A, Figure 5f) predate F_1 . Jurassic limestone and, rarely, schist developed into mylonites (e.g., 96P3, 96M22, Figure 5f; and 96M24, Figures S2 and 6t). Deformation is localized and strong, indicated by multiple stacks of distinct stratigraphic units and rootless inverted F_1 limbs, producing fold nappes (e.g., sketch of the high strain zone, 96P3, and Akdjilga valley; Figure 5f). In the high-strain zones, mylonites and s_1 are folded by progressive F_2 shortening. Monoclinic Cal LPOs indicate top-to-~N shear (96P3, 96M22, Figure 5f; and 96M24, Figure S2). At lower temperature, and in Triassic Qtz schist, ductile-brittle, scaly sb fabrics developed (Figure 6u). Characteristically, these overall east striking shear zones comprise segments that enclose obtuse angles $\geq 120^\circ$ and have distinct oblique-slip components. Mylonites follow segments that strike ~NE and have a sinistral-shear component (e.g., 96P3, Figure 5f; 96M14–15, 96M17, 96M24, and 96M3, Figure S2); these formed prior to and syn-tectonically with the segments that have a dextral slip component and strike ~SE (e.g., 0828C, 96P3, 96M22, Figure 5f; P15 = P39, 96M17, 96M3, Figure S2). A general feature of deformation in clastic rocks is the development of tension gashes, commonly associated with fibers (Figures 5f, S2, 6w, and 6x). The gashes are associated with reverse faults and form the glide planes in

flexural-slip folds or stretch layers in folds; most were rotated during progressive folding. Conjugate s_2 and s_3 strongly stretched s_0 and s_1 during folding (e.g., station 96P2, Figure 5f); in station 96M24 (Figure S2), foliation boudins occur along conjugate sets of mylonitic s_2 that have s_1 as the bisector.

In contrast to the NMSZ hanging wall, D_3 structures are rare in the SMSZ hanging wall (e.g., 170913M–P, Figure S2). F_4 tightens and refolds the D_1 structures; we observed south vergence at a few stations (e.g., 96M18–19 and 96M22, Figure 5f). Synfolding to postfolding D_4 faults indicate ~N-S shortening; they commonly have a dextral strike-slip component (e.g., P15 = P39, P16 = P37B, Figure 5f; 96M17, 96M3, P34, and 96P1, Figure S2). Tension gashes and fibers also record fold axis parallel, ~E-W extension (e.g., P15 = P39, 96P2, P16 = P37B, Figure 5f; 96M14–16, P37A, and P33, Figure S2); extreme examples are provided by stations 96A9–10 and P30 (Figure 5f) southwest of the Shatput dome, where Triassic-Jurassic schist and pebbly sandstone intruded by Cretaceous granite have pencil structures developed where s_0 and s_1 are at high angles. There, a scaly s_3 fabric is steeply dipping where s_1 dips steeply, and a horizontal s_3 fabric occurs where s_1 is subhorizontal; both s_3 fabrics are accentuated by numerous tension gashes. Extension progressed by faults that grew out of the gashes. Structures, indicating synshortening, ~E-W stretch, are most widespread south of the transition zone between the Muskol and Sarez domes; characteristically, the Akbaital-Rangkul-Kalakdash thrust sheet, the highest tectonic unit of the Central Pamir, is preserved there. Unusual at these stations is the wide variation in the orientation of planar and linear structures; they describe (partial) great circle distributions around ~NE trending axes, locally parallel to open folds. This is also characteristic of the stations southwest of the western Shatput dome (Kalakdash and Guro-Otesch valleys; 11011F–H, Figure 5f; P34, 11010G, and 11011A–E, Figure S2), where ~NNE trending, open folds occur. The eastern limbs of these open folds are steeper than their western limbs; they fold the Akbaital-Rangkul-Kalakdash thrust sheet and its footwall at the kilometer scale.

Structures in the conglomerate-dominated Murghab-basin strata are identical to those in the underlying rocks (Figures 5f and S2). Due to the lack of weak layers, e.g., limestone, mylonites are not present. Ductile flow and crack-seal fracturing [Ramsay, 1980] accommodated strain in the glide planes of the ubiquitous F_1 ; crack-seal tension gashes locally make up 50% of the volume of the extended layers (Figures 6w and 6x). At nine sites of station P37A, we quantified the overall homogeneous stretch in these layers; the average $1 + e = 1.4$. Assuming plane strain, ~30% shortening accounts for this stretch. At four stations in the Murghab-basin strata and three stations in the underlying Triassic rocks, we used up to six separate rock faces to quantify intralayer strain using pebbles (R/ϕ technique). To avoid competence contrasts to the Cal cemented matrix, we used limestone pebbles only (Figures 6y and 6z). Strain is variable but to a first order plane strain and equivalent at all sites (Figure 9); the average strain indicates ~40% intralayer shortening. Whereas the principal shortening axes (Z) occupy a great circle distribution normal to $B_{1,4}$, the principal extension (X) and intermediate strain (Y) directions vary widely between vertical and ~E-W.

3.8.3. Interpretation

The identical ~20 Ma radiometric ages of the metabasalts and the metamorphically grown or reset Bt ($^{40}\text{Ar}/^{39}\text{Ar}$), Ser (K-Ar), and Zrn and Ap (apatite; fission track) in the Murghab-basin and underlying Triassic-Jurassic rocks [Rutte *et al.*, 2017] imply that the basalt ages date metamorphism and not crystallization; there is, so far, no support for Vlasov *et al.*'s [1991] suggestion that the Murghab-basin strata reach into the Neogene. Unconformities below the Cretaceous and below the Jurassic indicate pre-Cenozoic deformation. The pebbles in the Murghab-basin rocks testify to reworking of the underlying Triassic-Jurassic rocks, in particular the Jurassic carbonates. Metamorphic grade in the Bozbaital-Pangazdjilga fold-thrust belt is low except in the hanging wall of the SMSZ, where the Ab, Bt, and Chl porphyroblasts and a rapid increase in grade toward the SMSZ indicate heat conduction from the rising domes. The characteristic D_1 structures are tight-isoclinal folds and fold nappes, with the limbs developing into mylonitic shear zones. The overall structure of these fold and fold nappes shows segmentation in which sinistral-oblique thrusts are connected by dextral-reverse shear zones; these folds and fold nappes south of the Muskol dome form a network that accommodated ~N-S shortening with subvertical and significant ~ESE-WNW stretching. The basal detachment of the folds and thrusts is in the Carboniferous strata, as no deeper unit crops out. Whereas the strain intensity obtained from our pebble and tension-gash data may not be representative of the bulk strain in the Bozbaital-Pangazdjilga fold-thrust belt due to the large lithologic variation and the strain concentration in incompetent rocks (e.g., limestone mylonites), the orientation of the principal strain axes may be characteristic. The pebble data indicate ~N-S shortening with rotation of s_0 and s_1 (X - Y planes of the strain ellipsoid;

Figure 9) during folding ($F_{1,2,4}$). We interpret the great variability of the X and Y strain axes as indicating interaction between thickening and fold-axis parallel stretching, the latter emphasizing the \sim E-W extension that we observed during all phases of deformation. Sets of dextral and sinistral strike-slip faults—postdating $F_{1,2}$ —indicate that the overall deformation geometry did not change significantly during D_4 .

The relative timing of the along-strike extension is difficult to determine, because B_1 (folding s_0), B_2 (folding s_1 and D_1 high strain fabrics), and B_4 (tightening F_1 and F_2) are parallel. We associate most of the tension gashes and the overall fold-axis parallel extension to D_2 , because the gashes are folded with s_1 and lie along great circle distributions. South of the Muskol-Shatput transition, the sb fabrics and faults that indicate \sim E-W extension are mostly D_4 , as they cut across all structures. The \sim NE trending, open folds in the same area spatially correlate to a change in regional strike from \sim W to \sim NW; the latter is the overall strike along the southern margin of the Shatput dome. We interpret these open folds as related to the \sim E-W extension in the Aksu region; they likely represent culmination and trough axes (swells and pinches) along $F_{2,4}$, indicating bulk along-strike extension coeval with \sim N-S shortening. Their occurrence coincides with the largest kilometer-scale trough (pinch) along the domes—the transition from the Muskol to the Shatput dome.

3.9. Kalaktash and Kozyndy Klippen and the Akbaital-Rangkul-Kalaktash Thrust Sheet

3.9.1. Overview

South of the Muskol-Shatput dome transition and south of the Shatput dome, *Yushin et al.* [1964] mapped a dozen isolated occurrences of Cambro-Ordovician to Devonian strata in contact with Triassic units (Figures 2a and 2d and 3). A rich detrital plant flora in the Triassic and brachiopods and trilobites in the Paleozoic strata solidly define the local stratigraphy [*Dronov et al.*, 2006]. We classify the Paleozoic strata as the Kalaktash-Kozyndy klippen, tectonically emplaced onto the Triassic rocks, and link them with rocks of identical lithology, fauna, and metamorphism in the Akbaital-Rangkul imbrications and at the top of the Tuzguny-Terezki thrust sheet; we combine these units into the dome-spanning Akbaital-Rangkul-Kalaktash thrust sheet.

3.9.2. Observations

We mapped the area south of the Muskol-Shatput dome transition to understand the structural relationships between the Triassic and the early Paleozoic units. In the Kjukjurt (Figure 2c) and Kalaktash (Figure 2d) valleys, steeply dipping faults separate the Paleozoic and Triassic strata. In the Kjukjurt valley, a \sim SW vergent, open anticline exposes Silurian and Triassic-Jurassic strata. The latter have tight, \sim SW vergent folds and are cut by folded reverse faults and a steep foliation (96M18-19, Figure 5f); the faults displace the Silurian southward onto the younger strata. Local Qtz and pyrite-rich Silurian phyllite shows dominant basal $\langle a \rangle$ slip in Qtz (LPO of 96M18b, Figure 5f) with top-to- \sim S flow. In the upper Guro-Otesch valley (Figure 2d; 11010G–11011E, Figure S2), a ridge exposes an anticline that folds a low-angle contact that places lower Paleozoic onto Triassic strata. The Cambro-Ordovician rocks host approximately east trending $F_{1,2}$ with a wavelength of \sim 1 km, similar to those observed in the Bozbaital-Pangazdjilga fold-thrust belt, and younger, open, east vergent folds (11011F–H, Figure 5f; 11010G, and 11011A–E, Figure S2). Low-angle thrusts imbricate the Cambro-Ordovician units and high-angle reverse faults cut the folded strata. At the outlet of the Akdjilga into the Pshart valley (Figure 2c), *Yushin et al.* [1964] and *Vlasov et al.* [1991] show a tectonic sliver of trilobite-bearing Cambrian limestone, imbricated with Murghab-basin rocks. All these Cambrian to Devonian strata south of the domes have lithologies and fauna identical to the lower Paleozoic units cropping out in the Akbaital-Rangkul imbrications north of the domes; consequently, *Yushin et al.* [1964], *Vlasov et al.* [1991], and *Dronov et al.* [2006] ascribed them to the same suites (Figures 2a and 3).

3.9.3. Interpretation

We interpret the high-angle faults in the Kalaktash and the Kjukjurt valleys as D_4 reverse faults, similar to faults observed elsewhere in the Bozbaital-Pangazdjilga fold-thrust belt (e.g., P16 = P37B, P38, and 96M8 (Figure 5f), and P37A, Figure S2). We identify the regional low-angle contact between the lower Paleozoic and the underlying Triassic strata south of the domes as the sole thrust of a large thrust sheet (orange fault contact in Figures 2a, 2c, and 2d). Identical lithologies, fauna, and low-grade metamorphism link these klippen with the Akbaital-Rangkul imbrications north of the Muskol dome, constituting the Akbaital-Rangkul-Kalaktash thrust sheet. We include the klippe of Cambro-Ordovician rocks ($Cm+O_1zr$ and O_2+3kz ; Figures 2c and 3; section 3.6), which rests on top of Cambro-Ordovician units of the Tuzguny-Terezki thrust sheet, and the horse of Cambrian limestone in the Akdjilga valley within this thrust sheet. The Upper Cretaceous strata within the thrust sheet (in the Akbaital-Rangkul imbrications) and the Maastrichtian to likely

Paleogene Murghab-basin rocks in its footwall constrain the maximum emplacement age as Paleogene. The offset by the NMSZ and SMSZ defines the minimum emplacement age, i.e., 22 Ma [Rutte *et al.*, 2017].

In an alternative interpretation, the contacts between the lower Paleozoic and Triassic units may constitute a faulted and folded high-angle unconformity. Two arguments speak against this interpretation: (1) In the southeast Pamir, the well-exposed Cimmerian unconformity—related to the closure of the Rushan-Pshart basin—lies between the Upper Triassic and Lower Jurassic (e.g., SW corner of Figure 2d) [Dronov *et al.*, 2006; Angiolini *et al.*, 2015] and not below the Triassic strata. (2) Less than 10 km to the north and east of the Kjukjurt and Kalaktash valleys, and ~30 km to the west, the Upper Triassic strata are underlain by >1500 m thick Carboniferous strata, with a disconformity only in the Permian [Yushin *et al.*, 1964].

We correlate the emplacement of the Akbaital-Rangkul-Kalaktash thrust sheet with $D_{1,2}$. Although structural evidence does not definitively constrain its emplacement sense, the underlying top-to-~N Bozbaital-Pangazdjilga fold-thrust belt and the overall northward progression of the deformation in the Pamir favor northward emplacement. The horse of Cambrian limestone at the lower Akdjilga valley—just north of the Rushan-Pshart suture—marks the southernmost outcrop of the Akbaital-Rangkul-Kalaktash thrust sheet; it may define its root zone, imbricated with rocks of the Bozbaital-Pangazdjilga fold-thrust belt along D_4 faults. We interpret the complex structure in the Kjukjurt valley to result from D_1 and D_4 superposition: F_1 , with unusual ~SW vergence (possible due to F_4 rotation), were overprinted by neocrystallized Bt as part of the static annealing along the southern margin of the Muskol dome. D_4 faults with a dextral component imbricated the Silurian and Triassic-Jurassic strata and built the large anticline (96M18–19, Figure 5f). This D_4 zone may continue in the Akbaital South and Karataash valleys (Figure 2c) along the vertical to southward overturned section of the SMSZ with a dextral oblique-slip shear component (section 3.7; 96M13, Figure 5e; 96M14–16, 96M2, and 96M3, Figure S2). The atypical south vergence of these D_4 structures fits into a regional ~ESE trending zone, here called the Trans-Muskol transpressional back thrust zone (Figure 2a, insert bottom left). It connects the south vergent D_4 structures of the Karataash-Kjukjurt valley area with the Akbaital imbrications and possibly the backthrusts along the reactivated Tanyamas suture farther northwest. Farther east, north of the Aksu river, the Trans-Muskol transpressional back thrust zone interacted with the Murghab-Aksu-Southeast Pamir thrust-wrench belt (section 3.10), as manifested by backthrusts to its north (96A3 (Figure 2d) and S2). On an even larger scale, this zone may extend into the southern Kozyndy klippen and may include backthrusts north of the eastern Rushan-Pshart suture (4725B, Figure 2a). The ~NW trending, en échelon arrangement of these back thrust belts implies a dextral strike-slip component (highlighted in inset bottom left of Figure 2a).

3.10. Murghab-Aksu-Southeast Pamir Thrust-Wrench Belt

3.10.1. Overview

The Murghab-Aksu-Southeast Pamir thrust-wrench belt deforms the West and East Pshart blocks and the northern southeast Pamir; its frontal structures are the Pshart thrust system and the East Pamir fault zone, approximately tracing the Rushan-Pshart suture (Figures 1b; 2a, inserts bottom; and 3). The Pshart-blocks and Aksu duplexes constitute a part of the thrust-wrench belt with a strong strike-slip component. The Murghab-Aksu-Southeast Pamir thrust-wrench belt accommodated ~N-S shortening and dextral wrenching. Active faults in the southeast Pamir, collectively known as the Aksu-Murghab strike-slip fault zone, root in the Karakorum fault zone of western Tibet and are linked kinematically to top-to-~N thrusts [e.g., Ruzhentsev, 1990; Strecker *et al.*, 1995; Schurr *et al.*, 2014].

3.10.2. Observations

The leading edge of the Murghab-Aksu-Southeast Pamir thrust-wrench belt is a broad deformation zone that encompasses the Pshart blocks and the Pshart thrust system (Figures 2c and 2d). Along section 96P4 (Figure 5g), Qtz-rich ultramylonite, derived from Pshart-block Triassic-Jurassic granite, is bound to the north by tectonic breccia and cataclasite with Cal marble (98%), dolomite, Qtz vein, and ultramylonite fragments, that transitions into faulted red-bed clastics of the Murghab basin. Mylonite in Cretaceous limestone below the Murghab-basin rocks to the north shows pure thrust kinematics. The Qtz ultramylonite marks a dextral strike-slip zone; the Qtz LPO implies dominant basal and rhomb <a> slip. The breccia-cataclasite and the Murghab-basin strata show ~NW-SE shortening along conjugate faults, with the dextral strike-slip set more prevalent. The eastern continuation of the leading edge of the Murghab-Aksu-Southeast Pamir thrust-wrench belt across the alluvium of the southern Akdjilga valley contains the exotic

sliver of Cambrian limestone (section 3.9). Farther east, the leading fault traces the topography along the southern margin of the Murghab basin, indicating intermediate south dip (Figure 2c). Stations A96M18–19 and 96A1–3 (Figures 2c and 2d, 5g, and S2) trace dextral wrenching eastward. A96M18–19 shows contact metamorphic rocks north of Triassic granite with Ser + Chl ± Bt ± Ms ± Grt ± St schist, and a mélange of Triassic cherty limestone, dolomite, metabasalt, and calcschist. Brittle-ductile s-c mylonite developed out of Qtz veins; newly grown Ser and chloritized Bt occur along sb. The Qtz LPO is compatible with prism and rhomb $\langle a \rangle$ slip. In calcschist and limestone, sz and faults are brittle-ductile to cataclastic; chocolate-tablet boudins are present. The foliation, a spaced cleavage overprinting older ductile fabrics, dips steeply south. Qtz-rich layers outline isoclinal, asymmetric folds.

Stations 96A1–3 encompass a profile from Triassic granite northward through Triassic clastic rocks to the leading edge of the Murghab-Aksu-Southeast Pamir thrust-wrench belt (the Pshart thrust system; Figures 2d, 5g, and S2). The weakly deformed granite has a decimeter to meter spaced cleavage with northward increasing deformation; the clastic rocks have local mylonite in quartzite, calcschist, and limestone. Tight-isoclinal F_2 fold s_1 ; one Cal mylonite is folded isoclinally into a-type folds. Sz and sb are dominantly dextral, strike (N)W, and are overprinted by brittle-ductile to cataclastic faults, formed in the same kinematic framework. Well-foliated and layered rocks have kinks and asymmetric folds on all scales, again recording dextral shear. The Qtz LPO in quartzite is nearly orthorhombic with basal $\langle a \rangle$ slip prevailing (96A2, Figure S2). The Cal LPOs, measured at two locations in the same Cal mylonite (96A2; Figures 5, S2, and 6a and 6b), are also orthorhombic. Mélange forms the boundary to the Murghab-basin rocks: Cal mylonite, dolomite, and phyllite breccia are stratified parallel to the boundary.

In the Karadjilga valley, which cuts the Pshart blocks south of the upper Pshart valley, sinistral and normal faults partly reactivated s_0 and s_1 (1106A–C, Figures 2c and S2); strike is anomalously ~NE. Thrusts imbricate the West and East Pshart-block rocks and involve Upper Cretaceous strata, implying Cenozoic deformation. These thrusts merge with the general east trending leading edge of the Murghab-Aksu-Southeast Pamir thrust-wrench belt and a similarly east striking, top-to-~N thrust to the south (Figures 2a and 2c). This structure constitutes the Pshart-block duplex (see section 3.10.3.). Farther east is a similar structure—the Aksu duplex (Figure 2a). The latter has tight to isoclinal, partly northwesterly overturned, ~NE trending folds in its western part. These folds initiated before the Jurassic, as they are overlain by the Cimmerian unconformity. Open to tight folds within the Jurassic and locally within Upper Cretaceous–?Paleogene strata above the unconformity show that Cenozoic shortening tightened the older folds. This fold belt changes to an eastward trend farther east. The Aksu fault cuts this fold belt (including a few thrusts) to its south (Figures 2a and 2d). It branches off the Aksu-Murghab fault zone in the west, constitutes an out-of-syncline thrust within Jurassic strata farther east, cuts obliquely ($\leq 30^\circ$) across the pre-Jurassic folds, and imbricates and thrusts Triassic onto Jurassic strata. At 96A4 (Figures 2d and 5g), the principal slip surface of the Aksu fault dips steeply south, reactivated the local s_0 in a syncline of red sandstone, and constitutes a mélange zone, mixing sandstone, basalt, and yellow dolomite, likely all Triassic; it is accompanied by numerous subparallel faults with pure dextral strike-slip kinematics. Folds in the Jurassic limestone just north of the Aksu fault, are mostly open and north vergent. Tension gashes and fractures reflect ~ENE-WSW, along-strike and vertical extension. Two fault sets formed postfolding; the younger conjugate strike-slip fault set has a tensional component with accompanying fractures and gashes and breccia-bearing faults, implying along-strike extension. P35 (Figures 2d and S2) characterizes one of the faulted folds within the Aksu duplex where openly folded Jurassic limestone is in fault contact with ~170 Ma (U-Pb Zrn) granite. The fold hinge shows crest and troughs. Abundant tension gashes and an older conjugate strike-slip fault set emphasize ~E-W, fold axis-parallel stretch. Postfolding ~N-S shortening activated s_0 along dextral-oblique thrusts. 96M8 (Figures 2d and S2), along the southern boundary of the Aksu duplex, at the very western end of the Aksu basin in Jurassic limestone shows dextral strike-slip faults.

Stations P21–22 record the near-field deformation along the western Aksu fault in the Murghab valley (Figures 2a and S2). P21, within contact metamorphosed, penetratively foliated gneiss and marble in the aureole of a ~119 Ma (U-Pb Zrn) granite, and P22, within Permian quartzite, lie in the southern East Pshart block north of the Aksu fault. The marble flowed ductilely and is isoclinally folded—as is the quartzite—indicating early ~N-S shortening. In P21, an early Chl-coated fault set reactivated s_1 sinistrally, suppressing a weakly developed dextral fault set; in contrast, at P22, Qtz-coated faults reactivated s_0 dextrally. At both stations, younger faults cut through the older structures along conjugate sets, with the dextral, ~NW-striking set outlining the principal fault. Cimmerian deformation is preserved southwest of the Aksu-Murghab fault zone, in the westernmost

Murghab-Aksu-Southeast Pamir thrust-wrench belt, here called the Peak Sarez region (Figure 2a, insert bottom left). There, the pre-Jurassic folds trend ~N(E); these folds are refolded by younger, likely Cenozoic, east trending folds, that locally form dome-and-basin (type 1) interference patterns [Ramsay, 1967]. The Cimmerian fold trends become progressively more easterly and the overprinting folds become more pervasive toward the Aksu-Murghab fault zone. P24–25 (Figures 2a, 5g, and S2) characterize the near field of the latter along the southwestern margin of the Pshart-block duplex. The Jurassic limestone/marble at P24 deformed in ductile-brittle fashion along a steeply ~SSW dipping foliation and a subhorizontal str, with dextral shear documented by sb and af. Crack-seal boundinaged Fe-carbonate layers with Cal flowing ductilely and the Fe-carbonate fracturing outline the principal stretch direction. The dextral and normal faults are partly active [Strecker *et al.*, 1995]. Faults in the ~100 Ma (U-Pb Zrn) granite of P25 are brittle-ductile (Chl coated) and ~NW striking, identical to those in P24. The southern far field of the Aksu-Murghab fault zone (station 96M27; Figures 2a and S2) is also characterized by dextral transpressional faulting.

Stations 4723C and 4725B characterize the East Pamir fault zone in the Dunkeldik valley (Figures 2d and 5g). 4723C, in the upper valley and in the far field of the fault, shows a complex fault and tension-fracture fabric, which was measured over a considerable area. The structures indicate bulk (N)E-(S)W extension; an alkali basalt dyke (most of the basalts are ~11 Ma pipes that contain lower crustal xenoliths [Hacker *et al.*, 2005]) strikes ~NW, subparallel to the major set of tension fractures. The range front fault—studied in ~77 Ma (U-Pb Zrn) granite—is a thick cataclasite that likely outlines a dextral fault zone (Figure 5g). Strecker *et al.* [1995] described the active Karasu fault zone at a few sites; we studied a more easterly strand (96A7; Figures 2a, 5g, 6ac, and 6ad) that comprises a cataclastic mélangé zone between limestone-dolomite and shale with up to 3 m thick Cal veins that include the host reddish limestone as clasts. The fault core is ~1 m thick black gouge. Triassic shale, thrust onto Jurassic limestone that was flexed downward into an anticline, indicates a top-to-~SSE dextral-oblique slip component. P26 and P36 characterize strands of the seismically active Aksu-Murghab fault zone (Figures 2a and S2). In accordance with the few available fault plane solutions [Schurr *et al.*, 2014], we found dextral strike-slip and normal faults with ~N-S shortening and ~E-W extension, overprinting older thrusts.

3.10.3. Interpretation

The near and far field of the Rushan-Pshart suture zone was reactivated as a regional thrust and dextral wrench zone (Figure 2a). The kilometer-scale features include the Pshart-block and Aksu duplexes and the Aksu basin, which are interpreted as transpressional strike-slip duplexes and a transtensional basin, respectively. Characteristically, the duplex internal structures appear to have been rotated against the overall dextral transpressional shear (Figure 2a); where studied, the duplexes are bounded by dextral shear zones. South of the Pshart and Aksu duplexes, from the Aksu fault in the north to the broad belt that marks the seismically active Aksu-Murghab fault zone in the south, folding, fold-axis parallel extension, and distributed dextral strike-slip faulting accommodated ~N-S shortening. Characteristically, the folds in this zone bend sigmoidally into the East Pamir fault zone that parallels the strike of the units south of the eastern Shatput dome (Figure 2a). The Murghab-Aksu thrust-wrench belt narrows westward into the dextral transpressional fold-thrust belt around Lake Sarez and widens again farther west, encompassing the Rushan-Bartang-Sarez belt (Figure 1b) [Stübner *et al.*, 2013a; Schurr *et al.*, 2014].

In detail, we interpret the leading edge of the Murghab-Aksu-Southeast Pamir thrust-wrench belt in the upper Pshart valley to record progressive deformation along a dextral shear zone that has ductile rocks—the Qtz ultramylonite—in the south, and Murghab-basin strata in the north, which also record thrust shortening. The footwall Cal mylonite shows the typical Bozbaital-Pangazdjilga fold-thrust belt kinematics and likely relates to D_{1,2}. All sections of the leading edge of the Murghab-Aksu-Southeast Pamir thrust-wrench belt in the eastern part of the Pshart valley suggest thrusting of the Pshart-block onto the Murghab-basin rocks. The apparently high-T prism <a> slip in the low-T mylonite A96M18 may arise from hydrous flow conditions; the sample stems from a mylonitized Qtz vein. The Aksu fault and its western continuation, the Aksu-Murghab fault system, record dextral transpression along the southern margins of the Pshart and Aksu duplexes. The observed structures imply along-strike extension in addition to ~N-S shortening: fold hinges show crest and troughs, abundant tension gashes and conjugate strike-slip fault sets emphasize that ~E-W, fold-axis parallel stretch, locally exceeded the vertical stretch. Cenozoic east trending folds overprinted pre-Jurassic folds southwest of the Aksu-Murghab fault zone—most clearly in the Peak Sarez region (Figure 2a). Progressive bending of these Cimmerian folds into the Aksu-Murghab fault zone indicates a

Table 1. Estimates of Shortening Across the Central Pamir

Thrust Sheet/Structure	Overthrust Distance	Internal Shortening
Akbaital-Rangkul-Kalaktash	>30 km (section A)	>14 km (>47%)
Bozbaital-Pangazdjilga-Karasu	>19 km (section C)	9 km (47%; section A)
Muskol and Shatput domes		>20 km (Figure 7; Gurumdy)
Akbaital imbrications	3 km (section A)	
		total: >95 km shortening

broad zone of dextral shear. The poorly exposed East Pamir fault is a thick cataclastic zone with dextral shear and, possibly, a transtensional component. We interpret the Quaternary Aksu basin as a pull-apart basin between the Aksu, Karasu, and East Pamir faults. Radiometric ages out of the deformation zones of the Murghab-Aksu-Southeast Pamir thrust-wrench belt imply late Miocene activity [Rutte *et al.*, 2017]; this emphasizes its out-of-sequence nature, formed mainly during D_4 , after the emplacement of the major fold-thrust belts of the Central Pamir and the exhumation of the domes.

4. Cross Sections and Shortening Estimates

Figure 8 integrates lithology, stratigraphy, strata thickness, and the new structural data (Figures 2, 3, 5, and S2) into three sections across the eastern Central Pamir. They run ~N-S (Figure 2a), perpendicular to B_{1-4} and parallel to str_3 . The depicted fold shapes mimic the field observations; parallel folds are characteristic for the low-grade Akbaital-Rangkul-Kalaktash thrust sheet, whereas similar folds are typical of the higher grade and incompetent strata of the Bozbaital-Pangazdjilga fold-thrust belt and the crystalline rocks of the domes. The sections depict ~N-S displacements and neglect strike-slip flow out of the cross-section planes, which—albeit significant (section 3)—does not disturb the illustration of the first-order thrust-fold geometries.

Sections A and B show the Murghab-Aksu-Southeast Pamir thrust-wrench belt in the south. The structural contacts in the Pshart-block duplex (section A) are from Leven [1995]. Tightly folded Permian and Triassic strata below the Cimmerian unconformity oppose open to tight folds in the hanging Jurassic rocks (section B); reverse and dextral strike-slip faults cut the entire stratigraphic sequence. The internal imbrications and the leading and rear thrusts are top-to-~N. Imbricated and deformed Upper Cretaceous rocks demonstrate that a significant amount of the deformation is Cenozoic. The root zone of the Akbaital-Rangkul-Kalaktash thrust sheet is sketched in sections A and B with the inferred thickness of the entire Phanerozoic section in this sheet (~7 km; Figure 3); the root zone is cut out by the leading edge of the Murghab-Aksu-Southeast Pamir thrust-wrench belt.

The fold geometries in the Bozbaital-Pangazdjilga fold-thrust belt south of the domes are those of the upper Paleozoic to Mesozoic strata along section A—the best outcropping section of this belt. The décollement at the base of the Carboniferous strata requires the imbrication of the Ediacaran-Cambrian to Devonian strata in the footwall of the Bozbaital-Pangazdjilga fold-thrust belt (schematically shown in section A). Equivalent imbricates constitute the fold nappes of the crystalline rocks of the Muskol and Shatput domes (section 3.3). In sections A and B, the lower Paleozoic strata of the Akbaital-Rangkul-Kalaktash thrust sheet overthrust Triassic, Jurassic, and locally Cretaceous-?Paleogene (Murghab basin) rocks, implying pre-Cenozoic erosion/relief. This thrust sheet crops out most extensively along section B (Kalaktash klippen); in sections A and C, the location of its sole thrust is hypothetical. The schematic imbricates in section B mimic the deformation required by the tight folds with ~1 km wavelengths in the underlying Bozbaital-Pangazdjilga fold-thrust belt. The three major décollements of the eastern Central Pamir are in (i) Ediacaran strata where they form the base of the fold nappes in the domes, (ii) Cambro-Ordovician strata at the base of the Akbaital-Rangkul-Kalaktash thrust sheet, and (iii) Carboniferous strata at the base of the Bozbaital-Pangazdjilga-Karasu thrust sheet (sections A and B). In the Muztaghata dome, the Central Pamir affine rocks are preserved as the Muztaghata and Shen-Ti klippen; there, these Ordovician rocks overthrust the North Pamir Karakul-Mazar belt rocks (shown schematically in section C [Robinson *et al.*, 2012]).

In the Gurumdy valley (Figures 2b, 4a and 4b, 7, and 8, section A), the Muskol dome is a large open antiform with the dome axis close to its southern margin. The dating of these suites (U-Pb Zrn ages; Figures 3 and S1) and regional mapping imply that they form a recumbent isoclinal fold nappe with the Ediacaran-Ordovician

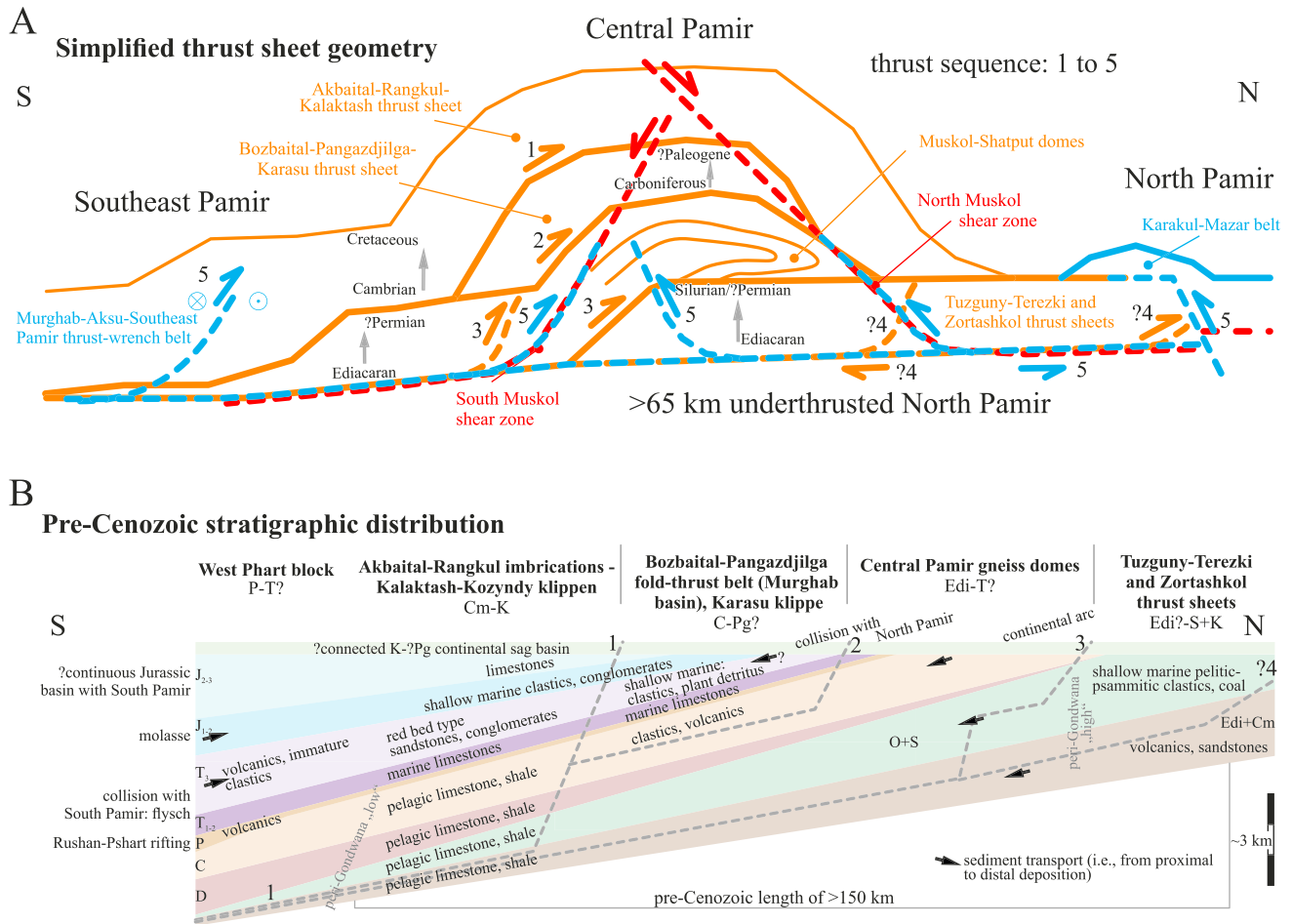


Figure 10. (a) D_1 (orange) thrust-sheet geometry with stratigraphic range of the eastern Central Pamir, synthesized from Figures 7 and 8. The central antiformal stack formed before ~22 Ma, i.e., before normal shear along the North and South Muskol shear zones (red). The lowermost imbricate, outcropping in the Muskol dome, has a fold-nappe geometry. The North Pamir, i.e., the Karakul-Mazar belt, was underthrust beneath this stack by at least 65 km. The blue lines visualize the re-activation of the Central Pamir by divergent thrusting-folding, postdating the normal shear. (b) Pre-Cenozoic distribution of stratigraphic units of the Central Pamir based on retrodeformation of the thrust sheets in Figure 10a. Thickness variations and generalized lithologies are from Figure 3. Isolated erosional remnants of marine and continental Cretaceous-?Paleogene strata in the South, Central, and southern North Pamir may indicate a continuous basin, overlying pre-Cretaceous relief.

paragneiss-metavolcanic rock-dominated Beletuin suite in its core and the Ordovician/Silurian-Permian marble-metapelite Sarylshilin suite along the northern and southern dome margins (Figure 7); the NMSZ thinned the Sarylshilin suite along the upright northern limb of the dome-spanning fold. Figure 7 shows the along-strike variation of the internal structure in the Muskol dome from the western Sasaksu to the eastern Akbaital South valleys; the fold nappe dies out and/or recedes southward toward the east.

In the Akbaital imbrications (Figure 8, section A), the normal-slip Akbaital fault separates Mesozoic strata in the south from mostly Paleozoic strata in the north. South-vergent folds indicate top-to-~S reverse-slip reactivation of the NMSZ (sections A and B). The fold-thrust geometries result from the top-to-~N emplacement of the Akbaital imbrications as part of the Akbaital-Rangkul-Kalaktash thrust sheet, ~N-S extension in the wide normal-fault belt north of the NMSZ (Rangkul imbrications, section B), and reactivation by top-to-~S folding-thrusting, affecting the Karakul-Mazar belt, Tuzguny-Terezki and Zortashkol thrust sheets, Akbaital imbrications, and NMSZ. Backthrusts that propagated even farther south (partly as blind thrusts) may be responsible for the Trans-Muskol transpressional back thrust zone (Figure 2a), with local overturning of the SMSZ, and late top-to-~S thrusting in the Bozbaital-Pangazdjilga fold-thrust belt, e.g., the cut-out of the root zone of the Akbaital-Rangkul-Kalaktash thrust sheet shown schematically in section B. The Tuzguny-Terezki thrust sheet is unconformably overlain by Cretaceous strata (Figures 2 and 8, section A), implying Mesozoic exhumation. In the Cenozoic, it was thrust southward onto the Akbaital-Rangkul

imbrications, and in turn overthrust by the Karakul-Mazar belt in the north (sections A to C). Cretaceous to? Paleogene deposits, similar to those covering the Tuzguny-Terezki and Zortashkol thrust sheets, line the footwalls of these top-to- \sim S backthrusts. In section B, the Karakul-Mazar belt was thrust >12 km over the Tuzguny-Terezki sheet along a low-angle fault; its activity may have been Permian to Jurassic (probably Triassic), purely Cenozoic, or Triassic with Cenozoic reactivation. We favor the purely Cenozoic scenario, as Permo-Triassic southward subduction along the Tanyamas suture calls for top-to- \sim N imbrication in the trench deposits of the Karakul-Mazar belt.

We estimated shortening by line-length balancing along the sections in Figures 7 and 8 and by measuring minimum overthrust distances in Figure 2 (Table 1). These estimates are minima and do not account for internal strain (see strain data; Figure 9). All units are fault-bounded; thus, undeformed pin lines do not exist. The overthrust distances of the Akbaital-Rangkul-Kalaktash and Bozbaital-Pangazdjilga-Karasu thrust sheet are >30 and >19 km, respectively, measured along sections A and C. Internal shortening in the Bozbaital-Pangazdjilga fold-thrust belt was estimated in section A, using the contact between the Triassic-Jurassic strata south of the Muskol dome. The contact is ~ 20 km long over a present distance of ~ 11.5 km, indicating ~ 8.5 km or $\sim 43\%$ shortening; this agrees with $\sim 47\%$ shortening determined along a short, but well-mapped section across the southern Murgab basin (Figure 9). Including the entire N-S extent of the Bozbaital-Pangazdjilga fold-thrust belt, its ~ 19 km of overthrust distance indicates a total internal shortening of ~ 9 km (D_{1-4}). We did not estimate the $D_{1,2}$ internal shortening of the Akbaital-Rangkul-Kalaktash thrust sheet due to insufficient exposure. Instead, we use the internal shortening of the underlying Bozbaital-Pangazdjilga-Karasu thrust sheet; that yields a value of >14 km for the ~ 30 km N-S range of this sheet given by its overthrust distance. The fold nappe in the Muskol dome (Gurumdy and Sasaksu valleys; Figure 7) records >20 km shortening. The northern Akbaital imbrications and the southernmost Cenozoic thrust in the Tuzguny-Terezki thrust sheet host >3 km of shortening without the possibility of quantifying the shortening by folding (section A). The total \sim N-S shortening in the present-day ≤ 50 km wide eastern Central Pamir (excluding the Tuzguny-Terezki and Zortashkol thrust sheets) is thus >95 km ($>66\%$, excluding rock-internal shortening, assessed only locally; Table 1). The predominate, initial N-S extent of the eastern Central Pamir was at least 150 km.

We estimated the extension along the NMSZ and the SMSZ from the metamorphic field gradient (vertical offset, given by $625\text{--}725^\circ\text{C}$ [Schmidt *et al.*, 2011; Stearns *et al.*, 2015] in the footwalls (dome interiors) and $200\text{--}300^\circ\text{C}$ and $300\text{--}350^\circ\text{C}$ in the hanging walls of the NMSZ and SMSZ, respectively, as provided by geothermochronometers [Rutte *et al.*, 2017] and the dip of the shear zones. Along the NMSZ, 5–20 km of throw, and dips between $25\text{--}40^\circ$, suggest 5 to 43 km of \sim N-S extension. Along the SMSZ, 5–15 km of throw, and a virtually unknown initial dip of 25 to 50° , suggest 4 to 32 km of \sim N-S extension. A realistic minimum value for extension across the domes is ~ 17 km, given the petrologically determined exhumation from ~ 30 km depth and an assumed 45° shear-zone dip; the maximum value is ~ 75 km. Both values may increase due to the stretch in the hanging wall of the NMSZ.

5. Discussion

As our understanding about how the thick Asian crust of the Pamir-Tibetan Plateau has been built is incomplete, the main aim in part 1 of this paper series—the structural study—is the description of the geometry, kinematics, and amount of deformation. In the following, we discuss the evolutionary stages, their implications for the formation of the Pamir-Tibetan Plateau, the possible drivers for large-scale syn-convergent extension, and the role of lateral extrusion, i.e., material transport from the Plateau into its western foreland. Although deformation is a key to understanding the involved orogenic processes, only the timing and the deduction of the involved rates—reported in part 2 [Rutte *et al.*, 2017]—allow drawing links between crustal deformation and the underlying mantle processes. Thus, in the following discussion, we focus on the implications of the structural data on the architecture of the Pamir and outline potential evolutionary scenarios. We use the full deformation-time data set to link the crust and mantle evolution over the Cenozoic India-Asia collisional history in part 2 [Rutte *et al.*, 2017].

5.1. Crustal Stacking in the Central Pamir

Thrust and fold-nappe tectonics built the thick Asian crust of the Central Pamir (sections 3 and 4). Figure 10a synthesizes the structural architecture as an antiformal stack. In-sequence, top-to- \sim N imbrication started with the emplacement of the Akbaital-Rangkul-Kalaktash thrust sheet, which includes the full Phanerozoic

stratigraphic sequence (Akbaital imbrications). The in-sequence Bozbaital-Pangazdjilga-Karasu thrust sheet cut out the Carboniferous to Cretaceous-Paleogene stratigraphic section, forming a horse with the sole thrust of the Akbaital-Rangkul-Kalaktash thrust sheet as its roof thrust, and its sole thrust within the Carboniferous clastic rocks. The remaining lower Paleozoic section likely was stacked in fold nappes below the Bozbaital-Pangazdjilga-Karasu thrust sheet. We speculate that the Tuzguny-Terezki and Zortashkol thrust sheets formed in sequence and constituted the leading edge below and in front of the Central Pamir thrust stack. We place the sole thrust to this Paleogene stack along the re-activated, south dipping Tanyamas suture (part 2 for timing; [Rutte *et al.*, 2017]). In Figure 10a, the NMSZ and SMSZ traces indicate where the post ~22 Ma extension cut this nappe stack, exhuming the deepest imbricates exposed in the Muskol and Shatput domes.

Figure 10b shows a reconstruction of the pre-Cenozoic upper crustal structure with the four major thrust sheets and the West Pshart block arranged in their prestacking order together with the three major décollements. The thickness variations and proximal-distal deposition relations are from Figure 3; they define the probable sediment transport directions. The shortening estimates indicate that the pre-Cenozoic N-S extent of the Central Pamir was >150 km. Over this distance, the early Paleozoic depositional facies changed from the volcanoclastic rocks of the Tuzguny-Terezki and Zortashkol thrust sheets in the north to the pelagic sedimentary rocks of the Akbaital-Rangkul-Kalaktash thrust sheet in the south. In the Carboniferous, the difference between the proximal volcanoclastic sequence of the Bozbaital-Pangazdjilga-Karasu thrust sheet in the north and the distal pelagic sedimentary rocks in the Akbaital-Rangkul-Kalaktash thrust sheet in the south point to the volcanic arc that existed along the northern margin of the Central Pamir (related to the Tanyamas suture [Schwab *et al.*, 2004]) and shed sediments southwards. Thus, in contrast to the current northerly position of the Akbaital-Rangkul imbrications, their Carboniferous position likely was south of the Bozbaital-Pangazdjilga-Karasu thrust sheet. The Permo-Triassic collision of the Central and North Pamir uplifted the northern section of the Central Pamir, in particular the northernmost Tuzguny-Terezki and Zortashkol thrust sheets, and eroded it down to the Silurian, while sedimentation continued farther south. We speculate that the depositional facies of the Central Pamir gneiss-dome rocks is transitional, with the lower suites being equivalents of the Tuzguny-Terezki and Zortashkol thrust-sheet rocks; the higher suites include Carboniferous to Permo-Triassic rocks, resembling the more southerly rocks of the Bozbaital-Pangazdjilga thrust sheet (Figure 3).

The ~66% Cenozoic shortening of the 7–10 km Central Pamir Ediacaran-Phanerozoic sedimentary sequence implies tripling of the upper crust of the Central Pamir. This shortening agrees with the burial of these units to depths of ~30 km during the Paleogene, traced by petrology and geochronology of the rocks of the domes [Schmidt *et al.*, 2011; Stearns *et al.*, 2013, 2015; Smit *et al.*, 2014]. Assuming a pre-Cenozoic >30 km thick crust for the Central Pamir, its thickness at ~22 Ma may have exceeded 90 km.

What lies below the Ediacaran-Phanerozoic upper crustal sequence of the Central Pamir? The Muztaghata dome of the Chinese Pamir [Robinson *et al.*, 2012] and the southward subduction polarity of the Triassic Tanyamas suture [Schwab *et al.*, 2004] provide an answer. In the Muztaghata dome, rocks equivalent to the Tuzguny-Terezki thrust sheet and the Ediacaran-lower Paleozoic strata of the Shatput dome overlie Karakul-Mazar belt rocks (part 2 for discussion, Rutte *et al.* [2017]). The minimum southward underthrusting is 65 km.

The structural data on the Pamir gneiss-domes offer details about how and how much the Asian crust thickened. In the Tibetan Plateau, Cenozoic upper crustal ~N-S shortening is often considered to have been insufficient to build the 60–80 km thick crust [e.g., DeCelles *et al.*, 2002; Kapp *et al.*, 2005; Robinson, 2015]. Explanations for this discrepancy include pre-Cenozoic thickening [e.g., Murphy *et al.*, 1997; Roger *et al.*, 2010], underthrusting by India [e.g., DeCelles *et al.*, 2002], lateral tectonic escape and orogen-parallel lower crustal flow [e.g., Tapponnier *et al.*, 1982; Royden *et al.*, 1997], localized intracontinental subduction [e.g., Tapponnier *et al.*, 2001], and magmatic growth [Mo *et al.*, 2006]. The Pamir domes—offering a window in the deep Asian crust—demonstrate that classical Alpine-type thrust-fold nappe tectonics [e.g., Schmid *et al.*, 1996] built the thick crust of the Pamir-Tibetan Plateau. Despite the uncertainties involved in our shortening estimates, excess crustal thickness (>90 km compared to the present 60–70 km) might have existed at the end of the Paleogene to drive gravitational adjustments and lateral material flow out of the Plateau area (see below).

5.2. Central Pamir Gneiss-Dome Formation: Slab Breakoff and Gravitational Collapse of Thick Paleogene Crust

Rey *et al.* [2001] defined gravitational collapse as “gravity-driven ductile flow that effectively reduces lateral contrasts in gravitational potential energy.” Did the Central Pamir gneiss domes originate from gravitational

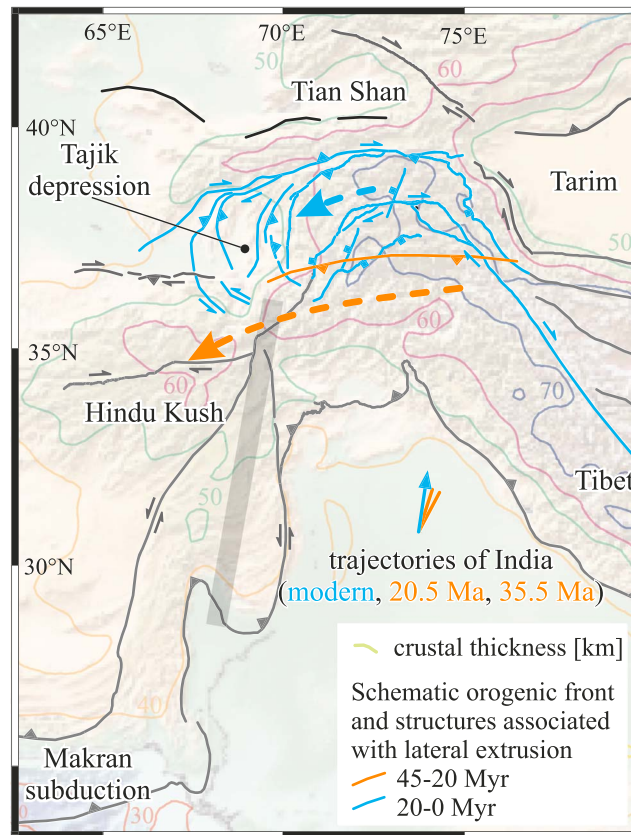


Figure 11. Topographic map of the western tip of the India-Asia collision zone with crustal thickness [Robert et al., 2015]. The crust of the Afghan western Hindu Kush is thick despite its position north of the oceanic Makran subduction zone and west of the India-Asia continent-continent collision. Schematic structures and their timing in the Pamir, Hindu Kush, and the Tajik depression visualize westward lateral extrusion that is likely responsible for thickening and basin inversion west of the collision zone.

collapse, and was there a trigger at the end of the Paleogene (~22 Ma)? The gneiss domes—structurally akin to core complexes in the sense of Lister [1988]—were exhumed by normal-sense crustal-scale shear/fault zones between ~22 and 12 Ma [Rutte et al., 2017]; subsequent crustal buckling may have contributed to the exhumation. Among others, Replumaz et al. [2010], DeCelles et al. [2011], and Stearns et al. [2013, 2015] suggested that the Indian slab broke off at 25–20 Ma, likely along the transition between Greater Indian and Cratonic Indian lithosphere (see section 1) [Kufner et al., 2016]. The long Paleogene shortening history, the possibly >90 km thick crust in the Central and South Pamir (and likely in the Hindu Kush and Karakorum farther south), and the Indian slab breakoff imply enhanced gravitational potential energy stored in the Pamir Plateau, a thermally weakened crust, and an enhanced basal heat flow through asthenospheric upwelling, resulting in a high Moho temperature. Together with a weak foreland upper crust, given by the regional evaporite detachment beneath the low-elevation Tajik depression [e.g., Nikolaev, 2002], these factors favor gravitational collapse

with the formation of metamorphic core complexes in the plateau crust—in analogy to Rey et al.'s [2010] numerical experiments. Gravitational collapse of the thick and hot Central and South Pamir crust—in the latter given by the giant Shakh-dara-Alichur dome [Stübner et al., 2013a, 2013b]—may have triggered the relocation of the active deformation front from the Central Pamir to the North Pamir, where foreland deformation in the Tajik depression and along the Main Pamir thrust system likely started at ~20 Ma [e.g., Sobel and Dumitru, 1997; Coutand et al., 2002]; in this scenario, the significant extension along the NMSZ may indicate gravitational sliding of the former plateau edge onto its foreland. The continuing northward underthrusting of Indian lithosphere in the aftermath of the slab breakoff likely terminated the collapse within a few Myr (at ~12 Ma in the Central Pamir gneiss domes [Rutte et al., 2017]). The northward advance of deep India may also explain why extensional gneiss domes occur in the Pamir, within the northern half of the thickened crust: India's underthrusting likely changed stresses from tensional to compressional earlier in the south. Additionally, lateral crustal flow into the Tajik depression (see below) likely drove the protracted crustal extension in the Shakh-dara dome, as outlined by Stübner et al. [2013a, 2013b], Schurr et al. [2014], and Stearns et al. [2015].

What localized the Paleogene deformation front along the northern margin of the Central Pamir and what caused the antiformal stack of the Central Pamir? We speculate that the Central Pamir stack formed at the southern edge of Cratonic Asia—before the delamination and rollback of its lithosphere. Paleogene shortening may have effectively thickened the crust of the amalgamated Cimmerian (Gondwana-derived) terranes that form the Pamir, Hindu Kush, and Karakorum crust today; this lithosphere was weakened rheologically by a long history of subduction, accretion, arc formation, and tectonism (section 1). Shortening may have

spread quickly northward (see the ~35 Ma Lu-Hf prograde garnet ages throughout the South and Central Pamir [Smit *et al.*, 2014]) but may have become localized and confined to the deformation front along the southern margin of rigid Cratonic Asia. At the time (~12 Ma) when deep Cratonic India encountered deep Cratonic Asia and initiated the delamination and retreat of Asian lithosphere [Kufner *et al.*, 2016], out-of-sequence shortening started: the northern Central Pamir was reactivated as a back thrust belt and the shortening in the Murghab-Aksu-Southeast Pamir thrust-wrench belt intensified [Rutte *et al.*, 2017], marking the resumption of distributed thickening in the amalgamated terranes of the Pamir. Then the exhumed and cooled gneisses of the Central Pamir domes began to act as a rigid backstop.

5.3. Dextral Wrenching: Lateral Extrusion

Lateral extrusion encompasses “extensional collapse, i.e., lateral gravitational spreading away from a topographic high in an orogenic belt, and tectonic escape, i.e., plane strain horizontal motion of wedges driven by forces applied to their boundaries” [Ratschbacher *et al.*, 1991]. Are dextral wrenching and ~E-W extension in the Pamir a feature of westward lateral extrusion? Paleogene recumbent isoclinal fold nappes in the Muskol and Shatput domes record crustal thickening during prograde metamorphism, and contain a ~ESE-WNW, along-strike flow lineation, implying orogen-parallel material transport. Stübner *et al.* [2013a] described similar high-grade, orogen-parallel flow in the Shakh dara dome; there, ~NE-SW stretch predated ~NNW-SSE ductile extensional flow that exhumed the crystalline rocks, similar to the Central Pamir gneiss domes. The younger (<~22 Ma) dextral wrenching and fold-axis parallel ~E-W extension in the Akbaital-Rangkul imbrications and Bozbaital-Pangazdjilga fold-thrust belts record orogen-parallel rock flow at shallower crustal level. The pinch and swell geometry of the domes and the culminations and troughs of the dome axis mark kilometer-scale, along-strike boudinage of the domes. The dextral wrenching was concentrated in the Murghab-Aksu-Southeast Pamir thrust-wrench belt south of the domes along the Rushan-Pshart suture. The ~E-W extension in the active Sarez-Karakul and Kongur Shan extensional systems that started at ~9 Ma [Robinson *et al.*, 2007] (likely ~12 Ma [Rutte *et al.*, 2017]) also relates to ~E-W material flow, as does the active dextral Aksu-Murghab strike-slip fault zone in the southeast Pamir, which roots in the Karakorum fault zone of western Tibet. We propose that the orogen-parallel material flow in the Pamir domes is related to an early stage of the geodynamic scenario that Schurr *et al.* [2014] derived from the seismotectonics of the Pamir: dominant ~N-S shortening building the Pamir Plateau is accompanied by lateral extrusion of material into depressions west of the Plateau. We envision that in the Paleogene lateral material transport contributed to crustal thickening in the western Hindu Kush of Afghanistan, where high topography and ~60 km thick crust [Robert *et al.*, 2015] remain puzzling given a geologic record of continuous oceanic subduction along the Makran trench in the south (Figure 11). Westward material transport since the mid-Miocene has been inverting the Tajik basin (Figure 11) [Stübner *et al.*, 2013a; Gagala *et al.*, 2014; Schurr *et al.*, 2014], which is ongoing [Schurr *et al.*, 2014].

6. Conclusions

We detailed the geometry, kinematics, and amount of deformation in the remote and high-elevation eastern Central Pamir to understand the orogenic processes involved in the building of the Pamir-Tibetan Plateau, i.e., the succession and interplay of thickening, thinning, and lateral transport of crust. Documented Cenozoic ~N-S shortening totals >95 km (>66%). A 7–10 km thick Phanerozoic upper crustal section was stacked and buried to ~30 km depth, consistent with the *P-T* conditions of the deepest exposed crust. The shortening was mainly accommodated by (1) top-to-~N emplacement of two large thrust sheets that span the Central Pamir, (2) tight to isoclinal folding and internal imbrication of these thrust sheets, and (3) Alpine-type fold-nappe emplacement. The sole thrust of the Central Pamir thrust-nappe stack reactivated the Triassic, south dipping Tanymas suture. During an intermittent, Miocene phase, parts of this crustal stack were exhumed along normal-sense shear zones, forming the Central Pamir gneiss domes. Fabrics along these shear zones record continuous exhumation from ductile flow to brittle fracturing. Post-extensional, out-of-sequence ~N-S shortening occurred along bivergent thrust-fold belts that reactivated the gneiss-dome margins, and had a dextral wrenching component expressed by regional strike-slip faulting, oblique thrusting, and kilometer-scale boudinage of the gneiss-dome rocks.

From the shortening estimates, it is possible that excess crustal thickness (>90 km compared to the present 60–70 km) at the end of the Paleogene drove gravitational adjustments and lateral material flow out of the

Plateau. The long Paleogene shortening history and the Indian slab breakoff at 25–20 Ma imply enhanced gravitational potential energy stored in the Pamir Plateau, a thermally weakened crust, enhanced basal heat flow, and a high Moho temperature. Together with a weak foreland upper crust, given by an evaporite décollement, these factors might have allowed gravitational collapse with the formation of extensional metamorphic core complexes in the orogenic hinterland—the Pamir gneiss domes. In addition, collapse may have triggered the relocation of the active deformation front from the Central to the North Pamir, as indicated by the onset of the foreland deformation in the Tajik depression and along Main Pamir thrust system at ~20 Ma. The continuing northward underthrusting of Indian lithosphere in the aftermath of slab breakoff likely terminated the collapse within a few Myr (at ~12 Ma in the Central Pamir gneiss domes). We speculate that the Paleogene deformation front and the antiformal stack of the Central Pamir localized above the southern edge of rigid Cratonic Asia that existed before the delamination and rollback of Asian lithosphere forced by the indentation of rigid Cratonic India. At ~12 Ma, when deep Cratonic India encountered deep Cratonic Asia, out-of-sequence shortening by bivergent thrusting-folding in the Central and South Pamir started, marking the switch from extensional collapse to resumption of distributed shortening.

The Paleogene fold nappes imply crustal thickening; the accompanying regional along-strike flow lineations imply orogen-parallel material transport before ~22 Ma. The post ~22 Ma dextral wrenching and fold-axis parallel, ~E-W extension in the upper crustal thrust sheets, the pinch and swell geometry of the gneiss domes, and the culminations and troughs of the dome axis record orogen-parallel material transport at shallower crustal levels. The dextral wrenching was concentrated in the Murghab-Aksu-Southeast Pamir thrust-wrench belt south of the domes along the Rushan-Pshart suture. The ~E-W extension in the active Sarez-Karakul and Kongur Shan extensional systems also relates to ~E-W material flow, as does the active dextral Aksu-Murghab strike-slip fault zone in the southeast Pamir. The interaction between ~N-S shortening by thrusting and folding, and the orogen-parallel material flow in the Central and South Pamir domes, mimics the geodynamic scenario given by the current seismic deformation: the dominant ~N-S shortening that is building the Pamir Plateau is accompanied by lateral extrusion of material into the depressions west of the Plateau. Currently, and over most of the Miocene, crust has been collapsing into the Tajik depression; in the Paleogene, lateral material transport thickened the crust in the western Hindu Kush of Afghanistan.

Acknowledgments

S. M. Gordon, J. Hofmann, E. Kanaev, N. Roziq, and J. Schmidt contributed to this study through joint field work and A. Friedrich contributed parts of the strain analysis. Data of this contribution are available in the supporting information and by contacting the corresponding authors. DFG bundle TIPAGE (PAK 443), bundle CAME project TIPTIMON, funded by the German Federal Ministry of Education and Research (support code 03G0809), and US-NSF grants EAR-0838269 and 1419751 funded this research. DAAD supported D.R., L.R., K.S., and S.S. with travel grants. Work in Tajikistan would have been impossible without the continuous support of the Tajik Academy of Sciences. We thank the TIPAGE members at GFZ Potsdam and TU Bergakademie Freiberg for discussions. We dedicate this paper to Victor Dronov and Vladislav Minaev (Tajik Academy of Sciences), two “rock stars” of the geology of the Pamir. Reviews by Djordje Grujic and Marc Jolivet are gratefully acknowledged.

References

- Angelier, J. (1984), Tectonic analysis of fault-slip data sets, *J. Geophys. Res.*, *89*(B7), 5835–5848, doi:10.1029/JB089iB07p05835.
- Angiolini, L., et al. (2015), From rift to drift in South Pamir (Tajikistan): Permian evolution of a Cimmerian terrane, *J. Asian Earth Sci.*, *102*, 146–169, doi:10.1016/j.jseas.2014.08.001.
- Bershaw, J., C. N. Garzzone, L. Schoenbohm, G. Gehrels, and L. Tao (2012), Cenozoic evolution of the Pamir plateau based on stratigraphy, zircon provenance, and stable isotopes of foreland basin sediments at Oytay (Wuyitake) in the Tarim Basin (west China), *J. Asian Earth Sci.*, *44*, 136–148, doi:10.1016/j.jseas.2011.04.020.
- Brunel, M., N. Arnaud, P. Tapponnier, Y. Pan, and Y. Wang (1994), Kongur Shan normal fault: Type example of mountain building assisted by extension (Karakorum fault, eastern Pamir), *Geology*, *22*, 707–710.
- Burg, J. P., and Y. Podladchikov (1999), Lithospheric scale folding: Numerical modelling and application to the Himalayan syntaxes, *Int. J. Earth Sci.*, *88*(2), 190–200.
- Burtman, V. S., and P. Molnar (1993), Geological and geophysical evidence for deep subduction of continental crust beneath the Pamir, *Spec. Pap. Geol. Soc. Am.*, *281*, 1–76.
- Coutand, I., M. R. Strecker, J. R. Arrowsmith, G. Hillel, R. C. Thiede, A. Korjenkov, and M. Omuraliev (2002), Late Cenozoic tectonic development of the intra-montane Alai Valley, (Pamir-Tian Shan region, central Asia): An example of intracontinental deformation due to the Indo-Eurasia collision, *Tectonics*, *21*, 1053, doi:10.1029/2002TC001358.
- DeCelles, P. G., D. M. Robinson, and G. Zandt (2002), Implications of shortening in the Himalayan fold-thrust belt for uplift of the Tibetan Plateau, *Tectonics*, *21*(6), 12–1–12–25, doi:10.1029/2001TC001322.
- DeCelles, P. G., P. Kapp, J. Quade, and G. E. Gehrels (2011), Oligocene–Miocene Kailas basin, southwestern Tibet: Record of post-collisional upper-plate extension in the Indus-Yarlung suture zone, *Geol. Soc. Am. Bull.*, *123*(7–8), 1337–1362, doi:10.1130/B30258.1.
- Dewey, J. F. (1988), Extensional collapse of orogens, *Tectonics*, *7*(6), 1123–1139, doi:10.1029/TC007i006p01123.
- Dronov, V. I., G. K. Melnikova, G. Ch. Salibajev, I. A. Bardashev, V. E. Minaev, M. M. Muchabatov, (2006), Stratigraphic dictionary of the Pamir (in Russian), edited by K. P. Stanek, Medienzentrums der TU Bergakademie Freiberg, 1–252, ISBN/EAN: 9783860122846.
- Faure, M., W. Lin, U. Schärer, L. Sun, Y. Sun, and N. Arnaud (2003), Continental subduction and exhumation of UHP rocks. Structural and geochronological insights from the Dabieshan (East China), *Lithos*, *70*, 213–241, doi:10.1016/S0024-4937(03)00100-2.
- Ferguson, C. C., and G. E. Lloyd (1984), Extension analysis of stretched belemnites: A comparison of methods, *Tectonophysics*, *101*, 199–206, doi:10.1016/0040-1951(84)90052-0.
- Gaetani, M. (1997), The Karakorum block in Central Asia, from Ordovician to Cretaceous, *Sediment. Geol.*, *109*(3–4), 339–359, doi:10.1016/S0037-0738(96)00068-1.
- Gagala, L., A. Kässner, S. Abdulhameed, A. Szulc, L. Ratschbacher, J.-C. Ringenbach, R. Gloaguen, N. Rajabov, and R. Mirkamalov (2014), Structure and exhumation of the Tajik depression (western foreland of the Pamir): Towards an integrated kinematic model, 14th International Conference on Thermochronology, Chamonix, 09/2014.

- Hacker, B., P. Luffi, V. Lutkov, V. Minaev, L. Ratschbacher, T. Plank, M. Ducea, A. Patiño-Douce, M. McWilliams, and J. Metcalf (2005), Near-ultrahigh pressure processing of continental crust: Miocene crustal xenoliths from the Pamir, *J. Petrol.*, *46*, 1661–1687, doi:10.1093/ptrology/egi030.
- Ischuk, A., et al. (2013), Kinematics of the Pamir and Hindu Kush regions from GPS geodesy, *J. Geophys. Res. Solid Earth*, *118*, 2408–2416, doi:10.1002/jgrb.50185.
- Ishii, K., K. Kanagawa, N. Shigematsu, and T. Okudaira (2007), High ductility of K-feldspar and development of granitic banded ultramylonite in the Ryoke metamorphic belt, SW Japan, *J. Struct. Geol.*, *29*(6), 1083–1098, doi:10.1016/j.jsg.2007.02.008.
- Jiang, Y.-H., Z. Liu, R.-Y. Jia, S.-Y. Liao, Q. Zhou, and P. Zhao (2012), Miocene potassic granite–syenite association in western Tibetan Plateau: Implications for shoshonitic and high Ba–Sr granite genesis, *Lithos*, *134*, 146–162, doi:10.1016/j.lithos.2011.12.012.
- Kapp, P., A. Yin, T. M. Harrison, and L. Ding (2005), Cretaceous–Tertiary shortening, basin development, and volcanism in central Tibet, *Geol. Soc. Am. Bull.*, *117*(7/8), 865–878, doi:10.1130/B25595.1.
- Kufner, S.-K., et al. (2016), Deep India meets deep Asia: Lithospheric indentation, delamination and break-off under Pamir and Hindu Kush (Central Asia), *Earth Planet. Sci. Lett.*, *435*, 171–184, doi:10.1016/j.epsl.2015.11.046.
- Kumar, M. R., J. Saul, D. Sarkar, R. Kind, and A. K. Shukla (2001), Crustal structure of the Indian shield: New constraints from teleseismic receiver functions, *Geophys. Res. Lett.*, *28*(7), 1339–1342, doi:10.1029/2000GL012310.
- Kurz, W., H. Fritz, V. Tenczer, and W. Unzog (2002), Tectono-metamorphic evolution of the Koralm complex (Eastern Alps): Constraints from microstructures and textures of the ‘Plattengneis’ shear zone, *J. Struct. Geol.*, *24*, 1957–1970.
- Law, R. D. (1990), Crystallographic fabrics: A selective review of their applications to research in structural geology, in *Deformation Mechanism, Rheology and Tectonics*, vol. 54, edited by R. J. Knipe and E. H. Rutter, pp. 335–352, Geol. Soc., London, doi:10.1144/GSL.SP.1990.054.01.30.
- Lee, J., B. R. Hacker, W. S. Dinklage, Y. Wang, P. Gans, A. Calvert, J. Wan, W. Chen, A. E. Blythe, and W. McClelland (2000), Evolution of the Kangmar Dome, southern Tibet: Structural, petrologic, and thermochronologic constraints, *Tectonics*, *19*(5), 872–895, doi:10.1029/1999TC001147.
- Leven, J. E. (1993), Main events in the Permian history of the Tethys and fusulinids, *Stratigr. Geol. Correl.*, *1*, 59–75.
- Leven, J. E. (1995), Permian and Triassic of the Rushan-Pshart Zone (Pamir), *Riv. Ital. Paleontol. Stratigr.*, *101*(1), 3–16.
- Lister, G. S. (1988), The origin of metamorphic core complexes and detachment faults formed during Tertiary continental extension in the northern Colorado River region, U.S.A., *J. Struct. Geol.*, *11*(1–2), 65–94, doi:10.1016/0191-8141(89)90036-9.
- Malavieille, J. (1987), Extensional shearing deformation and kilometer-scale “a”-type folds in a Cordilleran metamorphic core complex (Raft River Mountains, northwestern Utah), *Tectonics*, *6*, 423–448, doi:10.1029/TC006i004p00423.
- Malz, N., J. A. Pfänder, L. Ratschbacher, and B. R. Hacker (2013), Cretaceous–Cenozoic magmatism in the Pamir and a comparison with Tibet, *Geophys. Res. Abstr.*, *15*, EGU2013–3122.
- Means, W. D. (1989), Stretching Faults, *Geology*, *17*, 893–895, doi:10.1130/0091-7613.
- Mechie, J., et al. (2012), Crustal and uppermost mantle velocity structure along a profile across the Pamir and southern Tian Shan as derived from project TIPAGE wide-angle seismic data, *Geophys. J. Int.*, *188*, 385–407, doi:10.1111/j.1365-246X.2011.05278.x.
- Mo, X., Z. Hou, Y. Niu, G. Dong, X. Qu, Z. Zhao, and Z. Yang (2006), Mantle contributions to crustal thickening during continental collision: Evidence from Cenozoic igneous rocks in southern Tibet, *Lithos*, *96*(1–2), 225–242, doi:10.1016/j.lithos.2006.10.005.
- Molnar, P., and J. M. Stock (2009), Slowing of India’s convergence with Eurasia since 20 Ma and its implications for Tibetan mantle dynamics, *Tectonics*, *28*, TC3001, doi:10.1029/2008TC002271.
- Murphy, M. A., A. Yin, T. M. Harrison, S. B. Dürr, Z. Chen, F. J. Ryerson, W. S. F. Kidd, X. Wang, and X. Zhou (1997), Did Indo-Asian collision alone create the Tibetan Plateau, *Geology*, *25*, 719–722.
- Negredo, A. M., A. Replumaz, A. Villaseñor, and S. Guillot (2007), Modelling the evolution of continental subduction processes in the Pamir–Hindu Kush region, *Earth Planet. Sci. Lett.*, *259*(1), 212–225.
- Nikolaev, V. G. (2002), Afghan–Tajik depression: Architecture of sedimentary cover and evolution, *Russ. J. Earth Sci.*, *4*(6), 399–421.
- Pashkov, B. R., and E. A. Dmitriyev (1982), Muzkol crystalline massif (Central Pamir), *Int. Geol. Rev.*, *24*(3), 285–296.
- Passchier, C. W., and R. A. J. Trouw (2005), *Microtectonics*, pp. 366, Springer-Verlag, Berlin Heidelberg.
- Pegler, G., and S. Das (1998), An enhanced image of the Pamir Hindu Kush seismic zone from relocated earthquake hypocenters, *Geophys. J. Int.*, *134*(2), 573–595, doi:10.1046/j.1365-246x.1998.00582.x.
- Pryer, L. L. (1993), Microstructures in feldspars from a major crustal thrust zone: The Grenville Front, Ontario, Canada, *J. Struct. Geol.*, *15*(1), 21–36, doi:10.1016/0191-8141(93)90076-M.
- Ramsay, J. G. (1967), *Folding and Fracturing of Rocks*, pp. 531, MacGraw-Hill, New York.
- Ramsay, J. G. (1980), The crack-seal mechanism of rock deformation, *Nature*, *284*, 135–139, doi:10.1038/284135a0.
- Ramsay, J. G., and M. I. Huber (1983), *The Techniques of Modern Structural Geology: Strain Analysis*, pp. 307, Academic Press, London.
- Ratschbacher, L., W. Frisch, F. Neubauer, S. M. Schmid, and J. Neugebauer (1989), Extension in compressional orogenic belts: The eastern Alps, *Geology*, *17*(5), 404–407, doi:10.1130/0091-7613.
- Ratschbacher, L., W. Frisch, H.-G. Linzer, and O. Merle (1991), Lateral extrusion in the eastern Alps, Part 2: Structural analysis, *Tectonics*, *10*(2), 257–271, doi:10.1029/90TC02623.
- Ree, J.-H., H. S. Kim, R. Han, and H. Jung (2005), Grain-size reduction of feldspars by fracturing and neo-crystallization in a low-grade granitic mylonite and its rheological effect, *Tectonophysics*, *407*(3–4), 227–237, doi:10.1016/j.tecto.2005.07.010.
- Replumaz, A., A. M. Negredo, S. Guillot, and A. Villaseñor (2010), Multiple episodes of continental subduction during India/Asia convergence: Insight from seismic tomography and tectonic reconstruction, *Tectonophysics*, *483*(1), 125–134, doi:10.1016/j.tecto.2009.10.007.
- Rey, P. F., O. Vanderhaeghe, and C. Teysier (2001), Gravitational collapse of the continental crust: Definition, regimes and modes, *Tectonophysics*, *342*(3), 435–449, doi:10.1016/S0040-1951(01)00174-3.
- Rey, P. F., C. Teysier, and D. L. Whitney (2010), Limit of channel flow in orogenic plateaux, *Lithosphere*, *2*(5), 328–332, doi:10.1130/L114.1.
- Rey, P. F., C. Teysier, S. C. Kruckenberg, and D. L. Whitney (2011), Viscous collision in channel explains double domes in metamorphic core complexes, *Geology*, *39*(4), 387–390, doi:10.1130/G31587.1.
- Robert, A. M. M., M. Fernández, I. Jiménez-Munt, and J. Vergés (2015), Lithospheric structures in Central Eurasia derived from elevation, geoid anomaly and thermal analysis, *Geol. Soc. Lond. Spec. Publ.*, *427-10*, doi:10.1144/SP427.10.
- Robinson, A. C. (2015), Mesozoic tectonics of the Gondwanan terranes of the Pamir plateau, *J. Asian Earth Sci.*, *102*, 170–179, doi:10.1016/j.jseas.2014.09.012.
- Robinson, A. C., A. Yin, C. E. Manning, T. M. Harrison, S.-H. Zhang, and X.-F. Wang (2004), Tectonic evolution of the northeastern Pamir: Constraints from the northern portion of the Cenozoic Kongur Shan extensional system, *Geol. Soc. Am. Bull.*, *116*(7–8), 953–974, doi:10.1130/B25375.1.

- Robinson, A. C., A. Yin, C. E. Manning, T. M. Harrison, S.-H. Zhang, and X.-F. Wang (2007), Cenozoic evolution of the eastern Pamir: Implications for strain-accommodation mechanisms at the western end of the Himalayan-Tibetan orogen, *Geol. Soc. Am. Bull.*, *119*(7–8), 882–896, doi:10.1130/B25981.1.
- Robinson, A. C., M. Ducea, and T. J. Lapen (2012), Detrital zircon and isotopic constraints on the crustal architecture and tectonic evolution of the northeastern Pamir, *Tectonics*, *31*, TC2016, doi:10.1029/2011TC003013.
- Roger, F., M. Jolivet, and J. Malavieille (2010), The tectonic evolution of the Songpan-Garzê (North Tibet) and adjacent areas from Proterozoic to Present: A synthesis, *J. Asian Earth Sci.*, *39*, 254–269, doi:10.1016/j.jseas.2010.03.008.
- Royden, L. H., B. C. Burchfiel, R. W. King, E. Wang, Z. Chen, F. Shen, and Y. Liu (1997), Surface deformation and lower crustal flow in eastern Tibet, *Science*, *276*(5313), 788–790, doi:10.1126/science.276.5313.788.
- Rutte, D., et al. (2017), Building the Pamir-Tibet Plateau—Crustal stacking, extensional collapse, and lateral extrusion in the Central Pamir: 2. Timing and Rates, *Tectonics*, *36*, doi:10.1002/2016TC004294.
- Ruzhentsev, S. V. (1990), The Pamir, in *Tectonic Stratification of the Lithosphere and Regional Geologic Investigations* (in Russian), edited by Y. M. Pushcharovskii and V. G. Trifonov, pp. 214–225, Nauka, Moscow.
- Ruzhentsev, S. V., and V. A. Shvolman (1981), Tectonic zoning of the Pamirs and Afghanistan, in *Contemporary Geoscientific Researches in the Himalaya*, vol. 53–59, edited by A. K. Sinha, Bishen Singh Mahendra Pal Singh, Dehra Dun, India.
- Schmid, S. M., O. A. Pfiffner, N. Froitzheim, G. Schönborn, and E. Kissling (1996), Geophysical-geological transect and tectonic evolution of the Swiss-Italian Alps, *Tectonics*, *15*, 1036–1064, doi:10.1029/96TC00433.
- Schmidt, J., B. R. Hacker, L. Ratschbacher, K. Stübner, M. A. Stearns, A. Kylander-Clark, J. M. Cottle, A. Webb, G. Gehrels, and V. Minaev (2011), Cenozoic deep crust in the Pamir, *Earth Planet. Sci. Lett.*, *312*(3–4), 411–421, doi:10.1016/j.epsl.2011.10.034.
- Schneider, F. M., et al. (2013), Seismic imaging of subduction continental lower crust beneath the Pamir, *Earth Planet. Sci. Lett.*, *375*, 101–112, doi:10.1016/j.epsl.2013.05.015.
- Schurr, B., L. Ratschbacher, C. Sippl, R. Gloaguen, X. Yuan, and J. Mechie (2014), Seismotectonics of the Pamir, *Tectonics*, *33*, 1501–1518, doi:10.1002/2014TC003576.
- Schwab, M., et al. (2004), Assembly of the Pamirs: Age and origin of magmatic belts from the southern Tian Shan to the southern Pamirs and their relation to Tibet, *Tectonics*, *23*, TC4002, doi:10.1029/2003TC001583.
- Sippl, C., et al. (2013a), Deep burial of Asian continental crust beneath the Pamir imaged with local earthquake tomography, *Earth Planet. Sci. Lett.*, *384*, 165–177, doi:10.1016/j.epsl.2013.10.013.
- Sippl, C., et al. (2013b), Geometry of the Pamir-Hindu Kush intermediate-depth earthquake zone from local seismic data, *J. Geophys. Res. Solid Earth*, *118*, 1438–1457, doi:10.1002/jgrb.50128.
- Sippl, C., L. Ratschbacher, B. Schurr, C. Krumbiegel, H. Rui, L. Pingren, and U. Abdybachev (2014), The 2008 Nura earthquake sequence at the Pamir-Tian Shan collision zone, southern Kyrgyzstan, *Tectonics*, *33*, 2382–2399, doi:10.1002/2014TC003705.
- Smit, M. A., L. Ratschbacher, E. Kooijman, and M. A. Stearns (2014), Early evolution of the Pamir deep crust from Lu-Hf and U-Pb geochronology, and garnet thermometry, *Geology*, *42*(12), 1047–1050, doi:10.1130/G35878.1.
- Sobel, E. R., and T. A. Dumitru (1997), Thrusting and exhumation around the margins of the western Tarim basin during the India-Asia collision, *J. Geophys. Res.*, *102*(B3), 5043–5063, doi:10.1029/96JB03267.
- Sperner, B., and L. Ratschbacher (1994), A Turbo Pascal program package for graphical representation and stress analysis of calcite deformation, *Z. Dtsch. Geol. Ges.*, *145*, 414–423.
- Sperner, B., and P. Zweigel (2010), A plea for more caution in fault-slip analysis, *Tectonophysics*, *482*(1–4), 29–41, doi:10.1016/j.tecto.2009.07.019.
- Sperner, B., L. Ratschbacher, and R. Ott (1993), Fault-striae analysis: A Turbo Pascal program package for graphical representation and reduced stress-tensor calculation, *Comput. Geosci.*, *19*, 1361–1388.
- Stearns, M. A., B. R. Hacker, L. Ratschbacher, J. Lee, J. M. Cottle, and A. R. C. Kylander-Clark (2013), Synchronous Oligocene-Miocene metamorphism of the Pamir and the north Himalaya driven by plate-scale dynamics, *Geology*, *41*(10), 1071–1074, doi:10.1130/G34451.1.
- Stearns, M. A., B. R. Hacker, L. Ratschbacher, D. Rutte, and A. R. C. Kylander-Clark (2015), Titanite petrochronology of the Pamir gneiss domes: Implications for middle to deep crust exhumation and titanite closure to Pb and Zr diffusion, *Tectonics*, *34*, 784–802, doi:10.1002/2014TC003774.
- Stipp, M., H. Stünitz, R. Heilbronner, and S. M. Schmid (2002), The eastern Tonale fault zone: A ‘natural laboratory’ for crystal plastic deformation of quartz over a temperature range from 250 to 700°C, *J. Struct. Geol.*, *24*, 1861–1884, doi:10.1016/S0191-8141(02)00035-4.
- Strecker, M. R., W. Frisch, M. W. Hamburger, L. Ratschbacher, S. Semiletkin, A. Zamoruyev, and N. Sturchio (1995), Quaternary deformation in the Eastern Pamirs, Tadzhikistan and Kyrgyzstan, *Tectonics*, *14*(5), 1061–1079, doi:10.1029/95TC00927.
- Stübner, K., L. Ratschbacher, D. Rutte, K. Stanek, V. Minaev, M. Wiesinger, R. Gloaguen, and Project TIPAGE members (2013a), The giant Shakh-dara migmatitic gneiss dome, Pamir, India-Asia collision zone: 1. Geometry and kinematics, *Tectonics*, *32*, 948–979, doi:10.1002/tect.20057.
- Stübner, K., et al. (2013b), The giant Shakh-dara migmatitic gneiss dome, Pamir, India-Asia collision zone: 2. Timing of dome formation, *Tectonics*, *32*, 1404–1431, doi:10.1002/tect.20059.
- Tapponnier, P., G. Peltzer, A. Y. L. Dain, R. Armijo, and P. Cobbold (1982), Propagating extrusion tectonics in Asia: New insights from simple experiments with plasticine, *Geology*, *10*(12), 611–616, doi:10.1130/0091-7613(1982).
- Tapponnier, P., X. Zhiqin, F. Roger, B. Meyer, N. Arnaud, G. Wittlinger, and Y. Jingsui (2001), Oblique stepwise rise and growth of the Tibet plateau, *Science*, *294*(5547), 1671–1677, doi:10.1126/science.105978.
- Thiede, R. C., E. R. Sobel, J. Chen, L. M. Schoenbohm, D. F. Stockli, M. Sudo, and M. R. Strecker (2013), Late Cenozoic extension and crustal doming in the India-Eurasia collision zone: New thermochronologic constraints from the NE Chinese Pamir, *Tectonics*, *32*, 763–779, doi:10.1002/tect.20050.
- Vannay, J.-C., B. Grasemann, M. Rahn, W. Frank, A. Carter, V. Baudraz, and M. Cosca (2004), Miocene to Holocene exhumation of metamorphic crustal wedges in the NW Himalaya: Evidence for tectonic extrusion coupled to fluvial erosion, *Tectonics*, *23*, TC1014, doi:10.1029/2002TC001429.
- Vlasov, N. G., Yu. A. Dyakov, and E. S. Cherev (Eds.) (1991), *Geological map of the Tajik SSR and adjacent territories, 1:500,000*, Vsesojuznoi Geol. Inst. Leningrad, Saint Petersburg, Russia.
- Wilcox, R., T. Harding, and D. S. Seely (1973), Basic wrench tectonics, *Am. Assoc. Pet. Geol. Bull.*, *57*(1), 74–96.
- Yushin, I. P., M. E. Sass, S. S. Karapetov, S. M. Altukhov, I. C. Teplov, C. R. Raaikov, S. I. Harkov, and A. G. Davidchenko (1964), J-43-VIII, XIV, XV, XX, XXI, 1:200,000 maps of the Tajik SSR, Russian Geological Research Institute.
- Zubovich, A. V., et al. (2010), GPS velocity field for the Tien Shan and surrounding regions, *Tectonics*, *29*, TC6014, doi:10.1029/2010TC002772.